Master's thesis

NTNU
Norwegian University of Science and Technology
Faculty of Natural Sciences
Department of Materials Science and Engineering

Øyvind Lindgård

The Effect of Li Salts, Cosolvents, and Additives on the Performance of Silicon Anodes in Ionic Liquid Electrolytes for Lithium-Ion Batteries

Master's thesis in Nanotechnology
Supervisor: Professor Ann Mari Svensson
June 2020

NTNU
Norwegian University of
Science and Technology

Øyvind Lindgård

The Effect of Li Salts, Cosolvents, and Additives on the Performance of Silicon Anodes in Ionic Liquid Electrolytes for Lithium-Ion Batteries

Master's thesis in Nanotechnology
Supervisor: Professor Ann Mari Svensson
June 2020

Norwegian University of Science and Technology
Faculty of Natural Sciences
Department of Materials Science and Engineering

NTNU
Norwegian University of
Science and Technology

Preface

This thesis describes the work carried out in the course TMT4910 "Nanotechnology, Master's Thesis" during the spring of 2020. This work is partly based on the project thesis delivered by the author in the fall of 2019 with the title "Evaluation of LiTFSI as Electrolyte Salt in EmiFSI-based Ionic Liquid Electrolytes to be used with Silicon Anodes for Lithium-Ion Batteries", but have been extensively rewritten. The project thesis and this master thesis are related to the research project "Silicon anodes for Li-ion batteries, optimized binder, electrolyte and cathode" (SiBEC) and to the FME center (Centres for Environment-friendly Energy Research) "Mobility Zero Emission Energy System" (MoZEES).

The outbreak of the COVID-19 pandemic resulted in a six-week break from campus and a denied access to all labs, forcing some changes to be made to the original plan for this thesis.

I would like to thank my supervisor Professor Ann Mari Svensson for excellent guiding and feedback during the semester and for the many online meetings during the time away from campus. My co-supervisor Daniel Tevik Rogstad is sincerely thanked for participating in helpful discussions and assisting in lab work. The battery group at the Department of Materials Science and Engineering is thanked for its inclusive social and academic environment. Lastly, a huge thank you is given to Timini and to my fellow Nanotechnology students for making this semester and the previous five years a great experience.

XPS measurements in this work were performed with wonderful help from three great people. Firstly, Daniel Tevik Rogstad performed XPS characterization of the uncycled Si anode. Regarding the four cycled anodes, Maria Valeria Blanco, a Post-doc at the Department of Materials Science and Engineering, loaded the XPS sample holder into the inert transfer arm and Øystein Dahl, a SINTEF employee, operated the XPS. XPS data analysis for all samples was performed by the author, but Øystein Dahl is thanked for his help in the analysis process.

The Research Council of Norway is acknowledged for the financial support to SiBEC under the contract number 255195/E20 and for the support to the Norwegian Micro- and Nano-Fabrication Facility, NorFab, project number 245963/F50.

Abstract

This thesis aims at improving the performance and understanding of Si anodes in combination with ionic liquid (IL) electrolytes for Li-ion batteries (LIBs) for the purpose of supporting the quest for safer and higher-capacity energy storage. LIBs have been widely implemented in the past decades, revolutionizing the field of portable electronics and laying the foundation for the electrification of society, for instance through a widespread commercialization of electric vehicles. However, the graphite anode in the traditional LIB has reached its limiting capacity and further developments to this crucial technology are needed to allow LIBs to fulfill the role they can play in a greener future. Silicon has been recognized as one of the most promising next-generation anode materials. In addition, a replacement of today's flammable carbonate-based electrolytes should also be developed and ILs, despite their high viscosities, have been considered as a non-flammable electrolyte alternative for quite some time. To further address the challenges related to Si anodes and IL electrolytes, this thesis employed a threefold approach including **(1)** evaluating the effects that two different Li salts, *lithium bis(fluorosulfonyl)imide* (LiFSI) and *lithium bis(trifluoro-methanesulfonyl)imide* (LiTFSI), had on cycling stability, rate performance, and solid-electrolyte interphase (SEI) formation of Si anodes in two different ILs, *1-ethyl-3-methylimidazolium bis(fluorosulfonyl)-imide* (EmiFSI) and *trimethyl(isobutyl)phosphonium bis(fluorosulfonyl)imide* (P_{111i4}FSI), **(2)** assessing the use of *triethyl phosphate* (TEP) and *2-trifluoromethyl-3-methoxyperfluoropentane* (TMMP) as low-viscosity cosolvents for EmiFSI, and **(3)** evaluating *fluoroethylene carbonate* (FEC) as a potential SEI-forming additive in EmiFSI-based electrolytes with and without a cosolvent. The results showed that LiFSI is the preferred salt in P_{111i4}FSI electrolytes, but that there is a trade-off between improved capacity and a better Coulombic efficiency for LiTFSI and a better rate performance for LiFSI in EmiFSI-based electrolytes. These findings illustrate how the choice of Li salt affects cell performance and imply that careful consideration must be taken when choosing the electrolyte salt. Further, neither TEP nor TMMP appear to be suitable cosolvents for EmiFSI as TEP underwent a severe decomposition during the first charge cycle and TMMP was not miscible with EmiFSI at the concentrations tested in this thesis. The use of FEC as an additive resulted in worse rate performance and greater overpotentials, both with and without the cosolvent present, meaning that it is not suitable to be used with EmiFSI. Further research should focus on using additional characterization techniques to improve the understanding of SEI formation with LiFSI and LiTFSI salts, in addition to evaluating further alternatives for cosolvents and additives to improve the performance of Si anodes in IL electrolytes.

Sammendrag

Denne oppgaven fokuserer på å forbedre ytelsen og forståelsen av silisiumanoder i kombinasjon med elektrolytter av ioniske væsker for litsium-ionbatterier med formål om å støtte arbeidet med å utvikle energilagring som er tryggere og har høyere kapasitet. Litsium-ionbatterier har blitt kraftig implementert de siste tiårene og har revolusjonert bærbar elektronikk og lagt grunnlaget for elektrifiseringen av samfunnet, for eksempel via kommersialisering av elektriske biler. Nå har imidlertid grafittanoden i det tradisjonelle litsium-ionbatteriet nådd den teoretiske kapasiteten og det er nødvendig med videreutvikling for at litsium-ionbatteri skal kunne bidra til en grønnere framtid. Silisium er anerkjent som et av de mest lovende anodematerialene i neste generasjons batterier. I tillegg bør et alternativ til dagens brennbare karbonatelektrolytter bli utviklet. Ioniske væsker har, til tross for høy viskositet, blitt vurdert som en ikke-brennbar elektrolytt i mange år. For å videre adressere utfordringene knyttet til silisiumanoder og elektrolytter av ioniske væsker, har denne oppgaven tatt i bruk en tredelt tilnærming som inkluderer **(1)** å evaluere effektene som to litsiumsalt, *litsium bis(fluorosulfonyl)imide* (LiFSI) og *litsium bis(trifluoro-metansulfonyl)imide* (LiTFSI), hadde på opp- og utladingsstabiliteten, rateytelsen og dannelse av SEI ("solid-electrolyte interphase") med silisiumanoder i to forskjellige ioniske væsker, *1-etyl-3-metylimidazolium bis(fluorosulfonyl)-imide* (EmiFSI) og *trimetyl(isobutyl)phosphonium bis(fluorosulfonyl)imide* (P_{111i4}FSI), **(2)** å vurdere bruken av *trietylfosfat* (TEP) og *2-trifluormetyl-3-methoxyperfluoropentan* (TMMP) som kosolventer med lav viskositet for EmiFSI og **(3)** å evaluere *fluoretylenkarbonat* (FEC) som et mulig SEI-dannende tilsetningsstoff i EmiFSI-baserte elektrolytter både med og uten kosolvent. Resultatene viste at LiFSI er det foretrukne litsiumsaltet for P_{111i4}FSI-elektrolytter, men at det er en avveining mellom forbedret kapasistet og Coulombisk effektivitet med LiTFSI og en bedre rateytelse med LiFSI i EmiFSI-baserte elektrolytter. Disse funnene illustrerer hvordan valget av litsiumsalt påvirker celleytelsen og impliserer at nøye vurderinger må gjøres når litsiumsalt skal velges. Videre virker verken TEP eller TMMP å være aktuelle kosolventer for EmiFSI ettersom TEP gjennomgikk en kraftig dekomponeringsprosess under den første oppladingssyklusen og TMMP ikke var løselig i EmiFSI ved de konsentrasjonene som ble testet i denne oppgaven. Bruken av FEC som tilsetningsstoff resulterte i verre rateytelse og større overpotensial, både med og uten kosolvent tilstede, noe som betyr at den ikke er passende å bruke sammen med EmiFSI. Videre forskning bør fokusere på å bruke flere karakteriseringsteknikker for å forbedre forståelsen av SEI-dannelse med LiFSI og LiTFSI, samt evaluere flere alternative kosolventer og tilsetningsstoffer for å forbedre ytelsen av silisiumanoder i elektrolytter av ioniske væsker.

Abbreviations

IL	Ionic liquid
LIB	Lithium ion battery
LiFSI	Lithium bis(fluorosulfonyl)imide
LiTFSI	Lithium bis(trifluoro-methanesulfonyl)imide
SEI	Solid-electrolyte interface
EmiFSI	1-Ethyl-3-methylimidazolium bis(fluorosulfonyl)imide
P_{111i4}FSI	Trimethyl(isobutyl)phosphonium bis(fluorosulfonyl)imide
TEP	Triethyl phosphate
TMMP	2-Trifluoromethyl-3-methoxyperfluoropentane
FEC	Fluoroethylene carbonate
XPS	X-ray photoelectron spectroscopy
IFE	Institute for Energy Technology
LFP	$LiFePO_4$
EIS	Electrical impedance spectroscopy
SOC	State of charge
NMR	Nuclear magnetic resonance
DFT	Density functional theory
LUMO	Lowest unoccupied molecular orbital
HOMO	Highest occupied molecular orbital
EC	Ethylene carbonate
FTIR	Fourier-transform infrared spectroscopy
DEC	Diethyl carbonate
DMC	Dimethyl carbonate
EMC	Ethylmethyl carbonate
TMP	Trimethyl phosphate
HFE	Hydrofluoroether
CMC	Carboxymethyl cellulose

Contents

Chapter 1

Introduction

1.1 Background and motivation

The modern world is currently facing a serious climate crisis and a massive, collective effort is needed to limit global warming to below 1.5 °C to avoid the most disastrous consequences of climate change, as detailed in a recent IPCC report [1]. The transition from today's fossil fuel-dependent economy to a greener alternative will require both political willpower and technological innovations. Improved energy storage solutions will play an essential role in this transition and battery technology, with the LIB being the market leader, will likely be a key solution. The LIB is expected to be important in everything from the electric vehicle revolution [2] to overcoming the intermittency problem of many renewable energy resources [3]. In the fall of 2019, the LIB received additional attention when the 2019 Nobel Prize in Chemistry was awarded to its inventors [4]. Although the LIB is a well-researched technology, additional improvements are needed for it to continue to compete with fossil alternative [5].

The LIB system has not changed much since its commercialization by Sony in 1991 and a typical LIB still consists of a carbonaceous anode, a transition metal oxide cathode, and an organic liquid electrolyte. Graphite is used as active material in the anode due to its charge-discharge cycling stability [6], but the conventional LIB now faces the theoretical limit of its energy density [7] and it is necessary to find an alternative that can outperform the 372 mAh/g gravimetric theoretical capacity of graphite. Si has an almost ten times higher theoretical capacity, 3579 mAh/g, and is the leading candidate for next-generation anodes [7].

Implementing a Si anode comes with a set of challenges. Si can experience an enormous >300% volume expansion when alloying with Li [8]. This expansion results in cracking and fragmentation of the Si particles and deformation of the electrode, which may cause electrical isolation of the active material [9]. In addition, the expansion of Si has detrimental effects on the SEI layer. The SEI layer is a very thin, protective layer on the anode. The formation of the SEI layer happens during the initial charge cycles due to an irreversible reduction of the electrolyte when in contact with the anode [10]. The formation of the SEI layer represents an irreversible capacity loss, but a continuous electrolyte decomposition is usually avoided as the electrically insulating SEI acts as an electron barrier between the electrolyte and the anode, preventing further decomposition. However, the expansion of Si upon lithiation and the subsequent cracking of the SEI layer exposes "fresh" Si to the electrolyte, consequently promoting further electrolyte decomposition. The unstable nature of the SEI layer on Si gives

a reduced efficiency and lowers the capacity retained with each charge and discharge cycle [11].

The limited energy density is only one of the challenges that the traditional LIB faces. A profound safety hazard related to the electrolyte is also present. The electrolyte in today's LIBs is usually a blend of highly flammable carbonates [5] that have flash points around room temperature [12]. A damaged cell in combination with an ignition source can cause a fire or explosion. This has motivated a research effort to develop safer electrolyte alternatives.

An IL is a salt with a low melting point, usually defined to be $<100\,^{\circ}\mathrm{C}$, meaning that it exists as a liquid consisting of only ions even at relatively low temperatures. Room temperature ILs are a subset of ILs with melting points below room temperature. ILs have been considered as battery electrolytes for several decades [13] and their beneficial properties include negligible vapor pressure, wide electrochemical stability windows, sufficient ionic conductivities, and high chemical and thermal stability, making them a safe substitute for today's carbonate electrolytes [14, 15].

A large number of room temperature ILs have been successfully synthesized and this work investigates two of them. The first IL is the quite well-researched EmiFSI which is based on imidazolium, the cation present in many of the first ILs to be considered as electrolytes for LIBs [13, 16]. EmiFSI has a relatively low viscosity compared to other ILs [17] and have shown promising results with Si anodes [11, 18]. The second IL is the less investigated P_{111i4}FSI that has received attention in more recent years [19].

The choice of electrolyte salt has a large effect on the performance of an electrolyte. This thesis focuses on two salts, LiFSI and LiTFSI. LiFSI is less prone to hydrolysis and subsequent HF formation compared to the standard electrolyte salt, $LiPF_6$, and has shown that it can improve the performance of Si anodes in carbonate-based electrolytes [20]. LiFSI has also been tested with ILs and Si anodes, showing a stable reversible capacity of $\sim$2500 mAh/g at a rate of C/10 in EmiFSI [18] and an impressive capacity of $\sim$3000 mAh/g after 300 cycles at a rate of C/2.5 in P_{111i4}FSI [21].

LiTFSI is significantly cheaper compared to LiFSI and as long as it can yield similar or improved electrolyte performance, it would be the preferred alternative. LiTFSI is a larger salt than LiFSI and has stronger interactions between Li^+ and the anion [22]. Both of these effects contribute to a trend of increased viscosity in electrolytes with LiTFSI, where an increased viscosity usually is synonymous with worse ion transport properties [16]. On the other hand, LiTFSI is chemically [23] and thermally [24, 25] more stable than LiFSI. Further, it appears that LiTFSI in P_{111i4}FSI is a combination that has never previously been tested. In EmiFSI, LiTFSI has never been used with a pure Si anode, only with a Si-Ni-C composite [26].

A major disadvantage of IL electrolytes is their high viscosity compared to carbonate electrolytes [20, 27]. Attempts at tackling this challenge have been made by using carbonates as a cosolvent in IL electrolytes [28], but as even the co-presence of carbonates can make the cell vulnerable to safety issues [29], this solution is sub-optimal when it comes to electrolyte flammability. Using flame retardants as electrolytes or cosolvents has received attention in recent years [30] and this work tests a hydrofluoroether, TMMP, and a phosphate-based flame retardant, TEP.

Adding a small amount of a chemical is an effective and commonly used tactic to improve certain aspects of battery cell performance, in particular to promote a certain SEI formation [25]. FEC is one of the most studied additives for Si anodes in carbonate-based electrolytes for LIBs [31] and promotes the formation of a more ionically conductive SEI layer [32]. Although

only a minor research effort has so far been devoted to the investigation of additives for IL electrolytes, it has been shown that FEC can be preferentially reduced instead of the IL or the salt in an EmiTFSI-based electrolyte [33], making it a possible additive also for EmiFSI-based electrolytes.

1.2 Aim of this work

The overall aim of this work was to improve the performance and understanding of Si anodes in combination with ILs for LIBs. The approach was threefold and included (1) changing the electrolyte salt, (2) adding a cosolvent, and (3) adding an SEI-forming additive. The overall project goal can be divided into three subgoals:

1. Evaluate the effects that two different electrolyte salts, LiFSI and LiTFSI, have on cycling stability, rate performance, electrolyte decomposition, and ionic conductivity of battery cells with two different ILs, EmiFSI and P_{111i4}FSI. The SEI formation will be characterized by means of X-ray photoelectron spectroscopy (XPS) and related to electrochemical performance of the cells to further understand the differences between the two salts.
2. Assess the use of TEP and TMMP as possible cosolvents for EmiFSI by mixing electrolytes with different ratios of EmiFSI and TEP/TMMP and examining the effects on cycling stability, rate performance, electrolyte decomposition, and ionic conductivity of the cells.
3. Evaluate FEC as a potential additive to EmiFSI electrolytes with and without a cosolvent by investigating cycling stability, rate performance, and electrolyte decomposition of cells where FEC has been added to the electrolyte.

In this work, pseudo full cells with screen printed Si anodes from the Institute for Energy Technology (IFE) and capacitively oversized $LiFePO_4$ (LFP) cathodes from Customcells Itzeheo GmbH are used. The results from this thesis will hopefully broaden the understanding of IL-based electrolytes together with Si anodes and be a small contribution in achieving the implementation of safer and higher-capacity LIBs to promote a more electrified and greener future.

Chapter 2

Theory

2.1 Fundamentals of a Li-ion battery

2.1.1 Working principle

As an introduction to the theory behind LIBs, this first section will cover their basic working principle. Both this section, as well as the following, Section 2.1.2, are, unless otherwise stated, based on the book "*Lithium Batteries*" by Julien, Mauger, Vijh, and Zaghib [34] and the 2013 article "*The Li-ion rechargeable Battery: A perspective*" [35] by Goodenough and Park.

A battery is a collection of one or more interconnected electrochemical cells. An electrochemical cell is a system that can convert chemical energy into electrical energy via spontaneous chemical reactions or force non-spontaneous chemical reactions to occur using electrical energy. There are three essential components in an electrochemical cell; two *electrodes*, namely the anode and the cathode, and an *electrolyte*. In the case of the LIB, the electrodes store Li-ions and the electrolyte transports Li-ions between the two electrodes.

Batteries are categorized as primary or secondary batteries depending on their ability to readily be recharged. The LIB is rechargeable and is therefore a secondary battery. An illustration of the first LIB, as commercialized by Sony in 1991, is shown in Figure 2.1. This original setup will be used to further explain the working principles of the LIB.

Initially, some additional components should be introduced. Firstly, a thin *separator* is sandwiched between the anode and the cathode. Its electrically insulating properties prevent a short circuit between the electrodes while its porosity allows the transport of Li-ions back and forth in the electrolyte. Secondly, both the anode and the cathode are directly connected to metal foils called *current collectors*. The current collectors, illustrated as blue and red boxes in Figure 2.1, ensure that there is sufficient electrical contact between the *external electrical circuit* and the *active material* of the electrodes. In the first LIB, graphite was used as active material in the anode and $LiCoO_2$ was used in the cathode. Electrode materials will be extensively discussed in Section 2.2.

Strictly speaking, the cathode in an electrochemical cell is the electrode where the reduction reaction occurs and the anode is the electrode hosting the oxidation reaction. For secondary batteries, however, both electrodes host both oxidation and reduction reactions, as the reactions switch position between *charging* and *discharging* the battery. The usual convention is to assign labels based on the *discharge process*, i.e. the cathode is the positive

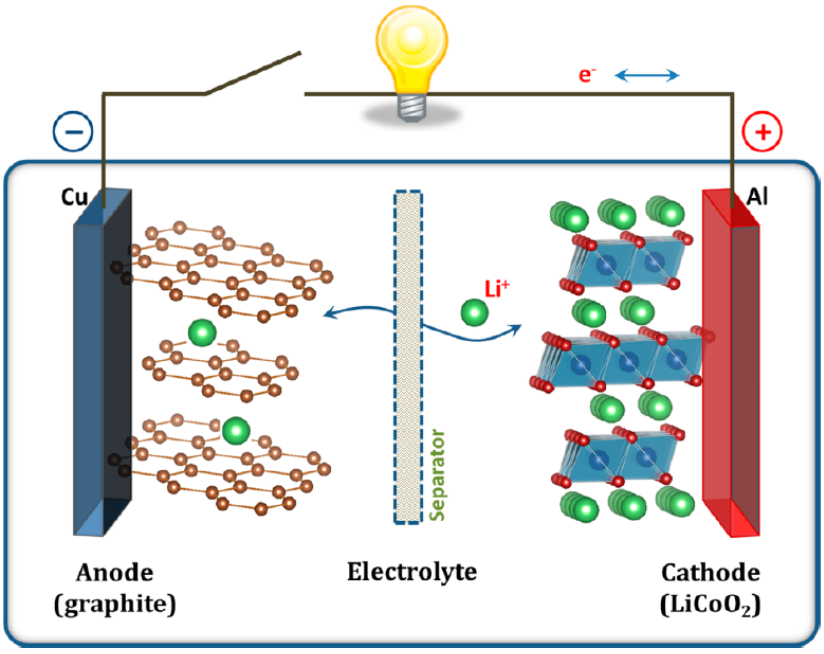

Figure 2.1: A schematic illustration of the first LIB consisting of a $LiCoO_2$ cathode and a graphite anode. Adapted from [35].

electrode where reduction reactions occurs during discharging and the anode is the negative electrode where oxidation occurs during discharging. This convention will be used throughout the report.

A LIB cell transforms energy through reduction and oxidation (redox) reactions facilitated by the reversible intercalation of Li-ions in the electrodes. When charging the cell, an external voltage is applied causing Li in the cathode to oxidize and to go into the electrolyte as positively charged Li-ions, according to the following reaction:

$$\mathrm{LiCoO_2} \rightleftharpoons \mathrm{Li_{1-x}CoO_2} + x\,\mathrm{Li^+} + x\mathrm{e^-}. \tag{2.1}$$

At the same time, Li-ions from the electrolyte are reduced at the anode:

$$x\,\mathrm{Li^+} + x\mathrm{e^-} + 6\,\mathrm{C} \rightleftharpoons \mathrm{Li}_x\mathrm{C}_6. \tag{2.2}$$

The top arrow in Equations (2.1) and (2.2) represents charging and the bottom arrow represents discharging of the cell.

Continuing on the description of the charging process, whereas electrons from the oxidation reaction at the cathode travel in the external circuit towards the anode, Li-ions are solvated by constituents of the electrolyte and move in the electrolyte, through the porous separator, and towards the anode. Here, the Li-ions are ideally desolvated from the electrolyte constituents, transported through possible surface layers (electrical double layer and/or SEI, which will be described in detail in Section 2.3), and are lastly incorporated into the anode where a reduction reaction happens. The incorporation of Li-ions in an electrode is called *lithiation*, while *delithiation* describes extracting ions from an electrode. When discharging, Li stored in the anode takes part in an oxidation reaction and the resulting Li-ions are transported

through surface layers, solvated in the electrolyte, and move through the separator and to the cathode.

Lithiation of the anode causes an *increase* in the electrochemical potential of the electrode. Conversely, delithiation causes a *decrease* in the electrochemical potential. The electrochemical potential is a thermodynamic measure that combines the concepts of energy stored in the form of chemical potential and electrostatics. Upon discharging, the difference in the electrochemical potential of electrons in the anode and the cathode is utilized to perform work as the electrons travel through the external circuit. The difference in the electrochemical potential, measured when no current is flowing, is the open-circuit potential, V_{oc}. However, when a current $I \neq 0$ flows, an extra voltage drop is caused by internal resistances in the cell, $R_{\mathrm{i}}(I)$. The internal resistance is a sum of contributions from: (1) resistance related to the transfer of charge across the electrolyte-electrode interphase and the electrode-current collector interphase, (2) intrinsic resistance of the electrodes, and (3) the electrolyte resistance to the ionic current. The voltage drop is called an overpotential and results in a decreased cell potential during discharging (V_{dis}) and an increased cell potential curing charging (V_{ch}):

$$V_{dis} = V_{oc} - IR_i(I) \tag{2.3}$$

$$V_{ch} = V_{oc} + IR_i(I). \tag{2.4}$$

Plotting electrical impedance spectroscopy (EIS) measurements in a Nyquist plot is a commonly used technique to determine properties of an electrochemical system. The intersection of the graph with the x-axis provides a measure of the high-frequency resistances in the cell, R_{HF}, which at this position can be assumed to be dominated by the electrolyte resistance, R_{el}. R_{el} can be related to the conductivity of the electrolyte, σ_{el}, but in a battery, the presence of the separator will alter this relationship. The relationship between R_{HF}, R_{el} and σ_{el} in a separator with porosity ϵ and tortuosity τ is [36]:

$$R_{HF} \approx R_{el} = \frac{d\tau}{\sigma_{el} A \epsilon}, \tag{2.5}$$

where d is the thickness of the separator and A is the area across which the ionic current is transferred. As d, A, τ, and ϵ can be assumed to be identical for cells where the only difference is the electrolyte, a comparison of R_{HF} allows for a qualitative comparison of ionic conductivities of the different electrolytes.

2.1.2 Physical terms and definitions

Some terms and definitions will be used frequently in this report. These are now introduced and discussed.

1. **Electrochemical potential (μ):** The change in Gibb's free energy (G) when the amount (m) of species i is changed:

   $$\mu_i = \frac{\partial G}{\partial m}. \tag{2.6}$$

   The electrochemical potential can also be expressed as:

   $$\mu_i = \mu_i^o + RT \ln(a_i) + z_i F \phi_i, \tag{2.7}$$

where μ_i^o is the standard chemical potential, R is the gas constant, T is temperature, a_i is the activity, z_i is the charge, F is Faraday's constant, and ϕ_i is the potential experienced by species i.

2. **Capacity (Q)**: The capacity of a given electrode represents the amount of charge it can store when charged with a current I:

$$Q(I) = \int_0^{\Delta t} I dt = \int_0^Q dq. \tag{2.8}$$

3. **Specific capacity (Q_{th}):** The capacity per mass of active material (Ah g^{-1}). This theoretical value is found using Faraday's law:

$$Q_{th} = \frac{1000 \times nF}{3600 \times M_W}, \tag{2.9}$$

where n denotes the number of electrons transferred in the reaction and M_W is the molar mass.

4. **Open-circuit potential (V_{oc}):** The potential between the anode and the cathode when no current is drawn, given by:

$$V_{oc} = V_{cathode} - V_{anode} = \frac{\Delta \mu_{e^-}}{z_{e^-} F} = \frac{\Delta G}{nF}. \tag{2.10}$$

5. **Energy:** The energy contained in a LIB is given by:

$$\text{Energy} = \int_0^Q V(q) dq, \tag{2.11}$$

where a charge dq is transferred between two electrodes with a potential difference of $V(q)$. The energy content is expressed in Wh. The gravimetric energy density (Wh g^{-1}) and volumetric energy density (Wh L^{-1}) are especially important. Equation (2.11) illustrates that both the capacity Q and the potential difference between the electrodes are important to maximize the energy content of the battery.

6. **Power:** The energy output of the cell per unit time, given in W:

$$\text{Power} = \frac{\text{Energy}}{\text{Time}}. \tag{2.12}$$

7. **State of charge (SOC):** The ratio of the charge currently stored in the battery (Q_e) to the battery's initial capacity (Q_o), given in %:

$$\text{SOC} = 100\% \times \frac{Q_e}{Q_o}. \tag{2.13}$$

8. **Overpotential (η):** When the cell is charged or discharged with a current I, a deviation from the open-circuit potential occurs due to the cell's internal resistance R_i, representing a voltage drop $\eta = IR_i(I)$. η is dependent on multiple factors, including SOC and I. The overpotential is also known as *polarization* or *overvoltage*.

9. **Coulombic efficiency (CE):** The ratio (in %) of the amount of charge extracted upon discharging (Q_{dis}) to the amount of charge inserted during charging (Q_{ch}) of the same cycle:
$$\mathrm{CE} = 100\% \times \frac{Q_{dis}}{Q_{ch}}. \tag{2.14}$$
A deviation from CE = 100% results in an irreversible capacity loss (ICL):
$$\mathrm{ICL} = Q_{ch} - Q_{dis}. \tag{2.15}$$

10. **C-rate:** A parameter that indicates the current needed to fully charge a battery in an hour. For a battery with a 1000 mAh capacity, $1C$ equals 1000 mA and $C/5$ equals 200 mA.

11. **Rate performance:** Describes how well a battery cell manages to maintain its capacity when subject to higher (dis)charging rates.

12. **Loading:** Describes the amount of electrode material deposited per area on the current collectors, either in terms of mass (mg/cm^2) or capacity (mAh/cm^2).

13. **Cycling stability:** Describes the ability of a battery system to maintain its original level of electrochemical performance upon consecutive cycles of charging and discharging, especially concerning the stability of the system's capacity. Cycling stability is closely related to the Coulombic efficiency.

14. **Lithiation and delithiation:** The terms *lithiation* and *delithiation* are sometimes preferred over the more ambiguous *charging* and *discharging*. This is due to the extensive use of Li metal half cells in battery research, where anode and cathode materials are separately tested versus a Li metal electrode. As both anode and cathode materials behave as a cathode relative to a Li metal electrode, some confusion can occur. Normally, charging involves *lithiation* of the anode, whereas in a half cell the anode will be *delithiated* during charging. However, as only full cells are used in this work, the two sets of terms can and will be used interchangeably.

2.2 Electrodes

2.2.1 Introduction to electrode materials

Electrode materials are and have been a key area of battery research for a long time and numerous material alternatives therefore exist today [37]. When speaking of electrode materials, one usually means the *active material*, but an electrode is not a solid block of a single material. In general, it is rather a mix of several components that play different roles in the electrode [34, 38]:

1. The *active material* is the electrochemically active component that takes part in the storage of Li-ions. It usually exists as micro- or nanoscale particles in order to facilitate a uniform lithiation of the entire volume of the active material.
2. An *electron-conducting additive* is added to improve the electrical conductivity between the individual particles of active material. In most cases, carbon black is used.

3. A *binder*, for instance *polyvinylidene fluoride*, is added to "glue" the particles of active material to each other as well as to the current collector.
4. Optionally, small amounts of certain *additive chemicals* can be added to tailor the performance of the electrode.

These electrode constituents are in direct contact with the current collector. Cu is used as current collector on the anode side and Al is used on the cathode side. The different choice of metals is based on the fact that Cu, unlike Al, does not significantly alloy with Li when exposed to the low potentials at the anode. Further, Cu dissolution at higher potentials prevents its use at the cathode, while Al can be used due to its ability to form passivating layers at higher potentials [39].

The remaining part of this section will focus on the active material of the electrodes. Inspired by a 2014 review paper "*Review on recent progress of nanostructured anode materials for Li-ion batteries*" written by Goriparti et al. [40], the following list of desired properties of active materials for LIBs can be compiled:

1. High reversible specific capacity
2. High rate of lithium diffusion
3. High electrical conductivity
4. High safety
5. Low cost
6. Low toxicity
7. Long cycle and calendar life

The *energy content* of a LIB is dependent on both the *capacity* and the *voltage* of the battery, as seen from Equation (2.11). Therefore, finding high-capacity electrode materials with a sufficient voltage difference is needed to create LIBs with a high energy content. The specific capacity and voltage (V vs Li/Li^+) of some of the most common classes of active materials are displayed in Figure 2.2.

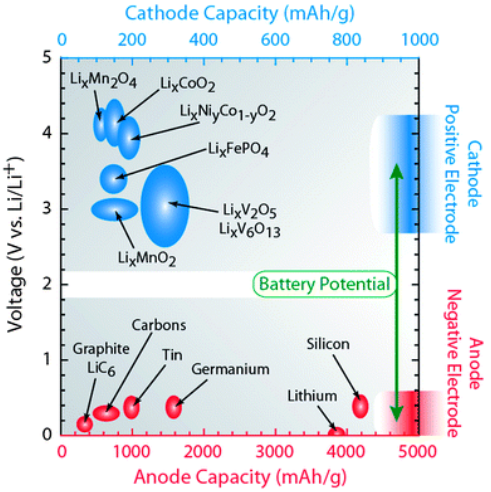

Figure 2.2: A diagram showing the specific capacity and voltage (V vs Li/Li^+) for some of the most common electrode materials. Adapted from [37].

Firstly, the focus will be the voltage of the battery, i.e. the potential difference between the two electrodes. Figure 2.2 shows that most anode materials lie quite close to the lower limit of 0 V vs Li/Li^+. This means that an improvement in the battery voltage must come from higher-voltage cathode materials. An absolute upper voltage limit does not exist, however issues with corrosion of cathode components [41] and decomposition of electrolyte constituents [35] nevertheless put some restrictions on how high the cathode voltage can be. A continuous electrolyte decomposition is usually avoided as the decomposition products can form a passivation layer on the electrode, limiting further decomposition. Such a passivating layer that kinetically stabilizes the electrode is called a SEI layer and will be extensively discussed in Section 2.3.

Now, capacity will be considered. Figure 2.2 shows that there is a substantial difference between the specific capacities of anode and cathode materials. Whereas most cathode materials have specific capacities ranging from 120 to 270 mAh/g [42, 43], some anode materials can achieve several thousand mAh/g. The commonly used graphite anode has a theoretical specific capacity of 372 mAh/g and one of the most promising alternatives, silicon, has a theoretical value of 3579 mAh/g, almost ten times as high as that of graphite [7].

The overall specific capacity of a battery is of course dependent on the specific capacity of *both* the anode and the cathode, as well as "dead weight" from other components such as external circuitry and the electrolyte. The specific capacity of a battery, when considering only the mass of the two active materials, is given by [44]:

$$\text{Specific capacity of a battery} = \frac{Q_\text{A} Q_\text{C}}{Q_\text{A} + Q_\text{C}}, \tag{2.16}$$

where Q_A and Q_C are specific capacities for the anode and the cathode active materials, respectively.

In order to visualize the effect of changing the anode material from graphite to Si, Equation (2.16) is plotted with a constant cathode specific capacity $Q_C = 131$ mAh/g in Figure 2.3. The plot shows how increasing the specific capacity of just the anode by a factor of ten only has a limited effect on the overall specific capacity of the battery, as long as the cathode remains unchanged. This illustrates the importance of improving *both* electrodes simultaneously.

Categories of electrode materials

Based on their mechanism of storing Li-ions, electrode active materials can be divided into three categories: intercalation electrodes, conversion electrodes, and alloying electrodes [37].

Intercalation electrodes have a crystal structure that allows for diffusion and storage of Li-ions in its interstitial sites. As ions are incorporated without breaking the crystal structure of the host, no chemical bonds are broken during (de)lithiation [45]. The diffusion pathway of the ions depends on the crystal structure of the host and can be in one, two, or three dimensions. Figure 2.4 shows the crystal structure and an example material of three common intercalation electrodes as well as their dimensionality of ion transport. The graphite and $LiCoO_2$ electrodes in the original LIB, as illustrated in Figure 2.1, are both intercalation electrodes with a layered crystal structure. Intercalation electrodes usually show great cycling stability, but are often limited by moderate Li storage capacities [37].

The second category of electrode materials, conversion electrodes, utilize a reversible chemical reaction with a Li transition metal oxide [46]. The conversion reaction is [37]:

$$\mathrm{M}_a\mathrm{X}_b + (bn)\mathrm{Li} \rightleftharpoons a\mathrm{M} + b\mathrm{Li}_n\mathrm{X}, \tag{2.17}$$

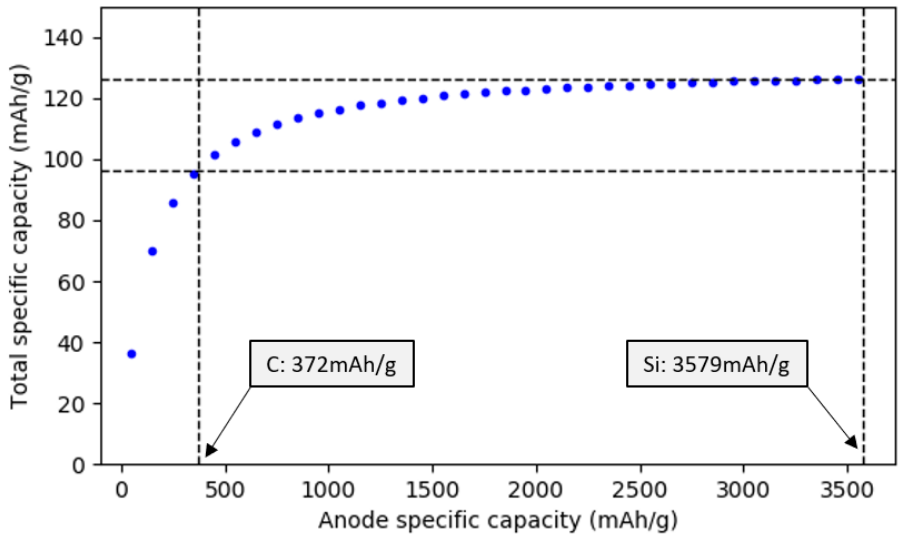

Figure 2.3: A plot of Equation (2.16) with a fixed cathode capacity of $Q_C = 131$ mAh/g. Specific capacity values for graphite and Si and the resulting total specific capacities are indicated.

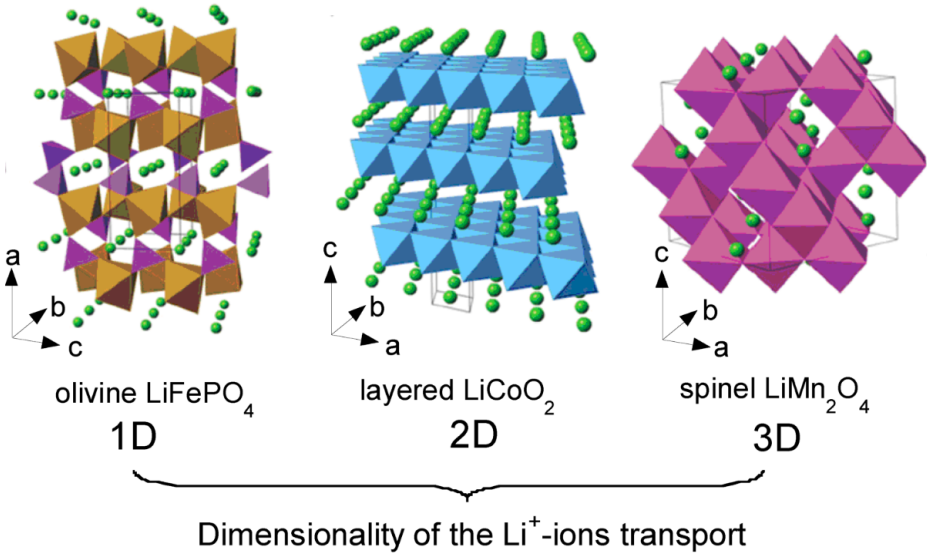

Figure 2.4: Crystal structure, dimensionality of Li-ion transport, and an example material of three common types of intercalation electrodes: olivine, layered, and spinel. Adapted from [43].

where M = transition metal, X = anion, and n is the formal oxidation state of X. Conversion electrodes for LIBs are currently only in a research stage and further understanding of fundamental characteristics and work on electrode design is required before a possible commercialization can happen [37].

The last category of electrode materials, alloying materials, has been extensively researched for more than three decades [34]. An alloying electrode relies on lithium metal alloys Li_xM_y (M = Al, Sb, Si, Sn, etc.) where Li-ions can reversibly form an alloy with the electrode material. Alloying electrodes can display impressively high specific capacities of several thousand mAh/g, but are usually accompanied by a massive volume change during (de)lithiation. This volume change causes mechanical degradation of the electrode and results in poor cycling stability [35].

2.2.2 Cathode materials

This thesis is mostly concerned with Si anodes and the effect of additives, cosolvents and two different electrolyte salts on the performance of ionic liquids. Cathodes are therefore of secondary importance. However, as a full cell setup with a Si anode and an LFP cathode is used in this work, a brief introduction to cathode materials and a consideration of some relevant aspects of the LFP chemistry seems appropriate.

A wide variety of cathode materials have been studied and commercialized following the initial $LiCoO_2$ cathode. These include, among others, phosphates such as LFP and various transition metal oxides, including $LiMn_2O_4$, $LiNiCoAlO_2$, and $LiNiMnCoO_2$ [2, 43]. Both the original $LiCoO_2$ cathode and most alternatives since contain cobalt, as cobalt has some unique properties beneficial for its use in cathodes [47]. However, a massive research effort is currently being made to develop cathodes where the cobalt content is reduced or even removed entirely, as the supply chain may have trouble in keeping up with future demand [47] as well as its link to child labor in the Democratic Republic of Congo [48].

LFP is a promising cathode material that does not contain any cobalt. It has a decent theoretical specific capacity of 170 mAh/g and has already been commercialized and put to use in the automotive industry [42]. Lithiation of LFP proceeds via a two-phase process [49, 50]. The Gibb's free energy composition diagram of Li_xFePO_4 for $0 \leq x \leq 1$ has two distinct energy minima corresponding to the composition of these two phases; a Li-rich and a Li-poor phase. These two minima promote phase separation into the corresponding phases at intermediate values of x, resulting in a constant $\frac{\partial G}{\partial x}$. A constant $\frac{\partial G}{\partial x}$ implies a constant open-circuit potential, as seen from Equation (2.10). This constant-voltage plateau occurs at 3.45 V vs Li/Li^+ [51] for $0.1 < x < 0.8$ and can be seen in Figure 2.5.

When testing full cells, as done in this thesis, it is usually impossible to determine if a feature in the voltage profile should be attributed to the anode or the cathode, at least unless a three-electrode setup is used. However, the voltage plateau of LFP allows for changes in the voltage profile to be assigned to the anode, at least for intermediate compositions. To extract the potential at the anode from the cell voltage, disregarding overpotentials, the following conversion can be used:

$$\text{Potential at anode (V vs } Li/Li^+) = 3.45 \text{ V vs } Li/Li^+ - \text{Cell voltage (V)}. \tag{2.18}$$

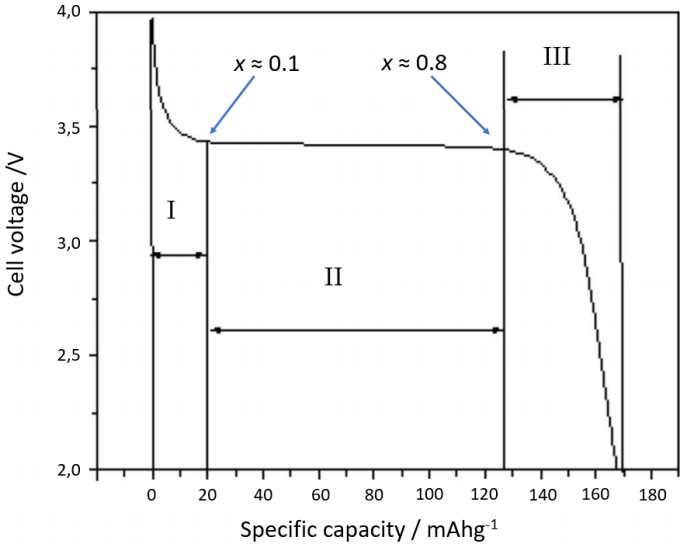

Figure 2.5: The voltage profile of an Li_xFePO_4 cathode versus Li metal showing a voltage plateau at 3.45 V vs Li/Li^+ (region II) for intermediate values of x. Adapted from [49].

2.2.3 Introduction to anode materials

Graphite has been the anode material of choice in most LIBs since its commercialization three decades ago. This is based on graphite showing many of the desired properties of a good active material, including high lithium (de)intercalation reversibility, sufficient availability, and stability in chemical, electrochemical, and thermal environments [40]. However, graphite has a theoretical specific and volumetric capacity of 372 mAh/g and 833 mAh/cm^3 [52], respectively, and alternative higher-capacity anode materials are highly requested to increase the energy density of future LIBs, of course in parallel with improvements to the cathode as well.

The 2014 review by Goriparti et al. [40] lists several materials that are being researched, along with their advantages and disadvantages. Some of these materials are also shown in Figure 2.2. In the category of *intercalation electrodes*, carbon-based materials beyond graphite is an alternative. These include carbon nanotubes, graphene and "hard carbons". Here, advantages of high safety and low operating potentials are weighed down by high costs, a low Coulombic efficiency and a high voltage hysteresis. Further, the various *conversion materials*, such as metal oxides (Fe_2O_3, Mn_xO_y, etc.) and metal phosphides/sulfides/nitrides (MX_y; M = Fe, Mn, Ni, Cu, etc. and X = P, S, N) show improved capacities compared to graphite and good environmental compatibility. These are, however, in a research stage and still show low Coulombic efficiency and unstable SEI formation. Lastly, *alloying materials*, including Si, Ge and Sn, exhibit very high capacities, but suffer from a large irreversible capacity and poor cycling stability.

A fourth "category" of anode material exists, namely pure Li metal. The theoretical specific capacity of Li metal is an impressive 3860 mAh/g [52] and it is therefore a natural choice as anode material. Indeed, Li metal has been continuously researched for 40 years and realizing such an anode would be a massive improvement compared to graphite. There are, however, two main challenges hindering the implementation of Li metal anodes, namely

dendrite formation and a low Coulombic efficiency [53], the former of posing a serious safety hazard if a short circuit between the anode and cathode is formed.

The following section will discuss the anode material in question in this thesis; silicon.

2.2.4 Silicon as anode material

Si is deemed one of the most promising anode materials to replace graphite in future higher-capacity LIBs [10, 40, 44]. Some of its advantages include:

1. Very high theoretical capacity
2. Low toxicity
3. High safety
4. Abundance
5. Low cost

The Si anode is an alloying electrode and thus relies on the Li_xSi alloy to be formed during charging and for it to subsequently de-alloy and release Li upon discharging. Si has one of the highest reported theoretical capacities, both specific and gravimetric, of all anode materials. Some claim that the specific capacity of Si is 4212 mAh/g for $Li_{4.4}Si$ [40], but others disagree and state that $Li_{4.4}Si$ is not the final phase at room temperature and that the true value is 3579 mAh/g, corresponding to $Li_{3.75}Si$ [54]. Phases with $x \geq 3.75$ are crystalline [55] and experience a less reversible delithiation compared to their slightly less lithiated amorphous counterparts, making them less relevant for battery applications. One might therefore argue that the actual specific capacity is somewhat lower than 3579 mAh/g. Either way, the theoretical capacity is very high compared both to graphite as well as most other potential replacement materials.

There are, however, some important disadvantages to using Si as the anode material which have so far hindered the commercialization of a pure Si anode. As previously mentioned, alloying electrodes are usually accompanied by a large volume expansion upon lithiation. Si is not an exception to this as it experiences a >300% volume expansion upon lithiation [10]. This expansion may result in the Si particles fracturing which can cause electrical isolation of the active material [9]. In addition, the SEI layer easily cracks as it is not mechanically stable enough to withstand the expansion of the Si particles. The necessity of a stable SEI-layer will be discussed in Section 2.3. Furthermore, Si is a semiconductor and has a low electrical conductivity at room temperature of $< 10^{-2}$ S/cm (depending on doping level) compared to graphite, which is in the range of 10^1-10^4 S/cm [56].

Fortunately, there are certain techniques that can be applied in order to overcome the above-mentioned drawbacks. Starting with the last issue; the electrical conductivity can be improved by incorporating conductive additives or coatings in the electrode [56].

Regarding the expansion issues, the perhaps most simple solution would be to not fully lithiate the Si particles, but to rather stop at for instance 50% of the maximum capacity. This would reduce the degree of swelling experienced by the particles and thus mitigate some of the issues related to expansion. As can be seen from Figure 2.3, a utilization of 50% instead of 100% of the Si anode capacity only results in a minor reduction of the total battery capacity, as long as the cathode capacity remains low. Although this solution can be readily implemented, there will still be expansion of the Si particles and some degradation and excess SEI growth will happen. It is therefore desirable to find a better solution than this.

Several innovative attempts are being made at tackling the expansion problems of Si with regards to design of the electrode and the active materials. These include: **(1)** nanostructuring the Si [40, 57], e.g. nanotubes, nanowires, and nanospheres, **(2)** creating porous (nano)structures [58, 59], **(3)** utilizing (nano)composite materials of for instance Si and graphite [7, 44], **(4)** using novel binder materials [60, 61], and **(5)** adding a protective coating of carbon, inorganic layers, or conductive polymers onto the Si particles [62].

Lithiation mechanism of Si

Ogata et al. [55] investigated the (de)lithiation mechanism of Si nanowires using *in situ* Li nuclear magnetic resonance (NMR) spectroscopy, *ex situ* X-ray diffraction (XRD), *ex situ* magic angle spinning NMR spectroscopy, and density functional theory (DFT). Their proposed (de)lithiation mechanisms are presented in Table 2.1.

The first cycle starts with lithiation of crystalline Si, as a Si anode is usually initially crystalline, and occurs via a two-phase mechanism in which Si is consumed to form highly lithiated amorphous Li_xSi with $x = 3.4 \pm 0.2$ [63, 64]. The amorphous phase is so highly lithiated because a very high concentration of Li atoms is needed at the interface to break the strong crystalline Si matrix [65]. Further lithiation generates crystalline $Li_{3.75}Si$ and possibly over-lithiated phases with $x \geq 3.75$. Upon delithiation, amorphous Si is created. Subsequent lithiation processes have amorphous Si as their starting point and therefore proceed differently than the first lithiation process.

Table 2.1: Experimentally observed (de)lithiation mechanism of Si nanowires as described by Ogata et al. [55]. Amorphous and crystalline phases are marked with *a* and *c*, respectively. $Li_{3.75+\delta}Si$ is an over-lithiated phase with δ in the range of 0.2 to 0.3.

Process/stage	Potential (V vs Li/Li^+)	Reaction
1st Lithiation		
1	0.10	c-Si $\rightarrow$ a-Li_xSi $\rightarrow$ c-$Li_{3.75}Si$ $\rightarrow$ c-$Li_{3.75+\delta}Si$
$\geq$ 2nd Lithiation		
2	0.30-0.25	a-Si $\rightarrow$ a-$Li_{2.0}Si$
3	0.10	a-$Li_{2.0}Si$ $\rightarrow$ a-$Li_{3.5}Si$
4	0.05-0.06	a-$Li_{3.75}Si$ $\rightarrow$ c-$Li_{3.75}Si$
5	0.03	c-$Li_{3.75}Si$ $\rightarrow$ c-$Li_{3.75+\delta}Si$
Delithiation		
1	0.05-0.15	c-$Li_{3.75+\delta}Si$ $\rightarrow$ c-$Li_{3.75}Si$ + c-$Li_{3.75-\delta}Si$
2	0.27-0.30	a-$Li_{3.5}Si$ $\rightarrow$ a-$Li_{2.0}Si$
3	0.43	c-$Li_{3.75}Si$ $\rightarrow$ a-$Li_{1.1}Si$
4	0.50	a-$Li_{2.0}Si$ $\rightarrow$ a-Si

2.3 SEI layer

2.3.1 A general discussion on the SEI layer

The SEI layer is considered to be "*the most important, but least understood component in rechargeable Li-ion batteries*" [66]. The concept of SEI was first introduced by Peled in 1979 [67]. The SEI layer is only a few nanometers thick and is a complicated, multi-component, porous structure comprised of various decomposition products of the electrolyte, making the attempts of understanding it challenging [10, 32, 66, 68].

Taking a step back; in order for an electrolyte to be thermodynamically stable, i.e. not spontaneously decompose, the electrochemical potentials at the electrodes must lie within the so-called *window of stability*, E_g, of the electrolyte. This means that the lowest unoccupied molecular orbital (LUMO) of the electrolyte must be positioned above the electrochemical potential of the anode, μ_A, and the highest occupied molecular orbital (HOMO) must lie below μ_C. Here, "electrolyte" includes all components of the electrolyte, i.e. the main solvent, salt, various additives and even impurities [32]. The electrolyte and its components will be discussed in Section 2.4.

An energy diagram illustrating a stable electrolyte window is shown in Figure 2.6. If the electrochemical potential of an electrode lies outside of E_g, the electrolyte will decompose on that electrode. This is indeed the case for most anode materials as well as for some cathode materials [34, 69]. However, as previously mentioned, a continuous electrolyte decomposition is usually avoided as the decomposition products can form a passivation layer on the electrode, the SEI layer, limiting further decomposition.

The SEI layer is primarily a feature of the anode, but cathodic SEI layers have also been reported for some materials, like $LiMn_2O_4$ and $LiCoO_2$ [69]. This work, however, will only focus on anodic SEI layers.

When charging the battery, the electrochemical potential μ_A increases and when it surpasses the LUMO of an electrolyte component, electrons from the anode will electrochemically reduce that component. Competing reduction processes of the various electrolyte components

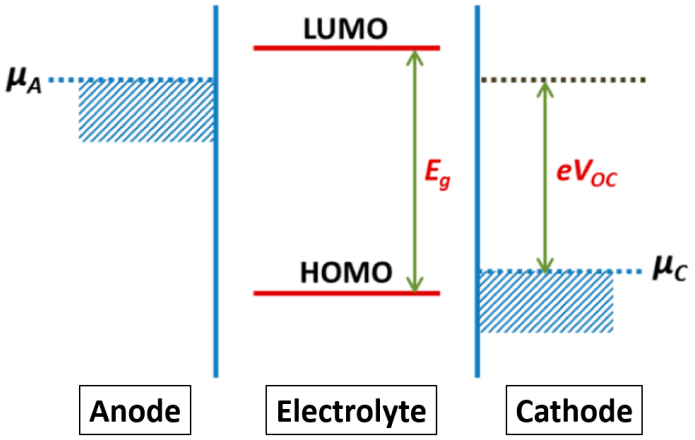

Figure 2.6: Schematic energy diagram of a stable electrolyte window, E_g, and the electrochemical potential at the electrodes. Adapted from [35].

lead to the formation of numerous organic and inorganic decomposition products at the surface of the anode. The decomposition of a standard organic solvent usually generates insoluble components like Li_2CO_3 and partially soluble semicarbonates and polymers, while the reduction of typical salt anions generally form insoluble components like LiF, LiCl, and Li_2O [32]. An example of a possible SEI layer that could form on a graphite or Li metal anode upon the reduction of a standard organic electrolyte is shown in Figure 2.7. This typical SEI structure includes a dense inner layer comprised mostly of inorganic compounds and an outer, more porous layer of mainly organic decomposition products.

A good SEI layer is electrically insulating, hence its ability to prevent further electrolyte decomposition by blocking electrons in the anode from reaching the electrolyte, i.e. kinetically stabilizing the electrode. The formation of the SEI layer therefore occurs mainly during the first charging cycle and to a certain degree also in the following cycles. The formation of the SEI layer is directly associated with an irreversible capacity loss as many of the decomposition products contain Li, thereby consuming some of the "active Li" available in the cell. Still, this irreversible capacity loss is a "necessary evil" as the formation of the SEI layer is crucial to attain a satisfactory cycling stability of the LIB.

Wang, Kadam, Li, Shi, and Qi state in their 2018 review article "*Review on modeling of the anode solid electrolyte interphase (SEI) for lithium-ion batteries*" [66] that two major challenges hinder a controlled design of the SEI layer. Firstly, the structure-property relationships of the SEI layer are mostly unknown. Secondly, the details of the electrolyte decomposition reactions near the electrode surface are unclear. The effect of these two challenges is that the design process of the SEI layer is always based on trial-and-error.

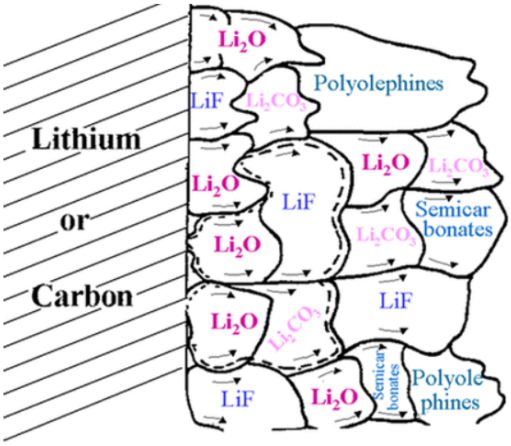

Figure 2.7: An example of the SEI structure that could form on graphite or Li metal when using a standard organic electrolyte. Adapted from [32].

2.3.2 SEI on silicon anodes

In comparison to the SEI layer that forms on the traditional graphite anode, SEI on Si is subjected to the massive expansion of the underlying Si particles upon lithiation. The SEI layer generally cannot withstand the mechanical stress and will break open [9]. This exposes fresh Si underneath and electrolyte decomposition will then occur, filling the cracks in the SEI layer. This process is illustrated in Figure 2.8.

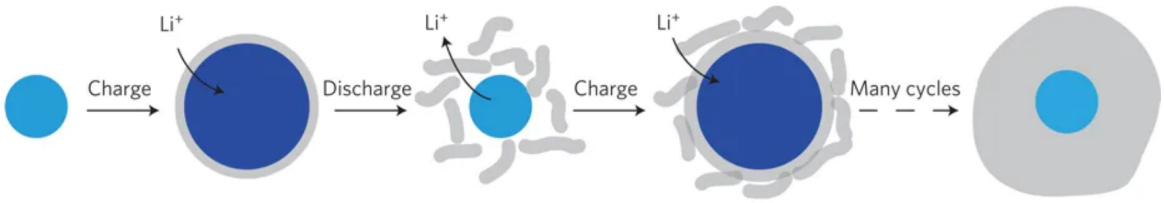

Figure 2.8: A sketch showing the formation of the initial SEI layer upon lithiation of Si, followed by consecutive breaking and reformation during later cycles, creating a thick SEI layer. Adapted from [57].

A thick SEI layer forming on Si is related to an *irreversible* capacity loss as active Li is consumed in its formation, in addition to a *reversible* capacity loss, as the increased overpotential related to a thicker SEI layer prevents some of the available capacity to be realized when a (de)lithiation current $I > 0$ is used. In addition to all the previously mentioned electrode-related attempts to tackle the expansion problems of Si, some try to find a solution by targeting the SEI layer itself. These attempts include adding electrolyte additives that are known to create a more stable and/or flexible SEI layer [70, 71] and testing novel electrolyte solvents [18]. These attempts will be further explained in Section 2.4.

The constituents of the SEI layer are closely related to the contents of the electrolyte, however some general trends exist when Si is used as the anode material. The surface of Si is normally covered by a native SiO_2 layer [70]. Philippe et al. [72] investigated Si nanoparticles in $LiPF_6$/ethylene carbonate (EC)-based electrolytes using both hard and soft XPS. They found that the inner part of the SEI layer to a large degree was dominated by the conversion of the native oxide layer to Li_xSiO_y, while the outer region of the SEI was similar to what would form on a carbonaceous anode. Their proposed mechanisms at play at the surface are shown in Figure 2.9. Nie, Abraham, Chen, Bose, and Lucht [10] investigated the SEI layer that forms on Si nanoparticles in $LiPF_6$/EC and $LiPF_6$/FEC electrolytes using transmission electron microscopy (TEM), solution NMR, XPS, and Fourier-transform infrared spectroscopy (FTIR). They came to the same conclusion as Philippe et al., namely that the inner part of the SEI layer consists of a large amount of Li_xSiO_y, while the constituents of the outer region were more electrolyte-dependent.

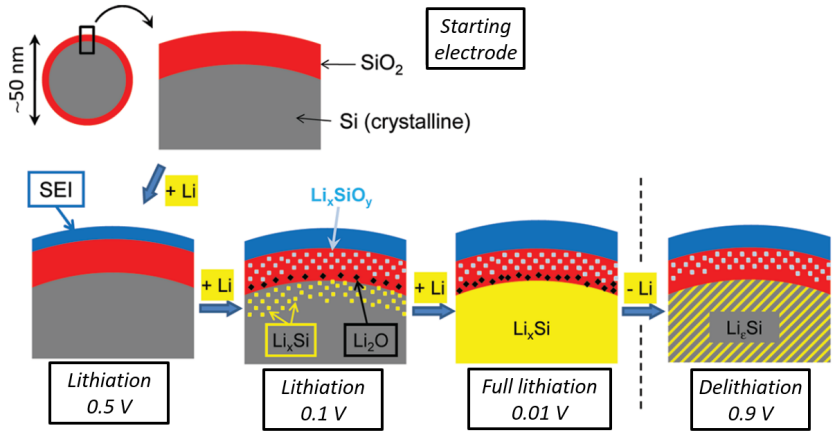

Figure 2.9: A schematic illustration of the surface of a Si nanoparticle with a native oxide layer during (de)lithiation. Adapted from [72].

2.4 Electrolytes

2.4.1 Introduction to electrolytes

As previously stated, the electrolyte consist of a solvent, a Li salt, and various additives. The primary task of the electrolyte in a LIB is to transport Li-ions between the two electrodes, however it must also fulfill an extensive set of requirements aside from just its ability to transfer ions. Based on the 2010 article "*Challenges for Rechargeable Li Batteries*" [5] by Goodenough and Kim and the 2017 review "*Electrolytes for Advanced LIBs*" by Feng [73], the following list of desired electrolyte properties can be compiled:

1. A large electrolyte window
2. Retention of the electrode/electrolyte interface during cycling when the electrode particles are expanding and contracting
3. A high Li-ion conductivity of $\sigma_{Li} > 10^{-4}$ S/cm over the temperature range of battery operation
4. A low electronic conductivity of $\sigma_e < 10^{-10}$ S/cm
5. A transport number as close to $\sigma_{Li}/\sigma_{total} \approx 1$ as possible, where σ_{total} includes conductivities by other ions in the electrolyte as well as $\sigma_{Li} + \sigma_e$
6. Chemical stability with respect to the electrodes, including an ability to rapidly form a passivating SEI layer, and to other cell components, e.g. separator and cell packaging materials
7. Chemical stability over ambient temperature ranges and temperatures in the battery under high power
8. Safe materials, i.e. preferably nonflammable and nonexplosive
9. Low toxicity and low cost

Goodenough and Kim state that "*meeting all these requirements proves to be a formidable challenge*" [5], and indeed, a massive research effort has been and is being made to improve existing electrolytes and create brand new alternatives.

The first commercial LIB was based on a propylene carbonate (PC) electrolyte, but PC was not stable with high-energy graphite-based anodes [73]. Fong, von Sacken, and Dahn [74] performed pioneering work on EC electrolytes and EC is still a common component of today's organic liquid electrolytes due to its contributions to a passivating SEI layer [5]. However, EC has a melting point of 36 °C [34] which is too high for it to be used without additional solvents. Other components in today's electrolytes include diethyl carbonate (DEC), dimethyl carbonate (DMC), or ethylmethyl carbonate (EMC). The electrolyte is usually a blend of carbonates and consist of both cyclic and linear components. Such a carbonate blend, for instance an EC:DMC mix, gives a synergetic effect as the favorable properties of the cyclic EC, namely the ability to form a good SEI layer, a high solubility of Li salts, and a high anodic stability on cathode surfaces are combined with the low viscosity of the linear DMC to promote rapid ion diffusion, in addition to its low melting point [25].

Although organic liquid electrolytes are used in commercial LIBs, they are far from perfect. Their perhaps greatest issue is posing a serious fire hazard as they are highly volatile and have flash points around room temperature [12]. In addition, they will generally not inhibit dendrite growth and realizing a Li metal anode is therefore difficult [35]. Xu lists numerous solvent

alternatives in his 2014 review "*Electrolytes and Interphases in Li-Ion Batteries and Beyond*" [16]. These include phosphorus- and silicon-based solvents, sulfones and sulfoxides, nitriles, esters, ethers, and ionic liquids. In addition, solid state electrolytes are also under heavy investigation [35]. The following section will describe ionic liquids as possible electrolytes in tomorrow's LIBs.

2.4.2 Ionic liquid electrolytes

An IL is a salt with a low melting point, usually defined to be $<100\,^{\circ}\mathrm{C}$. As a salt is comprised purely of ions, an IL is just what it sounds like, a liquid consisting of just ions. ILs have large ions with delocalized or sterically hindered charges, resulting in weak intermolecular forces and thus lowering the melting point [29, 75]. Room temperature ILs have melting points below $\sim 25\,^{\circ}\mathrm{C}$, making them the subset of ILs that are relevant for LIB applications. Other applications for ILs include supercapacitors, dye-sensitized solar cells, and polymer electrolyte membrane fuel cells [19].

Room temperature ILs have been around for more than a century [76], but the dramatic increase in research activity on the topic started about two decades ago [16]. ILs have properties that include negligible vapor pressures, adequate ionic conductivities, and compared to today's carbonate-based electrolytes; better thermal and chemical stability and wider electrochemical windows [14, 15]. A low vapor pressure and superior thermal stability make ILs nonflammable [12], which is the main reason why they have attracted a great deal of attention as possible replacements for flammable carbonates.

Sadly, ILs exhibit some disadvantageous properties as well. In their 2016 review article "*Different roles of ionic liquids in lithium [ion] batteries*" [29], Eftekhari, Liu, and Chen name four main challenges that must be solved and/or understood before neat IL electrolytes can be commercialized: (**1**) a high viscosity which is connected with poor conductivity, diffusivity, and wettability, (**2**) formation of a more severe and complicated electrical double layer than carbonate electrolytes, (**3**) a complex SEI formation, and (**4**) the solvation mechanism of Li^+. The poor conductivity, combined with the thermally stable nature of the ILs, make them especially appropriate in high-temperature operations where the slow diffusion is improved and carbonate electrolytes would need more extensive cooling systems.

The electrochemistry of ILs is fundamentally different to that of a conventional solvent. The presence of nothing but ions in an IL causes the usual assumptions behind commonly used equations of ion transport to be invalid, and more complex models, such as Stefan-Maxwell theory, must be used [29, 77]. Some of the behavior differences between ILs and standard solvents include strong interactions between the solvated Li^+ and the IL ions and the possibility for a frequent structural change of the IL through ion (de)pairing [29]. Both of these phenomena generally make diffusion in ILs hard to model and understand. Though, in recent years, a greater understanding of ILs and their interactions with Li^+ has been achieved, including how Li^+ migrates under an electric field in the ionic media, how Li^+ is solvated by counter-ions without the presence of solvent molecules, and how the anion and cation themselves interact to determine the electrochemical window of stability of the IL [16].

While ILs historically were thought to behave similarly to conventional liquids, i.e. being homogeneous, coherent, and generally irregular, recent advances in the field reveal that ILs show a large degree of structure both on microscopic (ion pairs, ion clusters) and mesoscopic length scales (H-bond networks, micelle-like morphologies) [75]. These structures are different

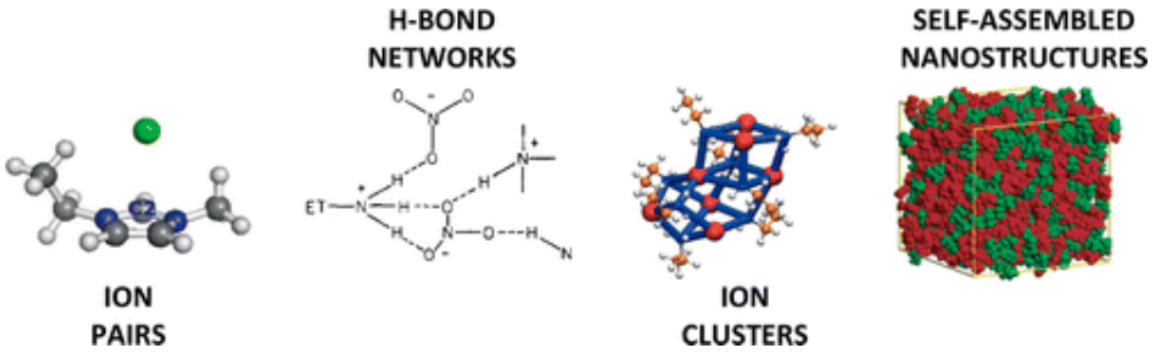

Figure 2.10: Different models for the bulk structure of an IL. Adapted from [75].

based on which ions are present in the IL and will influence the physical and electrochemical behavior of the IL. The various bulk structures an IL can show are illustrated in Figure 2.10.

Recent research activity has provided a long list of possible cations and anions for ILs. The different ions can provide vastly different properties and choosing the correct ions to match desired properties is a must. For instance, the choice of anion for a given cation will determine both the melting point and the electrochemical stability of the resulting IL [16]. These two properties are often in conflict, as the most electrochemically stable anions (PF_6^- and BF_4^-) give a higher melting point, while anions that decrease the melting point ($TFSI^-$, FSI^- and halides) typically are more reactive at higher potentials.

ILs based on the imidazolium cation were perhaps the first to be considered for LIBs [16], where the archetype was EmiTFSI. The TFSI anion proved to be sufficiently stable towards the cathode [14], but the main obstacle was a reduction of the imidazolium cation on the anode at potentials below 1 V vs Li/Li^+. Efforts were made to stabilize the imidazolium cation by coupling it with new anions [78] and replacing the active H atom at the R_2 position [79]. Among all these efforts, the FSI anion in combination with the Emi cation provided an interesting case as the complicated interplay between Li^+, imidazolium, and FSI resulted in an improved ionic conductivity and cathodic stability [16]. Goodenough and Kim stated in a 2010 article [5] that IL electrolytes based on the imidazolium cation appear to be the most promising candidates for LIBs. EmiFSI is chosen as one of the two ILs in this thesis. The chemical structure of imidazolium and the other IL cations that will be introduced in the following paragraphs is shown in Figure 2.11.

The pyrrolidinum cation was introduced in 1999 [80] and recieved a substantial amount

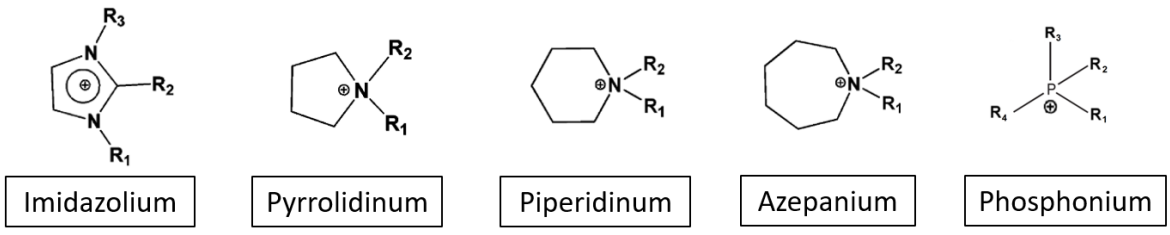

Figure 2.11: The chemical structure of five common IL cations.

of attention due to its superior cathodic stability compared to imidazolium [16]. The cation, in combination with the TFSI anion, showed a rather high ionic conductivity ($> 10^{-3}$ S/cm), a low viscosity, and a high Li^+-transference number (~ 0.4), together with a Li metal anode [81]. Further cyclic ammonium-based cations have been explored and include piperidinum and azepanium [16].

ILs based on the phosphonium cation have also been investigated in recent years. These ILs usually have higher melting temperatures, higher viscosities, and lower ionic conductivities than their ammonium-based counterparts [16], but some variants show promising physical and electrochemical properties [19]. The phosphonium cation has four side groups and the various alkyl- and alkoxy-based side chains that can be added give rise to a large number of possible cation structures. $P_{111i4}FSI$ is chosen as the second IL in this thesis. Not many research groups work with this particular IL and it appears that it has never before been tested with the LiTFSI salt.

This section will end with a critical and realistic look at ILs as battery electrolytes. While many articles praise ILs and the role they can play in future LIB electrolytes, Xu stated in his 2014 review "*Electrolytes and Interphases in Li-ion Batteries and Beyond*" [16] that "*there is no reason to be optimistic about the large-scale application of room temperature ILs in commercial LIBs in the foreseeable future*". He based his argument on the new interphasial challenges that must be addressed, the high cost of manufacturing and purification of most room temperature IL components, and what he describes as "*limited benefits*" compared to organic electrolytes. Xu also questioned the safety aspects of ILs and argued that "*nonflammability does not necessarily translate into higher tolerance against abuse in an electrochemical environment*", citing a study by Wang et al. [82] where accelerated calorimetry testing of the six most common ILs demonstrated that some of them were *more* reactive with partially lithiated electrode materials (including $Li_{0.45}CoO_2$ and Li_1Si) compared to typical carbonate-based electrolytes, making them a more hazardous alternative. However, Xu also added that "*this picture might change though, with any significant breakthroughs arising from room temperature IL electrolytes*".

2.4.3 Electrolyte salts

A salt is added in the electrolyte to ensure a sufficient Li-ion conduction. According to Xu [24], an electrolyte salt should meet the following minimal requirements:

1. It should be able to completely dissolve and dissociate in the nonaqueous media, and the solvated ions (especially lithium cation) should be able to move in the media with high mobility
2. The anion should be stable against oxidative decomposition at the cathode
3. The anion should be inert to electrolyte solvents
4. Both the anion and the cation should remain inert toward the other cell components such as separator, electrode substrate, and cell packaging materials
5. The anion should be nontoxic and remain stable against thermally induced reactions with electrolyte solvents and other cell components

$LiPF_6$ is the preferred salt for carbonate-based electrolytes for both graphite and Si anodes due to a series of well-balanced properties [25]. However, $LiPF_6$ is subject to decomposition

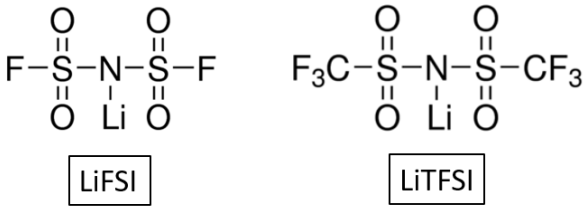

Figure 2.12: The chemical structure of LiFSI and LiTFSI.

in the presence of even trace amounts of water and decomposes to produce HF, a process that can degrade the battery as well as posing a safety hazard.

Compared to the impressive amount of electrode materials and electrolytes that are being researched, the choices of electrolyte salts are rather limited. Still, several possible replacements for $LiPF_6$ exist. Some salts that were investigated in the early stages of LIB research include the poorly conducting lithium trifluoromethanesulfonate (LiTf), the hazardous $LiClO_4$, the thermally unstable $LiBF_4$, and the toxic $LiAsF_6$ [24]. More recent alternatives are lithium bis(oxalato)borate (LiBOB) and lithium difluorooxalatoborat (LiDFOB) [16].

The two electrolyte salts under investigation in this thesis, LiFSI and LiTFSI, are both imide-based and have been proposed as alternatives to $LiPF_6$ due to their increased thermal and electrochemical stabilities, and their higher tolerance against small amounts of H_2O in the cell [23]. The chemical structure of both salts are shown in Figure 2.12. The synthetization of LiTFSI was first reported in 1984 [24], while LiFSI came eleven years later in 1995 [20]. LiTFSI is thermally stable up to 360 °C [24] and LiFSI is thermally stable up to 180 °C [25], although the latter is still under debate as some report a reduced thermal stability due to chlorine impurities in the salt [83].

Both salts have been tested and show promising results with a graphite anode in the EmiFSI IL [27]. With Si anodes, LiFSI in EmiFSI has shown a stable reversible capacity of ∼2500 mAh/g at a rate of C/10 [18] and ∼1200 mAh/g at 2C [11]. There are no signs in the literature that LiTFSI in EmiFSI has been tested with anodes where Si is the only active material, only with a Si-Ni-C composite [25, 26]. At 20 °C, LiFSI in EmiFSI has a conductivity of 6.8 mS/cm at 1.46 M and 11.2 mS/cm at 0.43 M, while LiTFSI in EmiFSI has a conductivity of 4.8 mS/cm at 1.46 M and 10.4 mS/cm at 0.43 M [27].

LiFSI has been tested with $P_{111i4}FSI$ with a Li metal anode [84] and with a Si anode [21], the latter maintaining a capacity of ∼3000 mAh/g after 300 cycles at a rate of C/2.5. A 1M LiFSI-$P_{111i4}FSI$ electrolyte has a conductivity of 3.3 mS/cm at 25 °C [85], i.e. a worse conductivity than its Emi-based counterpart. Regarding LiTFSI, it appears that it has never before been tested with $P_{111i4}FSI$, only with the related $P_{6,6,6,14}FSI$ [78].

When tested in an EC:EMC (3:7 vol%) electrolyte at 25 °C, LiFSI shows a lower viscosity than LiTFSI (2.96 mPa·s and 3.40 mPa·s, respectively) and a resulting higher conductivity (9.73 mS/cm vs 7.57 mS/cm) [20]. The same is true in an EmiFSI ionic liquid, as shown by Matsui et al. [27], where LiFSI-EmiFSI showed a higher conductivity than LiTFSI-EmiFSI for all relevant temperatures and where the difference in viscosities was 37 to 54 mPa·s at 25 °C for 1.46 M LiFSI and LiTFSI, respectively. For a $P_{111i4}FSI$-based electrolyte with 1 M LiFSI, the viscosity is 79 mPa·s at 25 °C [85]. No data exists for LiTFSI in $P_{111i4}FSI$. The difference in viscosity between LiFSI and LiTFSI can at least in part be explained by the

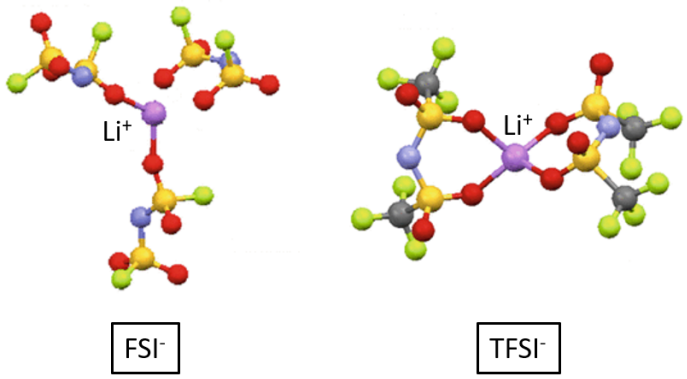

Figure 2.13: Possible solvation structures of Li^+ with FSI^- and $TFSI^-$ anions in EmiFSI and EmiTFSI. Li is purple, O is red, S is yellow, F is green, N is blue and C is grey. Adapted from [87].

difference in molar mass (287.1 g/mol and 187.1 g/mol for LiTFSI and LiFSI, respectively), where a 1M LiTFSI electrolyte will contain 53% more salt (measured by mass) than a 1M LiFSI electrolyte.

Perhaps the major disadvantage of LiFSI and LiTFSI is their corrosion issues with the Al cathode current collector at potentials above 4.0 V, which is the reason why LiTFSI did not make it into commercial LIBs in the early years of development [24]. This makes LiFSI and LiTFSI mostly suited for lower-voltage cathodes like LFP [16, 25]. It should be noted that corrosion is more prominent for LiTFSI than for LiFSI [20].

The benefits of utilizing a combination of FSI and TFSI anions have been investigated in recent years [86]. Mixing ions allows the benefits of both salts to be combined. Notable benefits include the reduced Al corrosion [20], reduced viscosity and improved conductivity [27] of FSI and the improved thermal [24] and chemical stability [23] of TFSI.

It is appropriate to discuss solvation of salt ions in solution, especially in an IL. The solvation of an ion in solution depends not only on the ion-solvent interactions, but also on the solvent/solvent interactions and/or the liquid structure of the IL [87]. The relative permittivity is often used as a measure of a solvent's solvation properties [16]. When an ion is introduced to an IL, the original liquid structure is broken and the ion is solvated by counter-ions to form a solvation cluster. This solvation cluster may not be permanent, as diffusion of ions in an ionic liquid has been associated with breaking and reformation of the solvation layer [22]. Fujii, Seki, Doi, and Umebayashi [87] used a combination of Raman spectroscopy and DFT calculations to determine the solvation number n and solvation structure of Li^+ in EmiFSI and EmiTFSI ILs. They found that, at room temperature, $n = 3$ for FSI^- and $n = 2$ for $TFSI^-$. Their proposed model for the solvation structures are shown in Figure 2.13.

The solvation of Li^+ when both FSI^- and $TFSI^-$ are present is not yet resolved, however some studies suggest that Li^+ is preferentially coordinated by $TFSI^-$ [86]. This could in that case be explained by the stronger interactions between Li^+ and $TFSI^-$ compared to Li^+ and FSI^- [22]. The stronger interactions with $TFSI^-$ can also help explain the increased viscosity of an ionic liquid when LiTFSI compared to LiFSI is added.

The strong Li^+-$TFSI^-$ interaction also affects the electrode/electrolyte interphase structure. Yamagata et al. [88] proposed a double-layer structure in Emi-ILs with FSI and TFSI

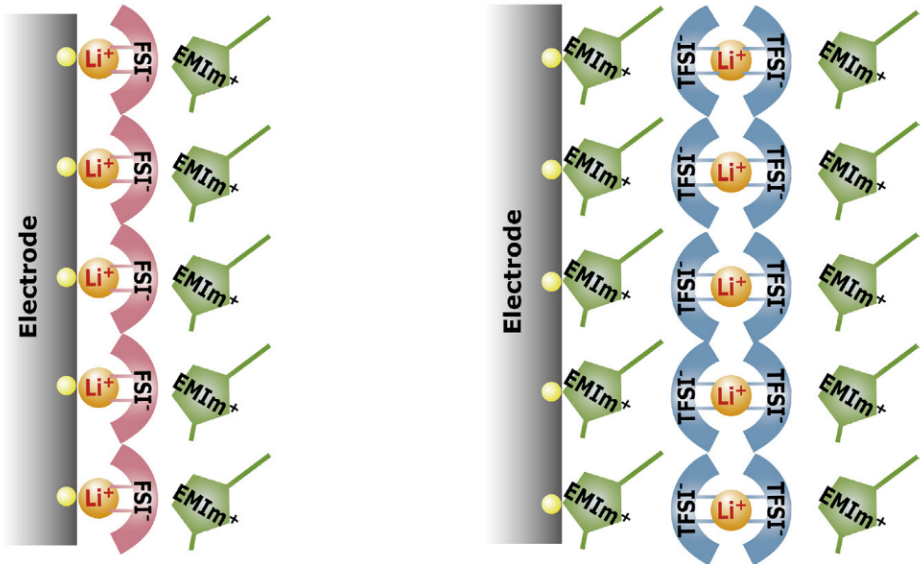

Figure 2.14: The structure of the electrode/electrolyte interphase with FSI^- and $TFSI^-$ anions in an Emi^+-based IL, as proposed by Yamagata et al. [88].

based on a modified Gouy-Chapman-Stern model. This study was performed with graphite anodes, however Matsui et al. argued that this would also be relevant for Si anodes [27]. The proposed model from Yamagata et al. is shown in Figure 2.14. In the model, the weaker Li^+-FSI^- interactions allow solvation clusters with FSI^- to break apart and for Li^+ solvated by a single FSI^- to be preferentially adsorbed onto the negative electrode. Meanwhile, the strong Li^+-$TFSI^-$ interactions make it so that Emi^+ cations are adsorbed onto the electrode, while the $[Li(TFSI)_2]^-$ solvation clusters are positioned further out. Yamagata et al. argue that FSI^- anions therefore can act as a shield against the decomposition of Emi^+ cations and that they can mobilize Li^+ to escape from what they call the "electrostatic inter-ionic cage" of the electrolyte to rather be adsorbed onto the electrode. This mobilization effect would be in addition to the previously mentioned beneficial conductivity properties that FSI^- would have in the bulk electrolyte.

The choice of anion also has a direct effect on the SEI formation on the negative electrode. In addition to the shielding effect of Emi^+ with FSI^- [88], the F-S bond in LiFSI is known to be more reactive than the F_3C-S bond in LiTFSI [23], resulting in a rapid release of F^- and generation of LiF in the SEI when LiFSI is used. The SEI layer with LiFSI is also dominated by other small inorganic species like LiOH, Li_2O, and SO_2^{2-} [11]. LiF in particular is known to promote structural stability of the SEI [70] and improve diffusion of Li^+ through the SEI [32]. LiTFSI, on the other hand, generally produces larger decomposition products such as SO_2CF_3 and Li_2CO_3 [23, 25]. Recent studies have shown a positive effect through the combination of Li_2CO_3 and LiF to reduce the electron leakage current and simultaneously improve Li^+ transport due to a charge accumulation at the grain boundaries between the two components [89]. The possibility of this synergetic effect is added to the previously mentioned list of benefits with a combination of FSI and TFSI anions.

2.4.4 Electrolyte additives and cosolvents

Adding a small amount of additive chemicals to an electrolyte is an efficient and economical way to achieve certain targeted functions [25]. Additives have been extensively studied during the past decades and are often incorporated to assist in SEI formation by being preferentially decomposed during the first few charging cycles. Further applications include improving thermal stability and electrochemical windows and increasing safety through the addition of fire-retardant chemicals [25].

Due to the massive volume expansion and possibility of extensive SEI growth, Si anodes in particular need an electrolyte with optimal SEI formation properties. The addition of additives is a good strategy to tackle this problem. Based on years of research on additives for graphite anodes, several additives for Si anodes have been proposed. The two most popular additives are FEC and vinylene carbonate (VC) [31] and their chemical structures can be seen in Figure 2.15. In carbonate-based electrolytes, both FEC and VC will promote the presence of polycarbonates in the SEI, but the detailed structure of the SEI will vary between the two. The SEI produced with FEC is generally dense and conducts Li^+ well which is believed to be due to the formation of nanocrystals of LiF and their incorporation into the SEI creating defects to promote Li^+ diffusion [32]. VC yields a more flexible SEI of mainly organic compounds, but the conductivity is decreased which can be a result of the absence of defects impeding diffusion through the layer [31].

There has not been so much research focused on additives for ILs, although VC has for instance successfully been combined with an imidazolium-based IL [90] and it has been shown that FEC can be preferentially reduced instead of the IL or the salt in a graphite anode half cell with an EmiTFSI-based electrolyte [33]. Instead, ILs themselves have been considered as additives in carbonate electrolytes due to their nonflammable properties [25]. In addition, mixtures of ILs and carbonate electrolytes show great promise [28, 29]. In these mixtures, both the IL and the organic components are present at comparable concentrations and it is therefore more appropriate to refer to them as *cosolvents* rather than *additives*.

When adding carbonates to an IL, the viscosity will decrease, promoting improved ionic conductivity. In addition, molecular dynamics simulations have shown that organic additives can further improve the ionic mobility by decreasing the coordination number of Li^+ [91]. Interestingly, an improved conductivity can also be achieved by doing the exact opposite: adding an IL to an organic electrolyte. This was exemplified by Guerfi et al. where adding an EmiTFSI IL to a 1M $LiPF_6$ EC/DEC + 2 wt% VC electrolyte [28] gave an optimal

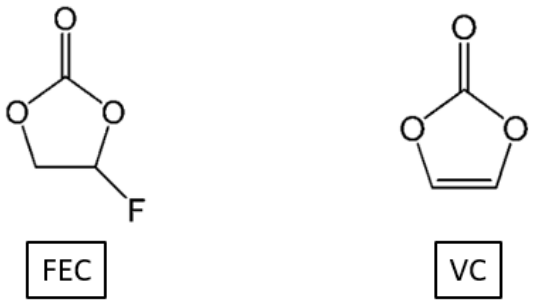

Figure 2.15: The chemical structure of FEC and VC.

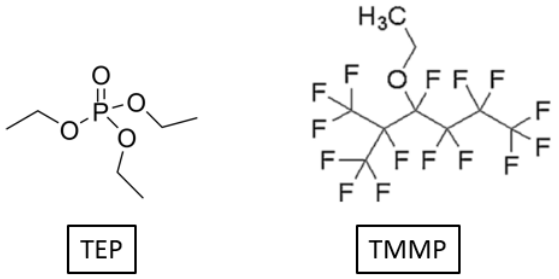

Figure 2.16: The chemical structure of TEP and TMMP.

compromise between viscosity and conductivity for an IL concentration between 30% or 40%.

The combination of an IL and a carbonate electrolyte can show significantly reduced flammability even with as much as 50% carbonate compounds present [28]. Although the flammability can be significantly reduced, the presence of carbonates can still make the cell vulnerable to safety issues [29]. Despite the promising electrochemical properties and apparent safety of IL-carbonate mixtures, it is relevant to look for non-carbonate cosolvent alternatives to reduce the viscosity and promote conductivity in IL electrolytes.

Using flame retardants as electrolytes has received attention in recent years [30], although they have not yet achieved a breakthrough necessary to overcome their challenges, particularly their poor electrochemical performance with graphite anodes [92]. So far, phosphate-based flame retardants, such as trimethyl phosphate (TMP), TEP, dimethyl methylphosphonate (DMMP), and diethyl ethylphosphonate (DEEP), appear to be one of the most promising alternatives and their stability is known to improve with the addition of FEC and VC [30]. These phosphate-based flame retardants have also been added as cosolvents to carbonate-based electrolytes, although a critical amount of carbonates or film-forming additives must be present for the electrolytes to provide stable electrochemical performance [92, 93, 94]. TEP has never before been used as a cosolvent with EmiFSI. TEP has a low viscosity of 1.6 mPa·s at 25 °C [95]. The chemical structure of TEP is shown in Figure 2.16.

Another family of nonflammable cosolvents are hydrofluoroethers (HFEs), particularly branched HFEs [96]. The chemical structure of one common branched HFE, TMMP, also known as Novec 7500, is shown in Figure 2.16. TMMP has been tested as cosolvent in carbonate electrolytes and show nonflammability, high rate capabilities, and no extra reductive decomposition occurs due to the TMMP [97]. TMMP has also shown compatibility with the LiTFSI salt [98], but it has not before been tested with EmiFSI.

Chapter 3

Experimental

3.1 Chemicals and electrodes

The following tables present details on chemicals and electrodes used in this thesis.

Table 3.1: An overview and details of the chemicals used in this work.

Chemical	**Full name**	**Purity**	**Producer**
LiFSI	Lithium bis(fluorosulfonyl)imide	99.9%	Am. Elements
LiTFSI	Lithium bis(trifluoromethane)sulfonimide	99.95%	Sigma-Aldrich
FEC	Fluoroethylene carbonate	99%	Sigma-Aldrich
EmiFSI	1-Ethyl-3-methylimidazolium bis(fluorosulfonyl)imide	99.5%	Solvionic
$P_{111i4}FSI$	Trimethyl(isobutyl)phosphonium bis(fluorosulfonyl)imide	??	??
TEP	Triethyl phosphate	$\geq$ 99.8%	Sigma-Aldrich
TMMP	2-trifluoromethyl-3-methoxyperfluoropentane	??	$3M^{TM}$

Table 3.2: An overview and details of the electrodes used in this work.

Active material (wt%)	**Si (eSi-400, unmilled)** (73.81%)	**$LiFePO_4$** (89.00%)
Loading (mg/cm^2)*	0.79	23.78
Conductive add. (wt%)	Carbon black (C65) (10.97%)	??
Binder (wt%)	CMC** (7.31%)	??
Buffer chemicals (wt%)	K+C+etc (8.54%)	??
Producer	IFE	Customcells Itz.

*Loading indicates mass of *active material* per area
**Carboxymethyl cellulose

3.2 Experimental procedure

3.2.1 Overview

Screen-printed sheets of Si anodes were received from IFE, in addition to sheets of LFP cathodes from Customcells Itzeheo GmbH. Different IL-based electrolytes were prepared and pouch cells with Si anodes and capacitively oversized LFP cathodes, i.e. pseudo full cells, were assembled in an Ar-filled glovebox maintaining H_2O and O_2 concentrations of <0.1 ppm. The cells underwent electrochemical testing and some were characterized by means of XPS. A flow chart showing the experimental work performed in this project is given in Figure 3.1.

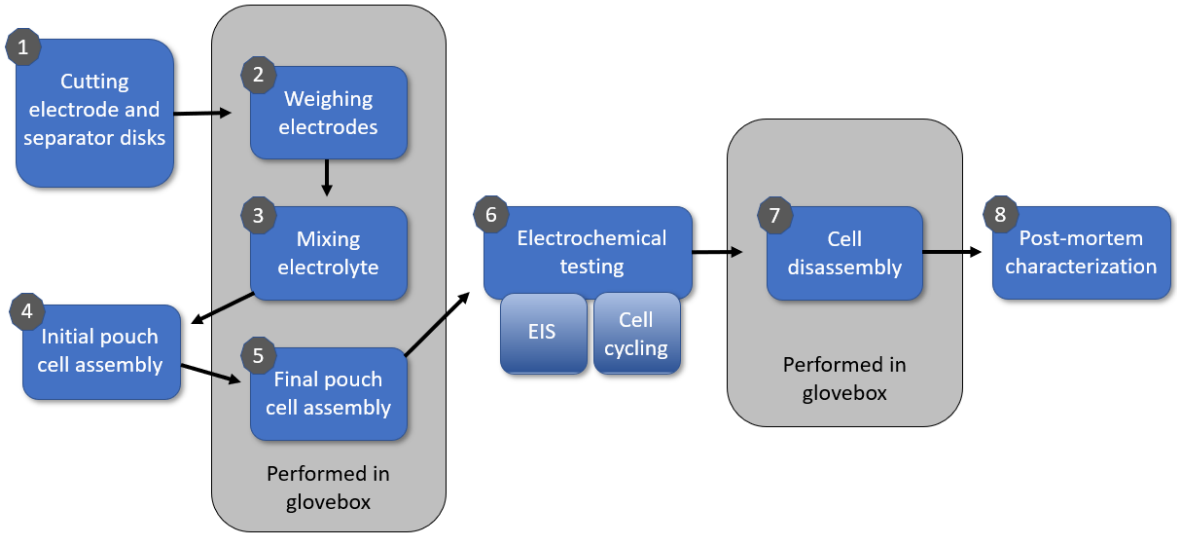

Figure 3.1: A flow chart showing the experimental work flow in this project.

3.2.2 Cell manufacture

Cutting electrode and separator disks

Electrode disks were cut from the pre-made electrode sheets using a Gelon Group GN-CP 20 manual punching machine. The Si anodes were cut to a diameter of 12 mm and the LFP cathodes were cut to 14 mm. Before being introduced to the glovebox, the electrodes were dried in a vacuum oven overnight for a minimum of 12 hours at 100 °C and 110 °C for Si and LFP, respectively. In the transporting process from the vacuum oven to the glovebox, the electrodes were exposed to ambient air for roughly two minutes.

Sheets of an Evopor^{TM} 5E02A separator, an ethylene vinyl alcohol copolymer (EVOH) hydrophilic separator, were cut to a diameter of 19 mm using a hammer and a manual punching cutter. The separators were dried in a vacuum oven at 80 °C overnight for a minimum of 12 hours before being introduced to the glovebox. This step is estimated to have exposed the separators to ambient air for roughly two minutes.

Weighing electrodes

All Si anodes were weighed using an analytical balance in the glovebox. Knowing the mass of the anode and subtracting the mass of the current collector, in addition to knowing the com-

position of the anode, allowed for an accurate determination of the loading on the individual anodes.

Mixing electrolytes

This work attempts at evaluating the improvement of IL electrolytes by using two different cosolvents, adding an electrolyte additive, and using two different Li salts. A total of eight electrolytes have been investigated in this project, all of which had salt concentrations of 1.0 M. It was not necessary to use a magnetic stirrer to dissolve the salts in the ILs. All work related to electrolyte preparation and mixing was performed in the glovebox.

Firstly, in order to remove moisture from the two cosolvents, TEP and TMMP, 3 Å molecular sieves (4×8 mesh) from Sigma Aldrich were added in a roughly 1:2 vol% ratio to the liquids. After >72 hours, the cosolvents were extracted using a syringe and filtered using 0.2 µm Whatman Polydisc TF filters.

The differences between LiFSI and LiTFSI were evaluated in two different ILs. Two P_{111i4}FSI-based electrolytes were prepared by mixing LiFSI or LiTFSI salt and the ionic liquid. In addition, two EmiFSI-based electrolytes with LiFSI and LiTFSI had been prepared in the Specialization project [99] preceding this Master project. Both ILs were used as received.

The least viscous of the two ILs used in this work, EmiFSI, was selected to evaluate the effect of adding cosolvents and/or an additive. Of the two Li salts, LiTFSI was chosen as LiTFSI in EmiFSI had shown better Coulombic efficiency and delithiation capacity after 50 cycles at C/5 than LiFSI in the Specialization project [99]. Two electrolytes with LiTFSI and different ratios of TEP and EmiFSI, 20:80 and 40:60 wt%, were prepared. The FEC additive was used as received and two additional electrolytes with LiTFSI were prepared by adding FEC in an amount of 5 wt% to EmiFSI and to the 20:80 mixture of TEP and EmiFSI.

An attempt was made to mix TMMP with EmiFSI, at first in a ratio of 25:75 wt%. Sadly, even after stirring the solution for a few minutes, the two components almost immediately separated into two distinct layers when allowed to rest, similar to oil in water. The solution was diluted with EmiFSI to a ratio of 15:85 wt%, but the two components were still immiscible. As a consequence, a continued effort on testing TMMP:EmiFSI electrolytes were not made.

The following list provides an overview of the electrolytes used in this work. Three cells were made with each electrolyte. The names that will be used when referring to the electrolytes are given in bold.

1. **LiFSI:Emi**: 1M LiFSI in EmiFSI
2. **LiTFSI:Emi**: 1M LiTFSI in EmiFSI
3. **LiFSI:Ph**: 1M LiFSI in P_{111i4}FSI
4. **LiTFSI:Ph**: 1M LiTFSI in P_{111i4}FSI
5. **TEP20**: 1M LiTFSI in TEP and EmiFSI (20:80 wt%)
6. **TEP40**: 1M LiTFSI in TEP and EmiFSI (40:60 wt%)
7. **Emi:FEC**: 1M LiTFSI in EmiFSI + 5wt% FEC
8. **TEP20:FEC**: 1M LiTFSI in TEP and EmiFSI (20:80 wt%) + 5wt% FEC

Initial pouch cell assembly

As illustrated by step 1 and 2 in Figure 3.2, the pouch cells were partially assembled before being taken into the glovebox. To start with, a 10x65 mm strip of a tesa® copolyester-based thermoplastic bonding film was fastened to a 70x80 mm polyethylene laminated Al-foil using

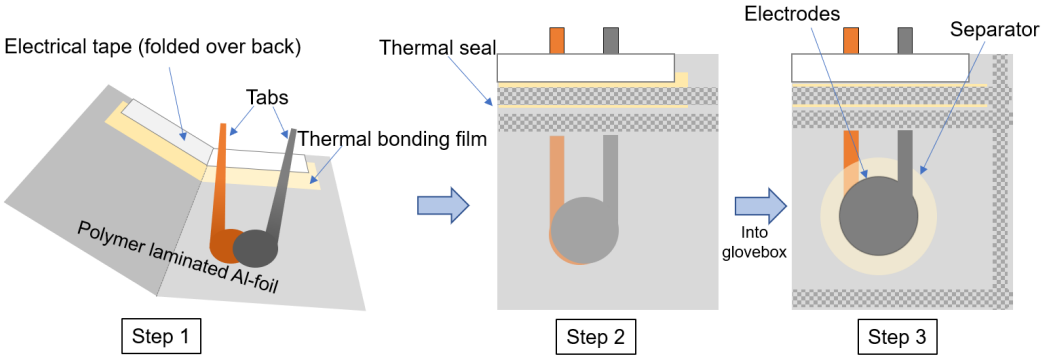

Figure 3.2: An overview of the pouch cell assembly process. Adapted from [100].

a 20x70 mm piece of electrical tape. The tape was folded over the edge and onto the backside. Quarter note-shaped pieces of Cu and Al foil with a diameter of the circle just larger than their corresponding electrodes and a tab length of 70 mm, that would later provide electrical contact between the outside of the pouch cell and the current collectors, were positioned as shown in Figure 3.2. The pouch cell was folded in half and the top part of cell was sealed using an Audion Magneta Motor heat sealer. The thermal bonding film, which was activated by the applied heat and pressure, provided a tight seal around the Cu and Al tabs, but was not needed for the two remaining seals in step 3.

Final pouch cell assembly

The partially assembled pouch cells were introduced to the glovebox. A Si anode was placed onto a support and 20 µL of electrolyte were applied using a micropipette. A separator was placed onto the anode and another 10 µL of electrolyte were added. Lastly, the cathode was placed onto the separator, making sure that the 14 mm cathode fully covered the 12 mm anode underneath. This electrode-separator stack was then positioned between the Cu and Al tabs in the partially assembled pouch cell as shown in Figure 3.2. The anode and cathode were in contact with the Cu and the Al, respectively. The pouch cell was sealed using an Audionvac VMS 53 vacuum sealer. The vertical seal in Figure 3.2 was done with a weak vacuum, whereas the final seal was done with a pressure of <30 mbar.

A moderate pressure was applied to the cell during EIS measurements and cycling by placing it between two 40x60 mm PVC pressure plates and attaching four 19 mm binder clips. Images showing the various components as well as how pressure was applied are presented in Figure 3.3.

3.2.3 Electrochemical testing

Electrochemical Impedance Spectroscopy

EIS measurements were taken of the cells before cycling using a Biologic VMP-300 potentiostat. EIS measurements were carried out the day after the cells were assembled to give the electrolyte sufficient time to fully wet the separator and the electrodes. The measurements were galvanostatic EIS with a 150 µA amplitude and a frequency range of 1 MHz to 1 kHz with a resolution of 20 points per decade. Data from the intersection with the x-axis was used together with Equation (2.5) to compare the conductivities of the different electrolytes.

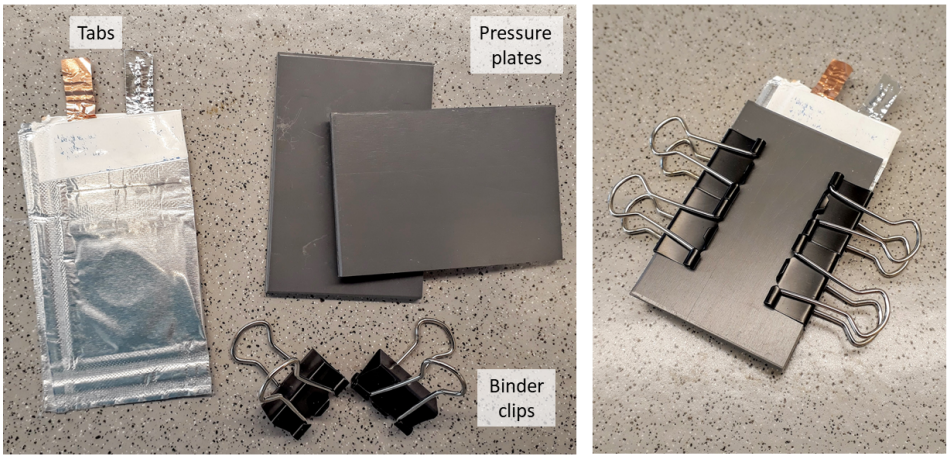

Figure 3.3: The left image shows a finalized pouch cell as well as the components used to apply pressure. The right image illustrates how pressure was applied to the cell during EIS measurements and cycling.

Electrochemical cycling

The cells were cycled using a Maccor Model 4200 potentiostat in a temperature-controlled room set to 20 °C. The cycling program was a rate test where each rate consisted of four cycles and a current I having the following values: C/20, C/5, C/2, 1C, 2C, and C/20, where the five increasingly faster rates show the rate performance of the cell and the last C/20 cycles indicate how much of the original capacity the cells retain after the first 20 cycles. Each cycle consisted of:

1. A constant current charging to a cut-off voltage of 3.41 V
2. A constant voltage charging until the current had dropped to $I/2$
3. A constant current discharging to a cut-off voltage of 2.2 V
4. A constant voltage discharging until the current had dropped to $I/2$

As LFP has a voltage plateau at 3.45 V, charging up to a cell voltage of 3.41 V meant that the potential at the anode was ∼40 mV, disregarding any overpotentials in the cell.

3.2.4 Post-mortem characterization

In order to investigate the initial SEI formation with LiFSI and LiTFSI salt in the two ILs, four extra cells were made using the electrolytes LiFSI:Emi, LiTFSI:Emi, LiFSI:Ph, and LiTFSI:Ph with the purpose of being characterized by means of XPS. The cells underwent a single charge and discharge cycle with a rate of C/20 and cut-off parameters as described in Section 3.2.3. In addition, an uncycled Si anode was also characterized with XPS.

Cell disassembly

The cells were introduced to the glovebox and cut open using an ordinary pair of scissors. The Si anodes were taken out and washed in a beaker with 2 mL of DMC for a few minutes in order to remove as much of the electrolyte and salt as possible. Roughly a quarter of each of the washed anodes were cut off using scissors and fastened on an XPS sample holder using Cu tape as seen in Figure 3.4.

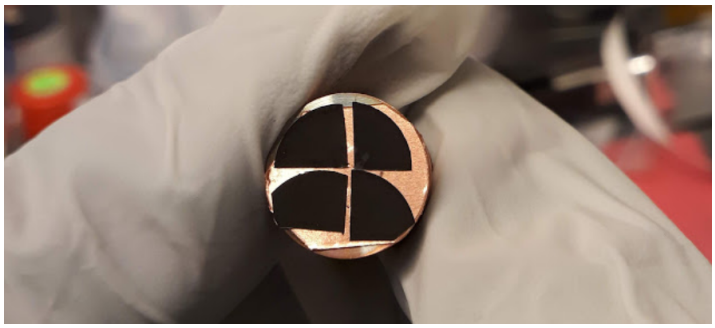

Figure 3.4: The XPS sample holder with the four anodes.

XPS

While still in the glovebox, the XPS sample holder was loaded into an inert transfer arm and brought to the XPS. The sample holder was mounted into the XPS without exposing the samples to ambient air.

Both for the uncycled anode and the four cycled anodes, a Kratos Axis Ultra XPS equipped with an Al monochromatic X-ray source with a photon energy of 1486.69 eV was used. The chamber pressure during characterization was $\sim 10^{-9}$ Torr and the area analyzed was 300x700 μm^2. Charge compensation was not used.

First, a survey scan consisting of 5 sweeps with a pass energy of 160 eV, a resolution of 0.5 eV, and a range of 0-1200 eV was taken to identify the elements present at the surface of the anode. Then, each core peak of interest underwent a detailed scan with a pass energy of 20 eV at a resolution of 0.1 eV. The detailed scans consisted of 10 or 20 sweeps depending on how many were needed to achieve a satisfactory signal-to-noise ratio. Two of the core peaks, F 1s and S 2p, showed a significant evolution of their spectra with each sweep, meaning that the prolonged exposure to X-rays and/or the strong vacuum altered the surface over time. For these peaks, further analysis was based on the initial sweep, while for the other core peaks, an average of all sweeps was used.

The CasaXPS software was used to perform data analysis. In order to be able to compare results with the literature, the data was shifted against a known energy reference. For the uncycled anode which had been exposed to ambient air before XPS testing, C-C at 284.8 eV from adventitious carbon in the C1s peak was used as a reference, corresponding to an energy shift of -0.5 eV. However, the detailed scan of the Si2p peak was left unshifted as the peak fitted well bulk Si positioned at 99.5 eV [72]. This was a sign of differential charging being present in the sample.

The cycled anodes had not been exposed to ambient air before XPS testing and adventitious carbon could therefore not readily be used as a reference. Further, since the cycled anodes were tested in the same XPS session, it was assumed that they experienced similar conditions and therefore should undergo the same energy calibration. Based on an expectation to find LiF at 685 eV [72], Na compounds at $\sim$1071.5 eV [101], carbon black at $\sim$283 eV [72], and C-C at $\sim$285 eV [68], an energy calibration of -2.0 eV was applied for the four cycled anodes.

The atomic composition of the samples were determined based on the survey spectra. The software uses an element library containing all relevant elemental information, including relative sensitivity factors, to determine the atomic percentages. Deconvolution of the core

peaks was done using the software's "quantify" tool where a region of interest was defined and the signal was approximated as a sum of component-specific peaks positioned at energy levels as found in literature. The mass balance between identical components found in the different core peaks was taken into consideration in order to strengthen the confidence in the deconvolution results. A Shirley background was used both for survey and core peak scans and the line-shape used in deconvolution was GL30 (30% Lorentzian and 70% Gaussian).

Chapter 4

Results

4.1 The effect of Li salts and cosolvents on electrolyte properties

4.1.1 Visual inspection of electrolytes

When mixing the various electrolytes, differences in viscosities and rates of separator wetting were observed. Electrolytes with $P_{111i4}FSI$ were more viscous and clearly wetted the separator more slowly compared to EmiFSI. With the larger LiTFSI salt compared to LiFSI, a slightly slower wetting and more viscous electrolyte was also observed for both LiTFSI:Emi and LiTFSI:Ph compared to LiFSI:Emi and LiFSI:Ph. Further, the addition of 20 and 40 wt% TEP to EmiFSI resulted in a visually observed reduction in viscosity that was more pronounced with a higher content of TEP.

The mixing of TMMP and EmiFSI resulted in a separation into two distinct layers within seconds after stirring ended. The mix of TMMP and EmiFSI was tested in ratios of 15:85 and 25:75 wt%, respectively, and the two liquids were immiscible at both ratios.

4.1.2 Electrolyte resistance measurements with EIS

Galvanostatic EIS measurements were carried out and the average values of the electrolyte resistance, R_{el}, which can be assumed to dominate the high-frequency resistance values extracted from EIS plots, are shown in Table 4.1. As the experiments are all performed in the same cell with the same separator, the measured high-frequency resistance may be assumed to be inversely proportional to the ionic conductivity.

Table 4.1: Average electrolyte resistances as measured by EIS.

Electrolyte	LiFSI:Emi	LiTFSI:Emi	LiFSI:Ph	LiTFSI:Ph	TEP20	TEP40
$\boldsymbol{R_{el}}$ (Ω)	1.76 ± 0.19	2.15 ± 0.31	3.84 ± 0.15	4.23 ± 0.34	2.00 ± 0.16	2.71 ± 0.27

Firstly, a clear difference between the two ILs can be seen as the electrolyte resistances with $P_{111i4}FSI$ are roughly twice that of EmiFSI. Secondly, LiFSI yields reduced resistances compared to LiTFSI, but the difference between the two salts is not as significant as the difference between the two ILs.

The two electrolytes with TEP contain LiTFSI and EmiFSI and should therefore be compared with the performance of LiTFSI:Emi. It can be seen that the addition of 20 wt% TEP reduces R_{el} slightly from 2.15 Ω ± 0.31 Ω to 2.00 Ω ± 0.16 Ω, however a higher concentration of TEP, 40 wt%, yields the opposite trend, namely an increased R_{el} of 2.71 Ω ± 0.27 Ω.

4.2 The effect of Li salts on cell performance and SEI formation

4.2.1 The effect of LiFSI and LiTFSI on cell capacity, rate performance, and electrolyte decomposition

The average delithiation capacities of cells comparing LiFSI to LiTFSI in EmiFSI and $P_{111i4}FSI$ are shown in Figure 4.1. First of all, all cells experience a massive reduction in capacity with increased (dis)charging rates, i.e. exhibiting a poor rate performance. The phosphonium electrolytes are the most affected by higher rates and both LiFSI:Ph and LiTFSI:Ph drop to <10% of their original capacity at C/2. LiTFSI:Ph exhibits a substantial loss in capacity already at C/5. Both EmiFSI electrolytes are also heavily affected by the incresed rates and pass below <10% of their original capacity at 1C. Further, electrolytes with LiTFSI show worse rate performance than those with LiFSI. LiFSI:Ph outperforms LiTFSI:Ph at all rates while in EmiFSI, LiTFSI achieves higher capacities at C/20 and C/5, but experience a more severe response to increased rates and fall below LiFSI at C/2.

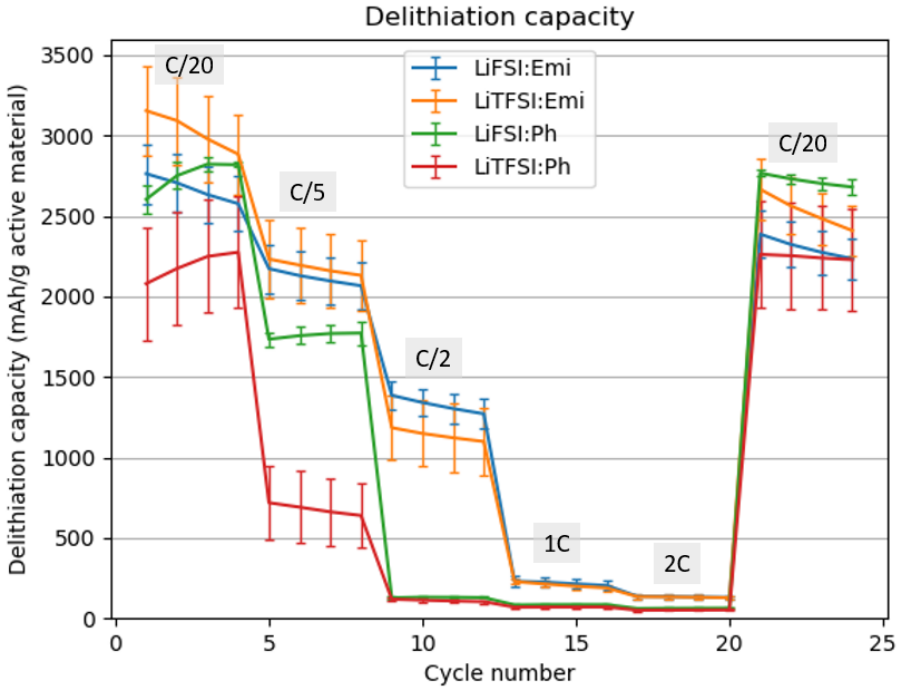

Figure 4.1: Average delithiation capacity of cells comparing LiFSI and LiTFSI showing an improved rate performance of LiFSI compared to LiTFSI.

Cells with LiTFSI:Emi display the highest initial delithiation capacities. While both EmiFSI electrolytes give a steadily decreasing cell capacity in the first four cycles, the $P_{111i4}FSI$ electrolytes show an *increasing* capacity. LiFSI:Ph maintains this behavior in cycle five to eight as well. In the last four cycles at the rate of C/20, all electrolytes show decreasing capacities from cycle 21 to 24, but both phosphonium electrolytes have a flatter curve, indicating a more stable cell performance over time. In addition, a comparison of the capacity in cycle four and 21 shows that LiFSI:Emi and LiTFSI:Emi experience more degradation than the two phosphonium electrolytes during cycling in the range C/5 to 2C.

The Coulombic efficiency of cells with LiFSI:Emi, LiTFSI:Emi, LiFSI:Ph, and LiTFSI:Ph is presented in Figure 4.2. The Coulombic efficiency of the first cycle provides a measure of the extent of electrolyte decomposition and SEI formation and the figure shows that more decomposition occurs for EmiFSI electrolytes than $P_{111i4}FSI$. The effect of the Li salt is different in the two ILs as LiFSI gives a lower initial Coulombic efficiency than LiTFSI in EmiFSI, but higher in $P_{111i4}FSI$. For the most part, these trends also continue for later cycles.

Figure 4.2 shows that the first cycle of each new rate exhibits a distinctly different Coulombic efficiency compared to the following three cycles of that rate. Whereas this for the very first cycle can be attributed to the formation of the SEI layer, the origin of the similar feature in later rates is unclear apart from it being some response to the new rate that stabilizes after the first cycle. The opposite effect is observed in the last rate, where the decreased (dis)charging rate yields an increased Coulombic efficiency for the first cycle.

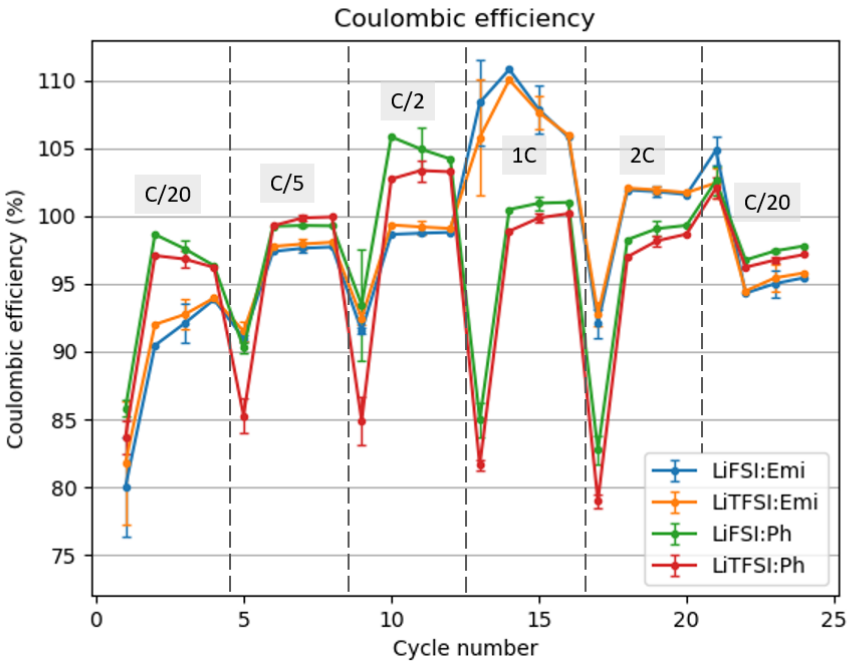

Figure 4.2: A plot of Coulombic efficiencies for LiFSI:Emi, LiTFSI:Emi, LiFSI:Ph, and LiTFSI:Ph showing a higher Coulombic efficiency for $P_{111i4}FSI$ than EmiFSI for most rates.

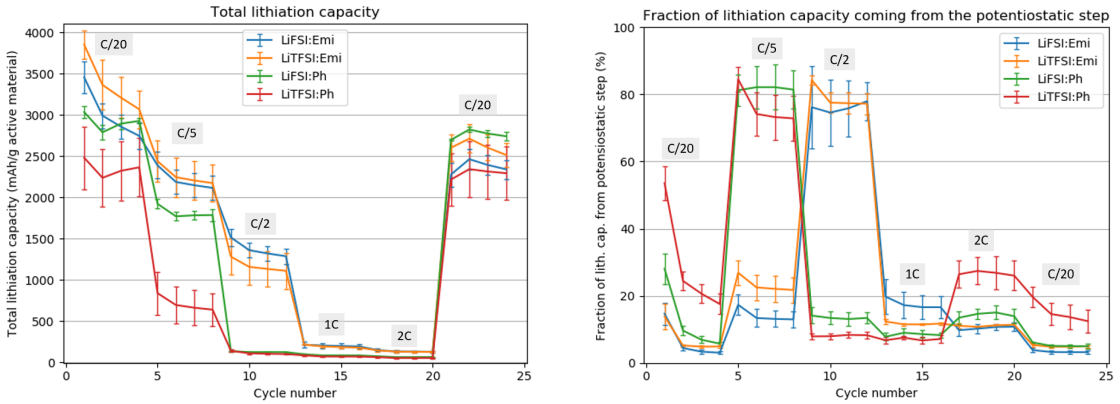

(a) Total lithiation capacity

(b) Hold step fraction

Figure 4.3: Graphs showing (a) the total lithiation capacity and (b) the fraction of the total lithiation capacity coming from the potentiostatic hold step for cells cycled in LiFSI:Emi, LiTFSI:Emi, LiFSI:Ph, and LiTFSI:Ph.

The lithiation capacity is plotted in Figure 4.3a. The *lithiation* capacities show qualitatively the same behavior as the *delithiation* capacities in Figure 4.1, with LiFSI and EmiFSI contributing to a better rate performance than LiTFSI and $P_{111i4}FSI$, respectively. In addition, the initial SEI formation due to electrolyte decomposition can be seen from the significantly higher capacities of the first cycle compared to the second. The SEI formation helps explain how the lithiation capacity of LiTFSI:Emi can surpass the theoretical specific capacity of Si, 3579 mAh/g, in the first cycle.

The total lithiation capacity is a sum of contributions from a galvanostatic step at the given current I and a potentiostatic step at a cell voltage of 3.41 V until the current reached $I/2$. With equilibrium charging conditions, which are only a theoretical possibility, the potentiostatic step would not contribute to the lithiation capacity. However, the presence of overpotentials in the cell increases the capacity contribution of the potentiostatic step. Analyzing the fraction of the total lithiation capacity coming from the potentiostatic step therefore provides a measure of the overpotentials in the cell which in some cases may be related to the thickness of the SEI layer or to the ionic conductivity of the electrolyte. This "hold step fraction" is plotted in Figure 4.3b.

First, Figure 4.3b shows that LiTFSI gives higher hold step fractions than LiFSI for both C/20 rates and that the effect is more pronounced for $P_{111i4}FSI$. Second, a clear difference between the two ILs can be seen when the rate is increased. While the capacity of LiFSI:Ph in Figures 4.1 and 4.3a is somewhat comparable to that of LiFSI:Emi and LiTFSI:Emi at C/5, Figure 4.3b shows an underlying difference with a vastly larger hold step fraction of ∼80% for LiFSI:Ph. A similar hold step fraction is seen for LiTFSI:Ph. This is an indication of the phosphonium cells operating at the edge of the rates they can handle and they both exhibit a very low capacity in the following rate. Likewise, the hold step fraction reaches ∼80% for both EmiFSI electrolytes at C/2 and at 1C, the capacity has dropped significantly.

In order to further investigate decomposition processes and overpotentials in the cells, potential vs capacity plots of cycle 1, 2, and 24 of one representative cell with each electrolyte are given in Figure 4.4. The overview of the first cycle shows that the overpotentials for

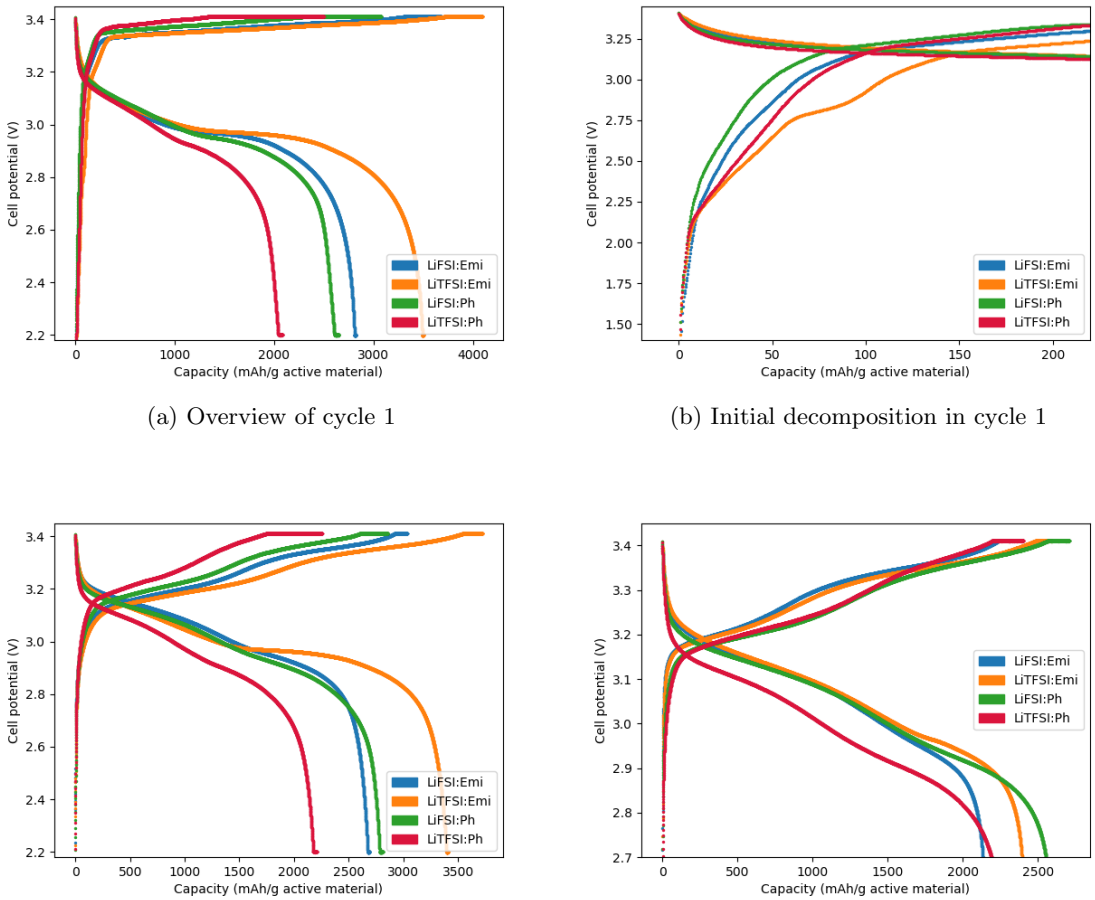

(a) Overview of cycle 1

(b) Initial decomposition in cycle 1

(c) Overview of cycle 2

(d) Overview of cycle 24

Figure 4.4: Potential vs capacity plots of representative cells from LiFSI:Emi, LiTFSI:Emi, LiFSI:Ph, and LiTFSI:Ph, showing (a) an overview of the first cycle, (b) the initial electrolyte decomposition in the first cycle, (c) an overview of the second cycle, and (d) and overview of the last cycle.

lithiation, as seen at roughly 3.35 V, are notably higher for $P_{111i4}FSI$ electrolytes than for EmiFSI, with LiTFSI:Ph having the largest overpotentials. The same trend continues in cycle 2, where the increased overpotential of LiTFSI:Ph is also more clearly visible for delithiation. In the last cycle, LiTFSI:Ph exhibits larger overpotentials for delithiation than the other electrolytes, but the same is not seen regarding overpotentials for lithiation.

The processes of (de)lithiation, as described in Table 2.1, can be seen from Figure 4.4. First of all, lithiation in the first cycle occurs at ∼3.35 V, in line with a potential 0.10 V vs Li/Li^+ at the anode being necessary to lithiate the initially crystalline Si matrix. In cycle 2 and 24, lithiation proceeds via a mechanism typical for the lithiation of initially amorphous Si, starting with a plateau at 3.15 V with lithiation of amorphous a-Si into a-$Li_{2.0}Si$, followed by a second plateau at 3.35 V corresponding to lithiation of a-$Li_{2.0}Si$ to a-$Li_{3.5}Si$. All delithiation processes also seem to follow the delithiation mechanisms presented in Table 2.1, with signs

of plateaus at roughly 3.15 V and 2.95 V corresponding to delithiation of a-$Li_{3.5}Si$ to a-$Li_{2.0}Si$ and further to a-Si, respectively.

A comparison of the plateaus related to lithiation in cycle 24 in Figure 4.4d seems to indicate that the cells with a phosphonium electrolyte achieved a higher degree of delithiation in the previous cycle than with EmiFSI electrolytes. This can be seen from the first plateau at 3.15 V being significantly wider for LiFSI:Ph and LiTFSI:Ph than for LiFSI:Emi and LiTFSI:Emi and the second plateau at 3.35 V being comparably more dominant with EmiFSI, i.e. lithiation of Si that is initially more delithiated contributes more to the lithiation capacity of cells with $P_{111i4}FSI$ than for EmiFSI. Similar conclusions can be drawn from the delithiation curves, with the plateau at 2.95 V contributing less to the delithiation capacity for electrolytes with EmiFSI.

The perhaps most interesting potential vs capacity plot is Figure 4.4b which shows the initial electrolyte decomposition in the first cycle. To begin with, a small amount of capacity originates from potentials below ∼2.15 V and electrolytes with LiFSI appear to be slightly more reactive at these low potentials. This capacity is assigned to a weak decomposition of the LiFSI salt [102] or impurities in the cell. Decomposition of the Li salt is also responsible for the increased capacity from ∼2.15 V and upwards [23], where both electrolytes with LiTFSI show more decomposition than LiFSI. Further, a clear plateau at 2.8 V in LiTFSI:Emi and a hint of a similar plateau in LiFSI:Emi can be seen. This corresponds to reduction of the Emi cation [88, 103]. Corresponding plateaus do not exist for the two phosphonium-based electrolytes. Figures 4.4a and 4.4b show that the onset for lithiation does not occur at 3.35 V, but rather at ∼3.2 V. This corresponds to lithiation of amorphous Si and is an indication that some amorphous Si is initially present in the electrode.

4.2.2 Characterization of SEI layers with XPS

The XPS survey spectra of a pristine Si anode and anodes having undergone one charging and discharging cycle in LiFSI:Emi, LiTFSI:Emi, LiFSI:Ph, and LiTFSI:Ph are shown in Figure 4.5. The atomic composition of the surface of the samples based on the survey spectra is given in Table 4.2. In addition to the elements given in the table, small amounts of K (0.1 at%), Na (0.9 at%), and Cu (0.2 at%) were found in the uncycled anode, with K being an additive in the electrode, Na coming from the binder (Na-CMC), and Cu being present in the current collector. These elements are not seen in survey spectra of cycled anodes. The P content in LiFSI:Ph and LiTFSI:Ph was 0.7 and 0.2 at%, respectively.

Table 4.2: Atomic percentages of the surface of an uncycled Si anode and anodes after one cycle in LiFSI:Emi, LiTFSI:Emi, LiFSI:Ph, and LiTFSI:Ph.

Peak	C 1s (at%)	F 1s (at%)	O 1s (at%)	N 1s (at%)	S 2p (at%)	Si 2p (at%)	Li 1s (at%)
Uncycled Si	57.1	0.6	26.8	-	-	14.3	-
LiFSI:Emi	33.6	3.2	28.2	5.6	5.8	0.7	22.9
LiTFSI:Emi	33.9	5.2	25.3	5.7	5.5	0.9	23.5
LiFSI:Ph	33.6	5.2	27.5	3.9	4.3	1.0	23.8
LiTFSI:Ph	31.0	5.8	27.6	3.4	4.5	1.2	26.3

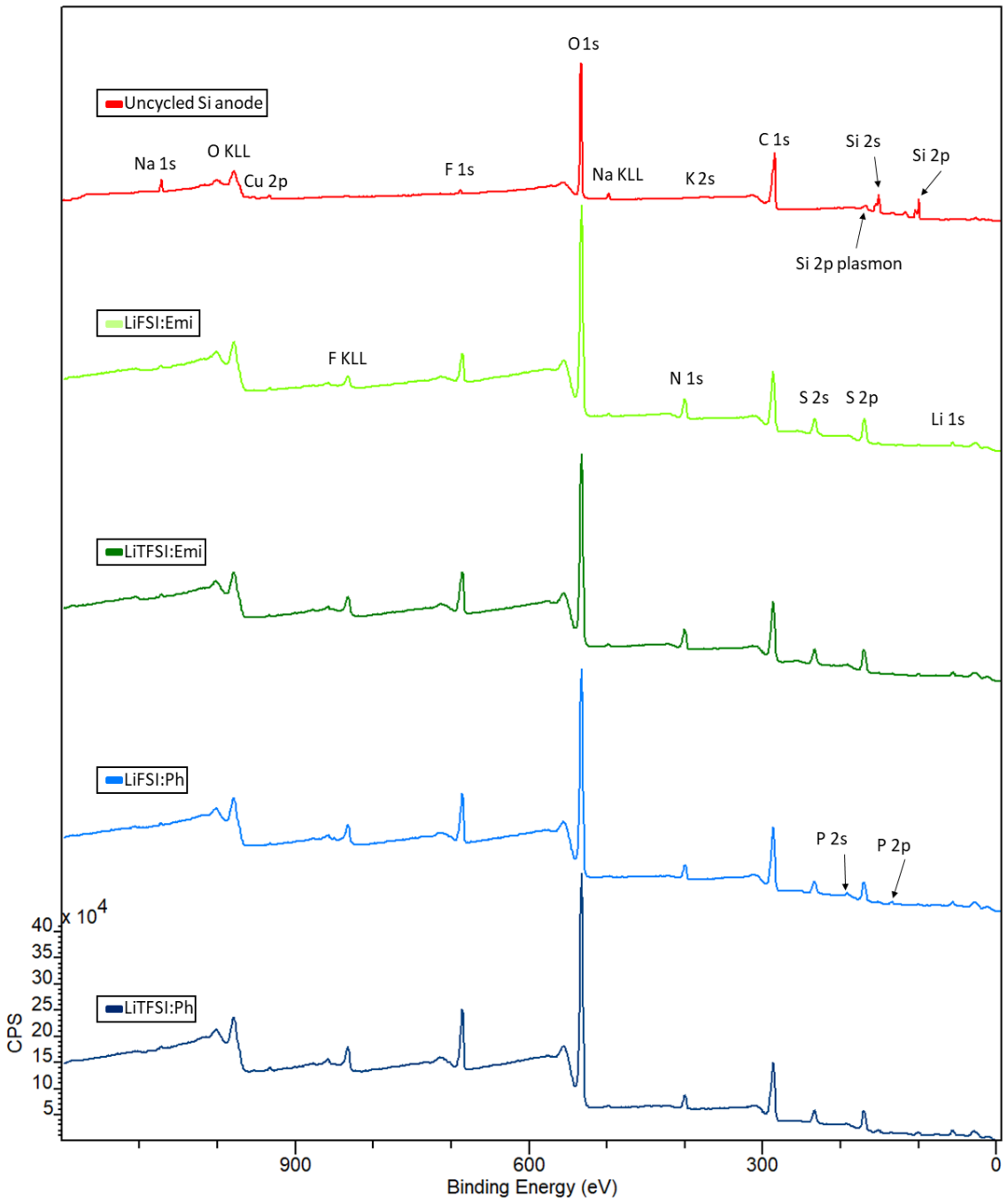

Figure 4.5: XPS survey spectra of an uncycled Si anode and Si anodes after one cycle in LiFSI:Emi, LiTFSI:Emi, LiFSI:Ph, and LiTFSI:Ph.

Table 4.2 and Figure 4.5 show that the surface of the pristine Si anode is dominated by carbon and oxygen species in addition to Si and some F. The strong carbon signal can be explained by carbon black and the CMC binder in the electrode, in addition to a substantial amount of adventitious carbon at the surface. Oxygen is likely present due to a combination of contamination from air, the CMC binder, and a surface oxide layer on the Si particles.

Anodes that have undergone cycling show a significantly altered surface with N, S, Li, and F now comprising a significant fraction of the atomic composition. C, O, and Li are the dominating elements. The Si signal is drastically reduced compared to the uncycled anode and accounts for roughly 1 % of the atomic percentage. There is a higher fraction of the signal coming from from N 1s and S 2p peaks with EmiFSI electrolytes than with P_{111i4}FSI.

Upon deconvolution of XPS spectra of the cycled anodes, it was clear that the four electrolytes gave the same peaks, although with somewhat different contributions from each peak to the overall spectrum. To illustrate the differences between an uncycled and a cycled anode and to show the chemical compounds and electronic states of elements detected at the surface, offset plots of core peaks from the uncycled anode and the anode cycled in LiTFSI:Emi for one cycle are now presented, with C 1s and O 1s in Figure 4.6, F 1s and N 1s in Figure 4.7, and S 2p and Si 2p in Figure 4.8. All spectra have been normalized with respect to the nearby background signal, except from Si 2p in Figure 4.8b. This was left non-normalized as the small Si content in the LiTFSI:Emi sample gave a spectrum where the deconvoluted peaks were not visible when compared to the large Si peak from the uncycled anode.

The C 1s and O 1s core peaks in Figure 4.6 have been deconvoluted and show various carbon and oxygen species. For the uncycled anode, the C 1s spectrum is fitted using four peaks corresponding to carbon black at 283.8 eV [72], C-C and C-H bonds at 284.8 eV [104], C-OH and C-O-C bonds at 286.7 eV [105], and C=O and O-C=O bonds at 288.7 eV [10, 106]. The anode cycled in LiTFSI:Emi shows similar chemical bonds, but the carbon black peak, which now may also be ascribed to lithiated carbon species [107], is shifted to lower energy levels and an additional CO_3 component is detected at 289.9 eV [72].

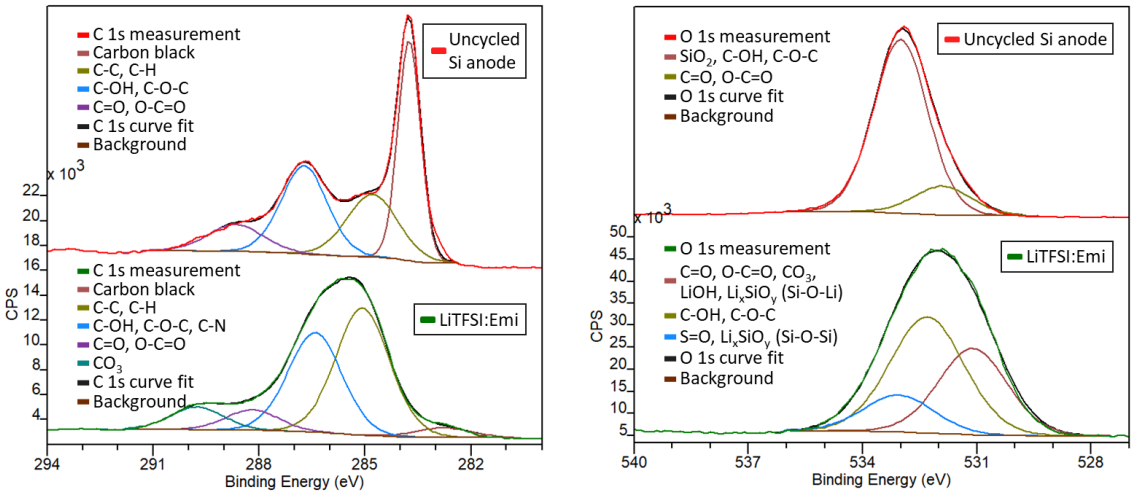

(a) C 1s

(b) O 1s

Figure 4.6: XPS spectra of (a) C 1s and (b) O 1s core peaks from an uncycled Si anode and an anode cycled in LiTFSI:Emi for one cycle.

In Figure 4.6b, the O 1s spectrum of the uncycled anode fits well with a dominating peak at 533.0 eV assigned to Si surface oxide and C-OH and C-O-C bonds [68, 72], in addition to C=O and O-C=O bonds at 531.9 eV [108]. The anode cycled in LiTFSI:Emi shows a somewhat overlapping set of peaks that are ascribed to C=O and O-C=O bonds, CO_3, LiOH, and Si-O-Li bonds in Li_xSiO_y at 531.1 eV [68, 108, 109], C-OH and C-O-C bonds at 532.3 eV [10], and Si-O-Si bonds in Li_xSiO_y and S=O bonds at 533.1 eV [109, 110].

The weak F 1s signal of the uncycled anode in Figure 4.7a is ascribed to organic F compounds at 687.9 eV [108] with an unknown origin. For the anode cycled in LiTFSI:Emi, a strong LiF peak is present at 684.9 eV [68]. The peak at 688.1 eV is assigned to the FSI and TFSI anions, in addition to their corresponding incomplete decomposition products [23].

For the N 1s core peak in Figure 4.7b, no signal is detected for the uncycled anode. The anode cycled in LiTFSI:Emi fits with peaks attributed to an unknown FSI/TFSI degradation product at 398.5 eV, undecomposed FSI/TFSI anions, C-N bonds or a degradation product related to X-ray exposure at 399.7 eV [111], and NSO_2^- components at 401.6 eV [110].

The S 2p and Si 2p spectra in Figure 4.8 are subject to spin-orbit splitting with $\Delta = 1.16$ eV and $\Delta = 0.63$ eV, respectively, and all detected components therefore have $2p_{1/2}$ and $2p_{3/2}$ peaks with a separation of Δ and the area of the $2p_{1/2}$ peak being half that of the $2p_{3/2}$ peak [108]. The $2p_{3/2}$ peak will consequently be used when referring to the position of these peaks. The S 2p spectrum for the uncycled anode fits well with a set of peaks at 167.6 eV that are ascribed to a plasmon artifact from the Si 2p orbital [112]. The anode cycled in LiTFSI:Emi have two sets of peaks corresponding to an unknown salt degradation product that might be Li_2SO_4 at 169.3 eV [113] and S=O bonds, an Si 2p plasmon effect, or an X-ray-induced degradation product at 166.7 eV [111, 112, 113].

The Si 2p spectra in Figure 4.8b show a clear reduction in the Si content for the cycled anode compared to the uncycled anode. The pristine Si anode shows two sets of peaks with Si-Si bonds at 99.4 eV and SiO_2 at 103.6 eV [72]. The spectrum of the anode cycled in LiTFSI:Emi fits well with Li_xSi components at 98.0 eV and Li_xSiO_y at 100.6 eV [72, 109].

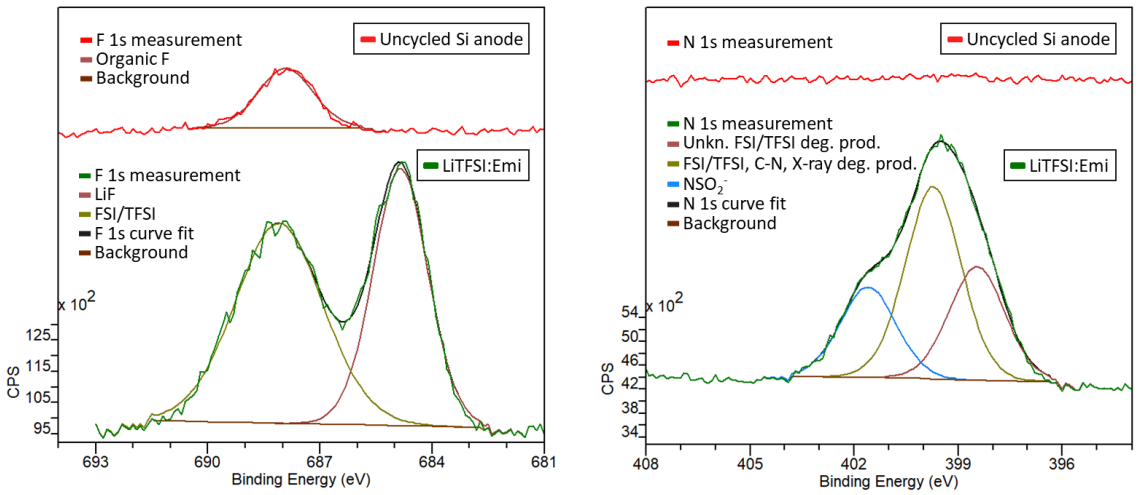

(a) F 1s

(b) N 1s

Figure 4.7: XPS spectra of (a) F 1s and (b) N 1s core peaks from an uncycled Si anode and an anode cycled in LiTFSI:Emi for one cycle.

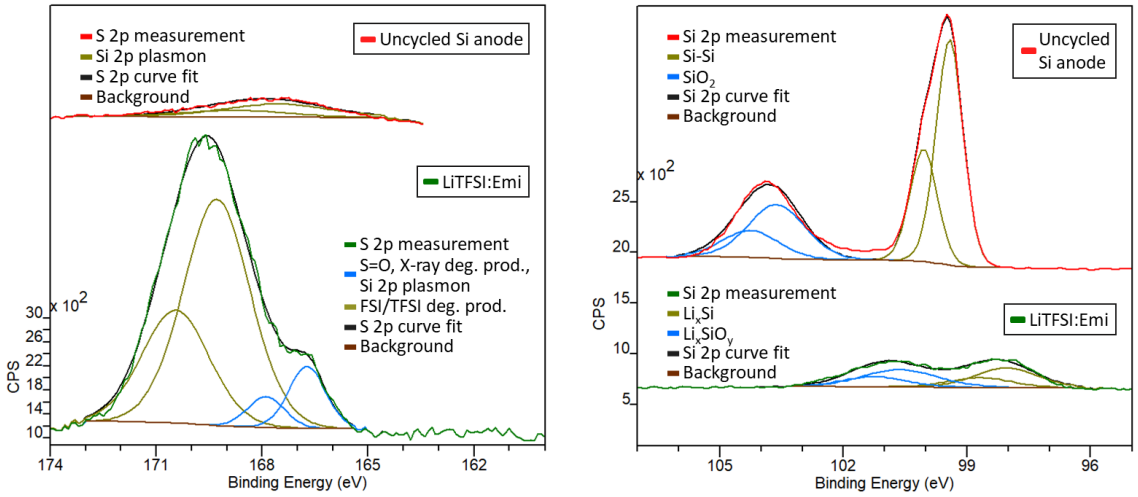

(a) S 2p (b) Si 2p

Figure 4.8: XPS spectra of (a) S 2p and (b) Si 2p core peaks from an uncycled Si anode and an anode cycled in LiTFSI:Emi for one cycle.

As the anodes cycled in LiFSI:Emi, LiFSI:Ph, and LiTFSI:Ph generally show very similar XPS spectra as LiTFSI:Emi, it is useful to compare these four sets of spectra using overlay plots to be able to distinguish subtle differences between them. Plots of C 1s and O 1s are given in Figure 4.9, F 1s and N 1s in Figure 4.10, S 2p and Si 2p in Figure 4.11, and P 2p and Li 1s in Figure 4.12. All spectra have been normalized with respect to the nearby background signal, however the background signal was already virtually identical for most peaks. Assuming that the surface roughness is similar for all anodes, it should be valid to compare the spectra both qualitatively and quantitatively.

A comparison of C 1s spectra in Figure 4.9a shows that electrolytes with $P_{111i4}FSI$ give far more C-C and C-H bonds in the SEI compared to EmiFSI, with LiFSI:Ph showing the highest peak. C=O and O-C=O bonds appear to be more present with EmiFSI electrolytes, whereas the peak ascribed to carbon black or lithiated carbon is similar for all electrolytes. The CO_3 content is higher with phosphonium electrolytes. Lastly, the part of the spectra corresponding to C single bonded to O and N may now also include C-P bonds [114]. This peak shows that LiTFSI:Ph gives the least amount of these bonds, while LiTFSI:Emi appears to give the most.

For O 1s spectra in Figure 4.9b, LiFSI:Emi gives less S=O bonds or Si-O-Si bonds in Li_xSiO_y in the SEI compared to the other electrolytes. LiFSI:Emi has a shift towards lower binding energies compared to LiTFSI:Emi. For binding energies close to C-OH and C-O-C bonds, LiTFSI:Ph has the strongest signal.

The F 1s spectra in Figure 4.10a show clear differences in the amount of LiF and FSI/TFSI components. Regarding LiF, $P_{111i4}FSI$ appears to give more LiF in the SEI than EmiFSI does and LiTFSI gives more than LiFSI. For the part of the spectra associated with FSI or TFSI anions and their incomplete decomposition products, LiTFSI gives more of these components than LiFSI in EmiFSI. For the two phosphonium ILs, the salt components are roughly equal.

The N 1s core peak presented in Figure 4.10b shows clear differences between the ILs, with far more N components being present with EmiFSI. LiFSI:Emi shows a clear shift to-

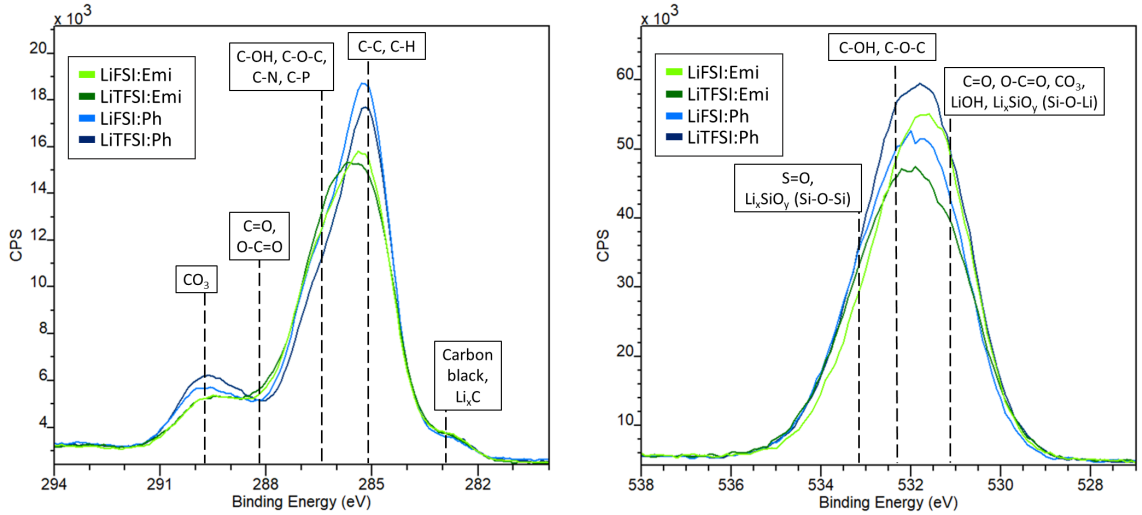

(a) C 1s (b) O 1s

Figure 4.9: XPS spectra of (a) C 1s and (b) O 1s core peaks from anodes cycled for one cycle in LiFSI:Emi, LiTFSI:Emi, LiFSI:Ph, and LiTFSI:Ph.

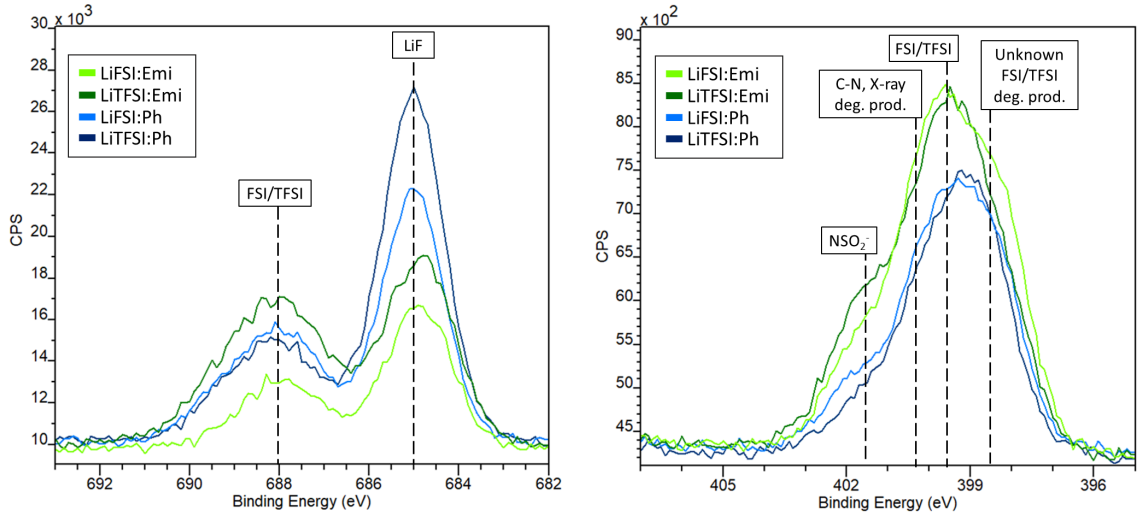

(a) F 1s (b) N 1s

Figure 4.10: XPS spectra of (a) F 1s and (b) N 1s core peaks from anodes cycled for one cycle in LiFSI:Emi, LiTFSI:Emi, LiFSI:Ph, and LiTFSI:Ph.

wards the unknown LiFSI decomposition product at 398.5 eV and LiTFSI:Emi gives more NSO_2^- components. The two $P_{111i4}FSI$ spectra are quite similar, but the shoulder of NSO_2^- components is more prominent for LiFSI:Ph.

Figure 4.11a shows that the S 2p spectra for LiTFSI:Emi, LiFSI:Ph, and LiTFSI:Ph are quite similar. The spectrum of LiFSI:Emi appears to be shifted towards lower binding energies in addition to showing significantly more S=O bonds, X-ray degradation products, or signal from the Si 2p plasmon artifact.

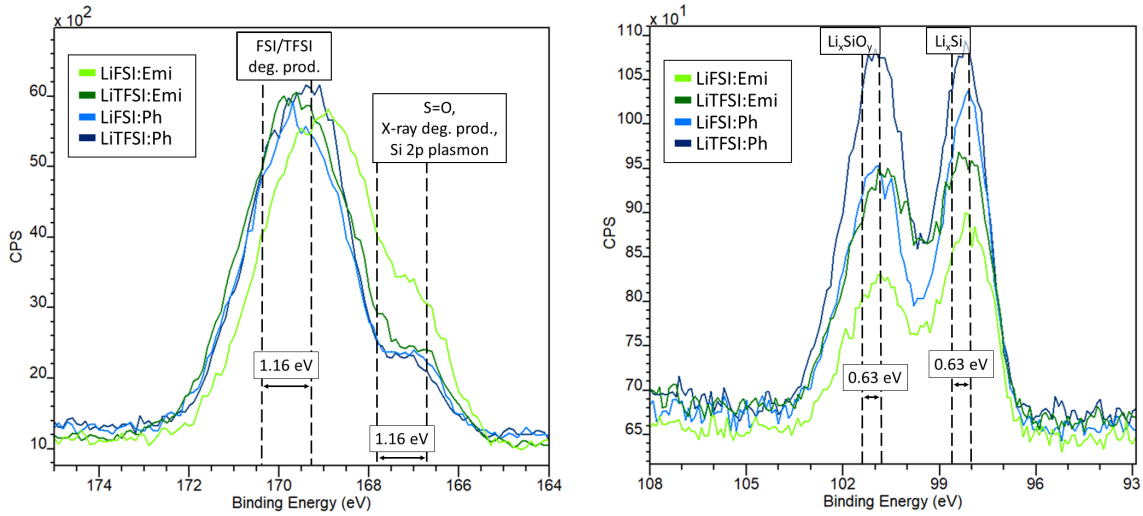

(a) S 2p (b) Si 2p

Figure 4.11: XPS spectra of (a) S 2p and (b) Si 2p core peaks from anodes cycled for one cycle in LiFSI:Emi, LiTFSI:Emi, LiFSI:Ph, and LiTFSI:Ph.

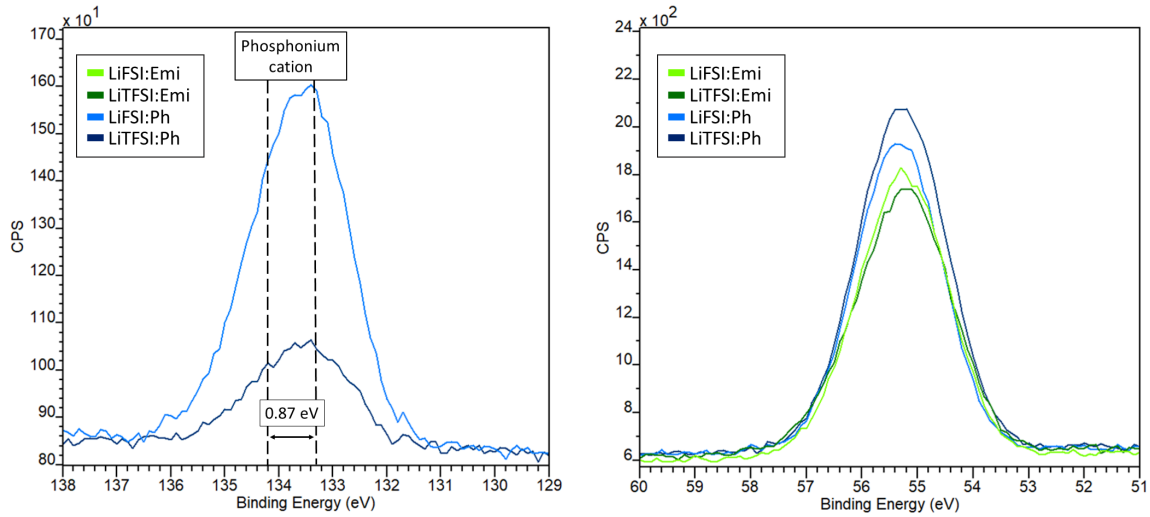

(a) P 2p (b) Li 1s

Figure 4.12: XPS spectra of (a) P 2p and (b) Li 1s core peaks from anodes cycled for one cycle in LiFSI:Emi, LiTFSI:Emi, LiFSI:Ph, and LiTFSI:Ph.

The Si 2p core peak in Figure 4.11b is largest in the LiTFSI:Ph sample. There seems to be a difference between the two Li salts, with LiTFSI giving similar amounts of Li_xSiO_y and Li_xSi, while LiFSI gives relatively more Li_xSi.

The P 2p core peak is presented in Figure 4.12a. The peaks display spin-orbit splitting with $\Delta = 0.87\,\text{eV}$ [108] and are ascribed to the undecomposed phosphonium cation [115]. A significantly larger amount of the cation appears to be incorporated into the SEI with LiFSI compared to LiTFSI. Lastly, Li 1s spectra are plotted in Figure 4.12b. The spectra are

qualitatively quite similar and have not been deconvoluted due to many possible overlapping peaks with inconsistent peak assignments in the literature. The main information to extract from this plot is the increased Li content at the surface of the anodes with the $P_{111i4}FSI$ IL.

4.3 The effect of TEP and FEC on cell performance

The average delithiation capacities of cells with LiTFSI:Emi, TEP20, TEP40, Emi:FEC, and TEP20:FEC are shown in Figure 4.13. The figure shows that the capacities are all heavily affected by the increased (dis)charge rates.

The use of TEP is first considered. TEP20 initially exhibits a quite good delithiation capacity of ∼2800 mAh/g, but shows poor rate performance compared to LiTFSI:Emi and reaches <10 % its original capacity at C/2. TEP40 initially shows a poor delithiation capacity of 1000 mAh/g that increases to 1500 mAh/g after four cycles. This increased capacity is attributed to improved wetting over time. A similar, but less pronounced increase is visible between the first and the second cycle for TEP20. TEP40 displays a poor rate performance and shows very little capacity from C/2. Comparing the first and last C/20 cycles shows that LiTFSI:Emi and TEP20 both lose some capacity, while TEP40 experience a slight increase in capacity.

The addition of FEC to the IL initially does not seem to have an impact on delithiation capacity, as LiTFSI:Emi and Emi:FEC show very similar behavior in the first four cycles. However, Emi:FEC appears to be less stable when the rate is increased and experience a more pronounced decrease in capacity than LiTFSI:Emi in C/5 and C/2. The situation reverses

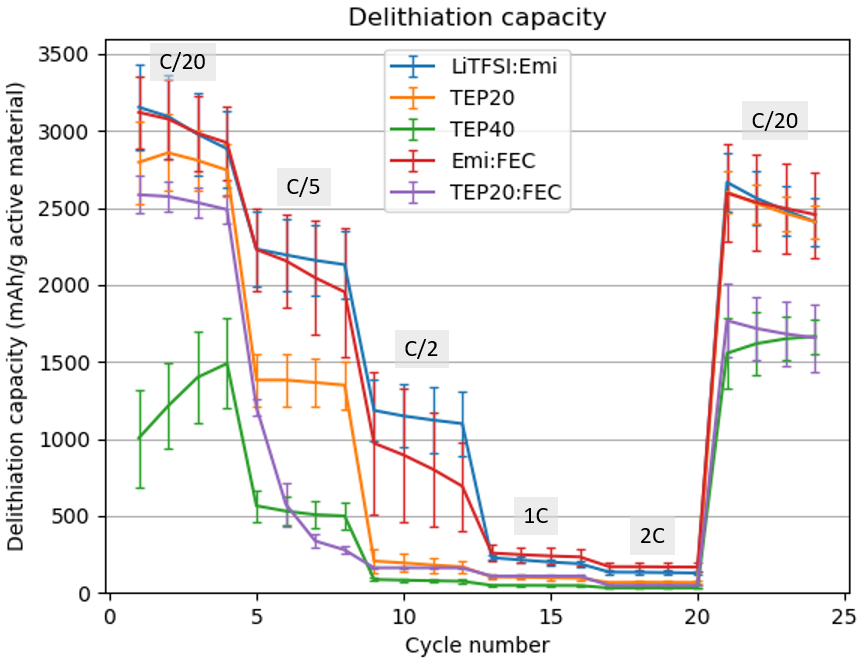

Figure 4.13: Average delithiation capacity of cells evaluating TEP and FEC as electrolyte components, showing a reduced rate capability with the addition of TEP and/or FEC.

at 1C and 2C where Emi:FEC slightly outperforms LiTFSI:Emi. TEP20:FEC displays less capacity than TEP20 for all cycles, except for 1C and 2C where they are equal. Further, TEP20:FEC has a declining capacity at C/5. In the last four cycles, TEP20:FEC has a significantly lower capacity than in the beginning, while LiTFSI:Emi and Emi:FEC experience a smaller and quite similar reduction in capacity.

A plot showing the Coulombic efficiencies of the cells is given in Figure 4.14. The figure shows that adding TEP has a devastating effect on the initial Coulombic efficiency, especially for TEP40. TEP20 has a lower Coulombic efficiency than LiTFSI:Emi for most rates and TEP40 is for the most part even lower than TEP20.

The addition of FEC decreases the initial Coulombic efficiency compared to both LiTFSI:Emi and TEP20. Though, the trend later reverses and in cycle four and the last C/20 cycles, electrolytes with FEC display higher Coulombic efficiencies than without FEC.

A distinct reduction of the Coulombic efficiency for the first cycle in a new rate is observed. This is the same behavior as seen in Figure 4.2.

Figure 4.15a shows the total lithiation capacity of cells comparing TEP and FEC. The figure shows qualitatively the same behavior as for delithiation capacities in Figure 4.13 with initial lithiation capacities between 3500 and 4000 mAh/g for all electrolytes except TEP40. The plot showing the potentiostatic hold step fractions is given in Figure 4.15b and shows that all three electrolytes containing TEP, i.e. both with and without FEC added, display an initial hold step fraction of >50 %. This immediately drops to below 20 % for TEP20 and TEP20:FEC in the following few cycles, but remains high for TEP40. Regarding TEP, both

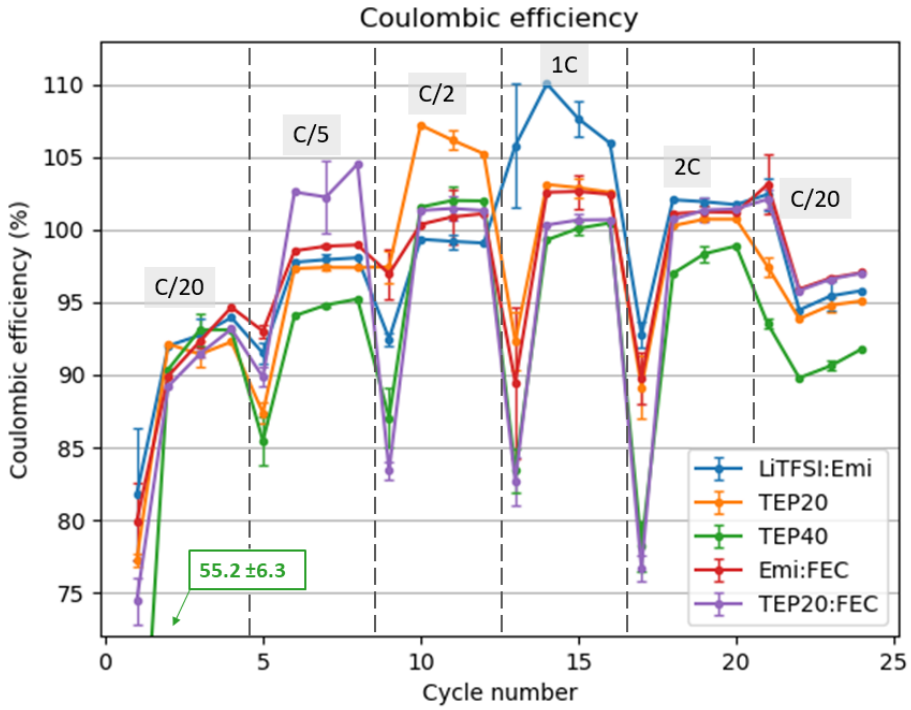

Figure 4.14: A plot of Coulombic efficiencies showing the effects of adding TEP and FEC.

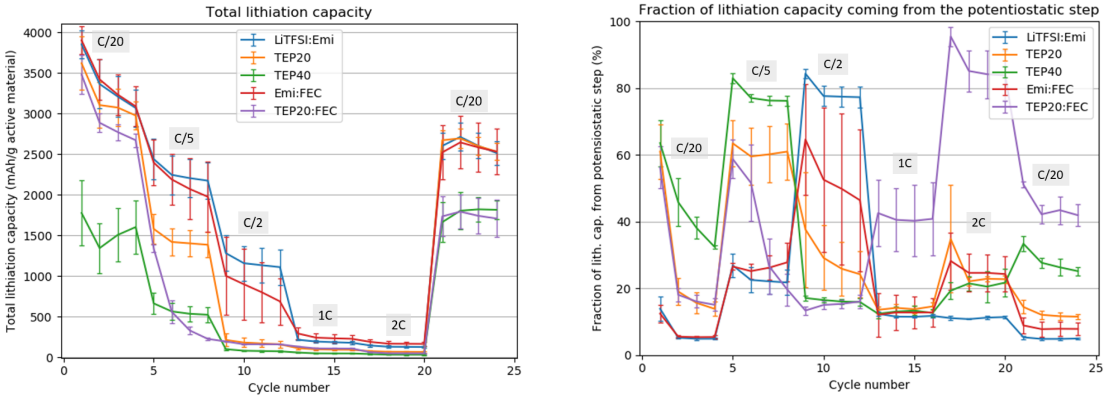

(a) Total lithiation capacity

(b) Hold step fraction

Figure 4.15: Graphs showing (a) the total lithiation capacity and (b) the fraction of the total lithiation capacity coming from the potentiostatic hold step for cells cycled in LiTFSI:Emi, TEP20, TEP40, Emi:FEC, and TEP20:FEC.

TEP20 and TEP40 have a very large hold step fraction at C/5. These drop down again at C/2, with LiTFSI:Emi now displaying the largest fraction. In the last C/20 cycles, LiTFSI:Emi displays the lowest hold step fraction of the three, followed by TEP20 and TEP40.

For the first four cycles, the hold step fraction of cells with FEC added is virtually identical to the corresponding electrolytes without FEC. Whereas TEP20:FEC exhibits a steeply decreasing hold step fraction in C/5 compared to TEP20, Emi:FEC increases slightly compared to LiTFSI:Emi. At C/2, both electrolytes show a reduced hold step fraction with FEC added, although the standard deviation is now quite large for Emi:FEC cells. In the last C/20 cycles, cells with FEC show a higher hold step fraction than cells without FEC, particularly for TEP20:FEC.

Potential vs capacity plots of the first, second, and 24th cycle of representative cells cycled in LiTFSI:Emi, TEP20, TEP40, Emi:FEC, and TEP20:FEC are shown in Figure 4.16. First, LiTFSI:Emi, TEP20, and TEP40 are considered. A comparison of cycle one in Figure 4.16a shows clear signs of a decomposition process at 2.7 V for TEP20 and 2.6 V for TEP40. Similar plateaus are not seen in the second cycle. As the amount of decomposition appears to be roughly doubled from TEP20 to TEP40, it is natural to believe that TEP itself is decomposing and this has also been reported for graphite anodes in the literature [116]. Cells with TEP20 and TEP40 lithiate with a significant overpotential compared to LiTFSI:Emi and this is especially visible for TEP40. A more detailed look at the initial decomposition in Figure 4.16b further highlights the massive decomposition of the two TEP electrolytes. Starting at ∼2.2 V, the LiTFSI:Emi electrolyte exhibits the highest capacity at this potential (prior to lithiation), assigned to reduction of the FSI/TFSI anions [23], and an increasing amount of TEP appears to give a shielding effect against salt decomposition. The reduction of the Emi cation at 2.8 V [88, 103] can be seen for LiTFSI:Emi, but a similar plateau for TEP20 and TEP40 cannot readily be seen.

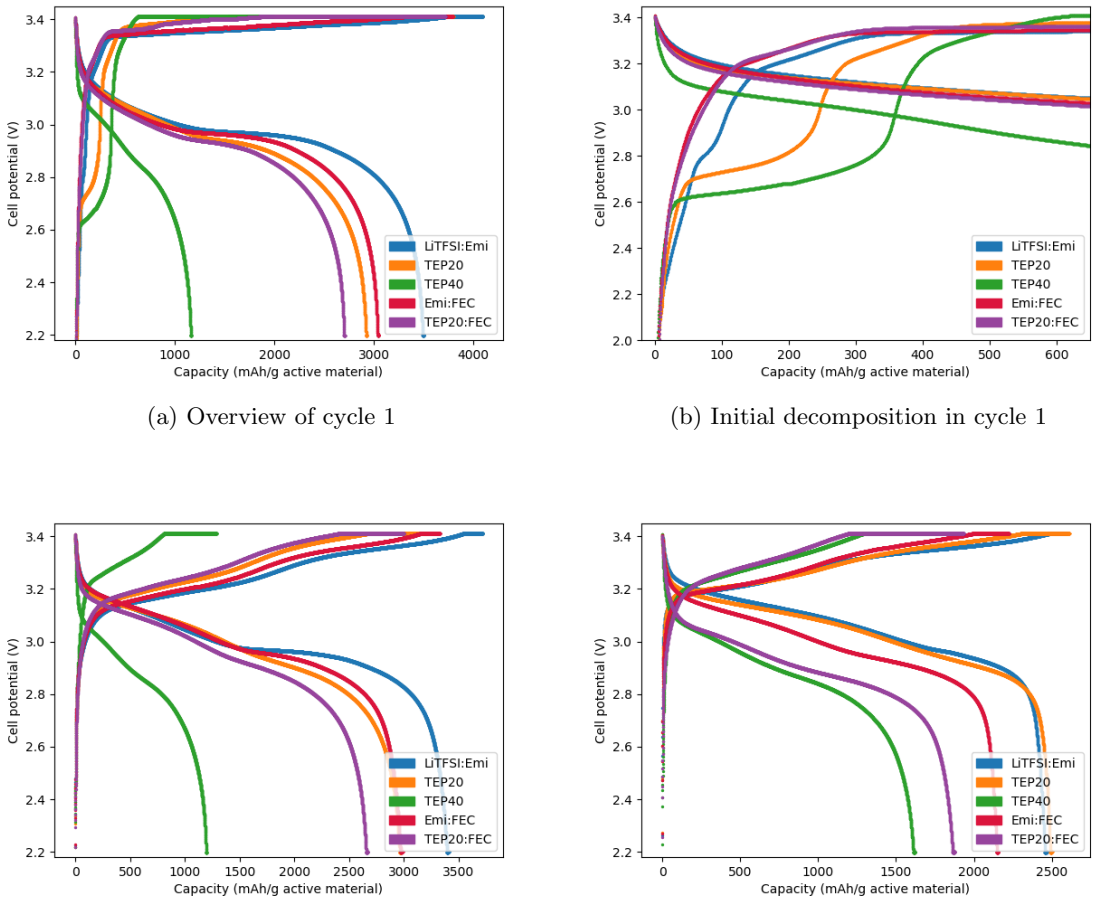

(a) Overview of cycle 1

(b) Initial decomposition in cycle 1

(c) Overview of cycle 2

(d) Overview of cycle 24

Figure 4.16: Potential vs capacity plots of representative cells from LiTFSI:Emi, TEP20, TEP40, Emi:FEC, and TEP20:FEC, showing (a) an overview of the first cycle, (b) the initial electrolyte decomposition in the first cycle, (c) an overview of the second cycle, and (d) and an overview of the last cycle.

Table 4.3: Initial electrolyte decomposition of cells with TEP and FEC measured by the capacity achieved up until a potential of 3.0 V and the number of moles of electrons corresponding to this capacity.

Electrolyte	LiTFSI:Emi	TEP20	TEP40	Emi:FEC	TEP20:FEC
Capacity (mAh/g)	99 ± 7	233 ± 24	364 ± 19	68 ± 4	65 ± 8
# mol e$^-$ (mmol)	73 ± 5	171 ± 17	267 ± 14	50 ± 3	47 ± 5

As a measure of the amount of initial electrolyte decomposition, the capacity achieved up to a potential value of 3.0 V and the corresponding number of moles of electrons involved are presented in Table 4.3. The table also includes values for Emi:FEC and TEP20:FEC.

Looking at the initial decomposition in Figures 4.16a and 4.16b, the addition of FEC

appears to suppress the decomposition of LiTFSI salt at 2.2 V and the Emi cation at 2.8 V in LiTFSI:Emi and TEP in TEP20 at 2.7 V. FEC itself decomposes at around 2.0 V [11, 31], but no large plateaus are observed at these potentials. The values for initial electrolyte decomposition presented in Table 4.3 show that both electrolytes with FEC added show less initial decomposition compared to LiTFSI:Emi. Further, Emi:FEC lithiates with a slightly larger overpotential compared to LiTFSI:Emi in the first cycle, whereas TEP20:FEC initially lithiates at a lower potential than TEP20, followed by similar potential curves after a somewhat sudden increase in potential at $\sim$1000 mAh/g. The overpotentials for delithiation appears to be slightly higher for both electrolytes with FEC compared to the corresponding electrolytes without FEC.

The increased overpotentials for lithiation for cells with FEC seem to continue in the second cycle, as seen in Figure 4.16c. The same is also true for TEP20 and TEP40 with TEP40 again showing the most extreme behavior. In the last cycle, shown in Figure 4.16d, TEP20:FEC displays a significant overpotential for lithiation compared to TEP20, while Emi:FEC lithiates quite comparably to LiTFSI:Emi. Regarding the last cycle, both electrolytes with FEC delithiate at lower potentials than their corresponding electrolytes without FEC. TEP20 lithiates at roughly the same potentials as LiTFSI:Emi, but delithiates at slightly lower potentials. TEP40 show large overpotentials for both lithiation and delithiation.

Chapter 5

Discussion

5.1 The effect of Li salts and cosolvents on electrolyte properties

From Table 4.1, it is clear that the choice of Li salt has a direct impact on the electrolyte resistance of a cell with an increased value of R_{el} when LiTFSI is used being seen for both P_{111i4}FSI and EmiFSI. These findings qualitatively match the relation between ionic conductivities of LiFSI:Emi, LiTFSI:Emi, [27] and LiFSI:Ph [85]. Regarding LiTFSI:Ph, a reduced ionic conductivity with LiTFSI compared to LiFSI has previously been demonstrated in both carbonate [20] and EmiFSI electrolytes [27] and it was expected that LiTFSI:Ph would show a higher value of R_{el} than LiFSI:Ph.

The comparison of ionic conductivities using electrolyte resistances is based on Equation (2.5) and an assumption that the area of the electrode and the thickness, porosity, and tortuosity of the separator are equal for all cells tested. More generally, the cells are regarded to be identical except for the electrolyte that was used. As the electrodes and separators were pre-made in sheets and cut using high-precision tools, the validity of these assumptions is regarded as good. Electrolyte decomposition products could potentially block pores in the separator and affect its porosity or cover the electrode surface and thereby alter the resistances in the cell, but the EIS measurements used high frequency currents of >1 kHz and were taken before cycling, thereby minimizing this effect. It should be noted that the standard deviation is rather large for some of the measurements, but a clear trend in differences between the two salts can nevertheless be seen. The variation in cell resistivity is believed to be related to the pouch cells themselves. The positioning of the electrode stack within the cell was done by hand and as the pressure was most likely not completely even across the PVC pressure plates, the resulting pressure differences might have affected cell performance. As a final comment, these EIS measurements do not account for the transport number of Li^+ which would be an important piece of information to further quantify the relevant transport phenomena in the cell.

The visually observed differences in viscosity between LiFSI and LiTFSI qualitatively agree with values found in the literature [27, 85]. The viscosity is known to have a major impact on ionic conductivity [16] and there is a correlation between observed viscosities and measured values of R_{el} for both Li salts in EmiFSI and P_{111i4}FSI. For EmiFSI, the mobilizing effect of FSI anions on Li^+ from the bulk electrolyte to the surface, as suggested by Yamagata

et al. [88], may also be a contributing factor to the improved ionic conductivity of LiFSI:Emi.

Surprisingly, the observed viscosities do not match R_{el} for cells when TEP is added. It would be expected that the reduced viscosity of TEP20 and TEP40 compared to LiTFSI:Emi would result in an improved ionic conductivity. TEP20 does indeed give a reduced electrolyte resistance compared to LiTFSI:Emi, however TEP40 gives a sudden *increase* of R_{el}. A possible explanation for this behavior is now presented.

The dielectric constant of a solvent is often used as a measure of its ability to dissolve the Li salt [16]. In carbonate electrolytes, EC is a key component due to its high dielectric constant ($\epsilon = 90.4$) [117]. TEP has a low dielectric constant ($\epsilon = 13.1$) [95] and it is therefore possible that the negative effect on ionic conductivity of reduced Li salt solvation for TEP40 outweighs the positive effect of a reduced viscosity, whereas the lower ratio of TEP to IL in TEP20 gives a sufficient salt solvation, making the beneficial effect of the viscosity the dominant factor.

It should be noted that the dielectric constant for EmiFSI is reported to be $\epsilon = 6.3$, which initially contradicts the idea of poor salt solubility with TEP as an explanation for the reduced ionic conductivity. However, the use of the dielectric constant to evaluate solvation in ILs is problematic. First of all, the dielectric constant of an IL cannot be measured by conventional methods due to its electrical conductance and alternative measurements methods, usually involving a measurement of the frequency-dependent dielectric permittivity and subsequent extrapolation to zero frequency, often give varying results [118, 119]. The reported value of $\epsilon = 6.3$ may therefore not reflect the true dielectric constant for EmiFSI. Second, and perhaps more important, the dielectric constant is not an appropriate measure of the polarity and solvation properties of an IL due to the fundamental electrochemical differences between ILs, that are purely ionic in nature, and conventional solvents [120]. Alternative parameters to quantify polarity and solvation parameters have been developed, and these accredit ILs with better solvation properties than their dielectric constants would indicate [119].

Lastly, a brief comment on the use of TMMP will be given. TMMP was not miscible with EmiFSI, neither at 15 nor 25 wt%. Testing a lower content of TMMP than 15 wt% would not be too interesting as TMMP cannot significantly alter the bulk electrolyte viscosity if its concentration gets too low. Previously, TMMP has been shown to be soluble for at least a concentration of 50 vol% in an EC:DEC (10:90 vol%) electrolyte [98] and its solubility in pure EC or DEC exceeds 75 vol% [97]. There are several reports regarding the miscibility of ILs with organic solvents, but none exist for TMMP and EmiFSI. In general, though, the miscibility gap of an IL and a solvent, i.e. concentrations for which a mix of the two components exists as two or more phases, is asymmetrical with a higher solubility of the solvent in the IL than vice versa [119]. This general trend would indicate that TMMP should not be expected to be miscible with EmiFSI for any immediate concentrations above 25 wt% TMMP. The unsuccessful mixing of the two liquids shows that TMMP cannot readily be used as a cosolvent with EmiFSI at these concentrations, however the two might be miscible at significantly higher concentrations and TMMP might be an appropriate cosolvent for other ILs.

5.2 The effect of Li salts on cell performance and SEI formation

5.2.1 The effect of LiFSI and LiTFSI on cell capacity, rate performance, and electrolyte decomposition

Initial remarks

In this work, the analysis of voltage profiles is based on an assumption that the LFP cathode displays a perfectly flat voltage plateau at 3.45 V vs Li/Li^+. Based on properties of LFP discussed in Section 2.2.2, it is clear that this is not the case for very lithiated and delithiated states. The cathodes used in this work are capacitively oversized compared to the Si anode, meaning that they would not be fully delithiated when the cell was charged. Further, the Coulombic efficiency of the first cycle is quite far below 100 %, indicating that a substantial fraction of the Li extracted from the cathode never returned after delithiation. The LFP would therefore for the most part exist in intermediate states of lithiation and thus not contribute significantly to the evolution of the voltage profiles. The only exception would be the beginning of the very first charge cycle, but the contribution of LFP to the voltage profiles would be equal for the different electrolytes and it is therefore not assumed that LFP has affected the voltage profile analysis by much.

The molar percentages of ions in the electrolytes are given in Table 5.1. The table shows that in electrolytes with LiTFSI, the FSI anion from the ionic liquid is still the dominating anion species. However, treating the different ions in the system just based on their molar percentages might not be appropriate as little is known about changes to the solvation structure upon addition of TFSI and FSI salts. Considering that Li^+ is believed to be preferentially solvated by TFSI anions [86], this could imply that the activity of Li^+ differs between electrolytes with mixed anions and only FSI^- present, which will also affect the SEI formation. The contribution of the TFSI anion to phenomena in the cell might therefore be greater than what its molar percentages in Table 5.1 would indicate.

Table 5.1: The molar percentages of ions present in LiFSI:Emi, LiTFSI:Emi, LiFSI:Ph, and LiTFSI:Ph calculated from the amount of the components added during mixing of the electrolytes.

Electrolyte	LiFSI:Emi	LiTFSI:Emi	LiFSI:Ph	LiTFSI:Ph
Li^+	8.7 %	8.7 %	9.7 %	9.6 %
Emi^+	41.3 %	41.3 %	-	-
$P_{111i4}{}^+$	-	-	40.3 %	40.4 %
FSI^-	50.0 %	41.3 %	50.0 %	40.4 %
$TFSI^-$	-	8.7 %	-	9.6 %

Cell capacity

LiFSI and LiTFSI have different effects on cell performance, as evident from results presented in Section 4.2.1. As seen in Figure 4.1, LiFSI:Emi achieves delithiation capacities of ∼2650 mAh/g at C/20 and ∼2150 mAh/g at C/5 that match well with a previously reported ∼2500 mAh/g capacity at C/10 [18]. However, the capacity of LiFSI:Emi within a given rate

is not particularly stable and the capacity drops to 2250 mAh/g during the last C/20 rate, i.e. not exhibiting the stable performance shown in the literature. This can also be seen from Figure 4.2, where, apart from the very first cycle involving SEI formation, LiFSI:Emi achieves Coulombic efficiencies lower than 96 % at both C/20 rates.

The initial and final delithiation capacity of LiTFSI:Emi is greater than that of LiFSI:Emi. This is opposite to what has been shown for graphite anodes by Matsui et al. [27], where the LiFSI salt yielded a slightly greater initial capacity than LiTFSI. As a LiTFSI:Emi electrolyte with a "pure" Si anode has not previously been reported in the literature, it is interesting to see that the effect of the Li salt on initial capacity appears to be opposite for Si anodes compared to graphite. Further, LiTFSI:Emi experience approximately the same reduction in capacity as LiFSI:Emi between the first and the last C/20 rate and the Coulombic efficiencies at C/20 are also quite poor (∼96.0 % for the last cycle), just slightly better than for LiFSI:Emi (∼95.5 % for the last cycle).

Regarding $P_{111i4}FSI$ in Figure 4.1, LiFSI:Ph exhibits a ∼2700 mAh/g capacity at the last C/20 rate. This is lower than achieved by Kerr et al. [21], where cells with LiFSI:Ph displayed a capacity of 3000 mAh/g after 300 cycles at C/2.5, though with a high salt concentration of 3.2 M. LiTFSI yields lower initial delithiation capacities than LiFSI. The hold step fraction (Figure 4.3b), voltage profile (Figure 4.4a), and electrolyte resistance measurements (Table 4.1) indicate that a substantial overpotential associated with LiTFSI:Ph might be the reason for its initial capacity being lower than LiFSI:Ph. Comparing the last C/20 rate (Figure 4.1) to the first cycles shows that both phosphonium electrolytes experience a very little reduction of capacity during the rate test compared to EmiFSI. This is also in agreement with a generally better Coulombic efficiency for $P_{111i4}FSI$ than EmiFSI at most rates.

Although the loss of capacity between the two C/20 rates seem to correlate with overall Coulombic efficiencies when comparing the two ionic liquids, the differences in Coulombic efficiency between the two Li salts in the last C/20 rate are not so easily explained. As seen from Figure 4.1, LiFSI:Ph experience a larger loss in capacity during the last C/20 rate than LiTFSI:Ph. Conversely, LiTFSI:Emi decreases more than LiFSI:Emi. This could be explained by LiFSI:Ph and LiTFSI:Emi initially having higher capacities than LiTFSI:Ph and LiFSI:Emi, respectively, which would indicate more capacity loss related to expansion of Si particles. The expansion and subsequent cracking of Si particles can promote electrolyte decomposition, however, this is not reflected in Coulombic efficiencies in Figure 4.2 where the Coulombic efficiency is slightly greater for LiFSI:Ph and LiTFSI:Emi than for LiTFSI:Ph and LiFSI:Emi, respectively. Cracking of Si particles can also lead to isolation of active material, a loss mechanism that would not necessarily yield a reduced Coulombic efficiency. Either way, the Coulombic efficiency and stability of the capacity in the last C/20 rate indicate that there are only minor differences between the two Li salts and that the choice of IL has a greater impact on the stability of cell capacity at low rates.

Lastly, an initially increasing delithiation capacity can be seen for both phosphonium electrolytes in Figure 4.1. This has previsouly been related to improper electrode wetting with a LiFSI:Ph electrolyte by Kerr et al. [21]. In their case, the initial capacity drops drastically during the first few cycles and gradually improves over the following ∼200 cycles. In this work, however, the phenomenon of increasing capacities appears to be "finished" after 24 cycles.

Rate performance
As seen in Figure 4.1, LiFSI yields better rate performance than LiTFSI in both EmiFSI and P_{111i4}FSI. Further, EmiFSI electrolytes clearly outperform P_{111i4}FSI. The improved rate performance of LiFSI:Emi compared to LiTFSI:Emi qualitatively match previous results using graphite anodes [27]. However, the poor 200 mAh/g capacity for LiFSI:Emi at 2C in this work does not coincide with previous results showing 1200 mAh/g at the same rate [11]. Similarly, the rate performance of LiFSI:Ph is worse than what can be found in the literature, with a >1000 mAh/g capacity at 1C reported by Kerr et al. [21] vastly exceeding the ∼100 mAh/g at 1C seen in Figure 4.1.

Continuing on the discussion of improved rate performance with LiFSI compared to LiTFSI; it is natural to believe that this is related to lower viscosities and higher ionic conductivities associated with LiFSI. Rate performance is intimately connected with overpotentials in the cell and EIS measurements (Table 4.1) showed that the electrolyte resistance, one important source of overpotentials in the cell, was higher for LiTFSI than for LiFSI. For the phosphonium electrolytes, hold step fractions and voltage profiles correlate well with R_{el} and show significantly larger overpotentials for LiTFSI than LiFSI at C/20. The picture is slightly more complicated with EmiFSI. Here, hold step fractions with LiFSI and LiTFSI are very similar, although slightly lower for LiFSI at most rates. The voltage profiles also behave quite similarly and it is hard to distinguish overpotentials between LiFSI and LiTFSI.

Electrolyte decomposition
Electrolyte decomposition processes can be evaluated with a combination of Coulombic efficiency plots in Figure 4.2 and the initial part of the voltage profiles of the first cycle, as seen in Figure 4.4b. LiFSI:Emi displays a lower Coulombic efficiency than LiTFSI:Emi for the first cycle. With an underlying assumption that all irreversible capacity loss directly contributes to the SEI layer, this means that the initial SEI layer is thicker when LiFSI is used. This assumption might not be entirely appropriate as some Li is likely trapped within the bulk Si after delithiation and a possible indication of this can be seen from Figure 4.4a where the voltage plateau related to delithiation of a-$Li_{2.0}$Si to a-Si in the first cycle appears to be comparably narrower for LiFSI:Emi than for LiTFSI:Emi, indicative of some Li remaining in the Si particles.

The voltage profiles in Figure 4.4b clearly show more decomposition at 2.15 V (attributed to the Li salt) and 2.8 V (Emi^+ reduction) for LiTFSI:Emi than for LiFSI:Emi. If the assumption of a Coulombic efficiency below 100 % being attributed solely to SEI formation is to be used, more decomposition of LiFSI:Emi should occur at higher potentials, alongside lithiation, for it to display the thickest SEI layer after the first cycle. The Coulombic efficiency in later cycles continues to be lower for LiFSI:Emi than LiTFSI:Emi, without it appearing to have a significant effect on the evolution of voltage profiles, hold step fractions, or delithiation capacities in later cycles. LiFSI is known to be chemically less stable than LiTFSI [23] and although LiTFSI:Emi gives more decomposition than LiFSI:Emi at 2.15 V in the first cycle, which also has been reported in the literature [23], LiFSI:Emi seems to give more decomposition at low and high cell potentials in the first cycle, in addition to a the lower Coulombic efficiency in later cycles.

For LiTFSI:Emi, Figure 4.4b shows a plateau in the voltage profile at 2.8 V attributed to decomposition of Emi cation [88, 103], whereas only a slight tilt of the voltage profile is seen for LiFSI:Emi. The decomposition of Emi^+ when the TFSI anion is present fits perfectly with the

double-layer model proposed by Yamagata et al. [88] that was discussed in Section 2.4.3. The FSI anions in LiFSI:Emi appear to effectively suppress reduction of Emi^+ and the presence of even just 8.7 mol% TFSI anions (Table 5.1) is apparently enough to greatly alter the shielding properties of the FSI anion. Though, as previously mentioned, the activity of FSI and TFSI anions might not be the same, which could make the "effective" concentration of TFSI anions greater than 8.7 mol%. The double-layer model was made for a graphite anode and it was suggested by Matsui et al. [27] that it would also be appropriate for Si anodes. As it seems that a Si anode has never been tested with a LiTFSI:Emi electrolyte before, it is noteworthy that this model indeed seems to apply also for Si anodes.

The voltage profiles of the two P_{111i4}FSI-based electrolytes in Figure 4.4b show no signs of a voltage plateau that can be attributed to the decomposition of the phosphonium cation. This possible lack of cation decomposition fits well with electrochemical reduction of $P_{111i4}{}^+$ supposedly taking place at -0.1 V vs Li/Li^+ [85]. The SEI layer is not necessarily void of phosphonium-related components, though, as Girard et al. [115] have shown through a combination of FTIR and XPS that undecomposed P_{111i4} cations can be incorporated into the SEI, at least for Li metal anodes.

The decomposition at 2.15 V in Figure 4.4b attributed to decomposition of the Li salts is also present for the phosphonium electrolytes. Again, significantly more decomposition occurs with LiTFSI than LiFSI. The phosphonium electrolytes seem to give slightly less salt decomposition than EmiFSI, but the reason for this is unknown. Further, the generally better Coulombic efficiency of P_{111i4}FSI compared to EmiFSI would indicate that the SEI grows more over time with EmiFSI electrolytes, at least as long as the aforementioned assumption of irreversible capacity loss only being attributed to SEI formation is employed. The hold step fractions and overpotentials in voltage profiles for cycle 24 show reduced differences between the two ILs compared to cycle 2. As the electrolyte can be assumed to be constant during cycling, this should mean that this behavior can be attributed to the electrode, with a thicker SEI layer over time with EmiFSI being a possible explanation. Lastly, it should be noted that what appears to be a higher degree of delithiation being achieved with P_{111i4}FSI in Figure 4.4d could affect hold step fractions and overpotentials seen from voltage profiles, but it is not known to which extent this would happen.

Closing remark

As an ending to this section, a short discussion on a notable feature of the electrochemical data is given, namely that a drastically different Coulombic efficiency is seen for the first cycle of a new rate. The Coulombic efficiency decreases when the rate is increased and increases when the rate is lowered. Comparing the lithiation capacity in Figure 4.3a to the delithiation capacity in Figure 4.1 shows that the reduced Coulombic efficiency is due to a better lithiation capacity in the first cycle of a new rate and not due to a reduced delithiation capacity. The Coulombic efficiency of a rate test is typically not reported in the literature and the origin of this effect is not known, but that does not mean that a few thoughts on the matter cannot be shared.

As delithiation of Si has been shown to be faster than lithiation [121], differences in (de)lithiation rates are unlikely the cause of the observed effect on the Coulombic efficiency. A plausible explanation can instead be related to inhomogeneous lithiation. When a higher rate is employed, the asymmetry in Li concentration at the surface compared to the core increases. It could therefore be the case that the surface experiences more Si expansion and

subsequent surface cracking and electrolyte decomposition when the rate is increased. In the next cycle, the surface is "already cracked" and much less electrolyte decomposition occurs, thus giving a stable Coulombic efficiency which does not change much until more cracking occurs the next time the rate is increased. Furthermore, the increased Coulombic efficiency observed upon lowering the rate might be related to trapped Li in the electrode being released when the rate is lowered.

5.2.2 Characterization of SEI layers with XPS

Discussion on energy calibration and the deconvolution process

Peaks in the XPS survey spectra were assigned to core peaks of different elements using the build-in Kratos Element Library in the CasaXPS software. Energy calibration for the uncycled Si anode was done using C-C and C-H bonds in adventitious carbon at 284.8 eV as a reference [101]. This method is far from perfect as the peak position has been reported to vary by as much as 1.44 eV [105], but it is still the most commonly used energy referencing procedure for samples that have been exposed to air. The Si 2p core peak was not shifted as the main peak was already positioned at 99.4 eV, the expected position for bulk Si [72]. This was a sign of a vertical differential charging phenomenon between the SEI layer and the underlying Si particles which probably have distorted the signal and broadened the peaks somewhat [122].

For the four cycled anodes that had not been exposed to air, a holistic referencing approach was used based on the expected peak positions of LiF, Na compounds, carbon black, and C-C bonds. The four cycled anodes had been positioned in a similar fashion on the same sample holder and tested during the same XPS session and it is therefore expected that they should require a similar energy shift.

Some comments on the deconvolution process of core peaks are now given. First, the deconvolution process of core peaks involve a high degree of user input with position, full width at half maximum, and number of peaks greatly affecting the output. As a measure to cope with this uncertainty, very closely positioned peaks, such as C-N and C-OH/C-O-C in C 1s, have generally been combined into *one* larger peak.

Second, the C 1s core peak of the uncycled anode is fitted with four peaks ascribed to carbon black, C-C and C-H bonds, C-OH and C-O-C bonds, and C=O and O-C=O bonds and is very similar to the spectrum of a similar Si anode presented by Philippe et al. [72]. They attribute the peaks of carbon bonded to oxygen solely to the CMC binder, but the exposure to air is also a likely contributor [105].

Third, as seen from Figures 4.6a and 4.9a, the C 1s spectra of the cycled anodes display signal at ∼290 eV that has been attributed to CO_3. As there are no immediate sources of carbonate components in the electrolyte, this peak is believed to most likely be an effect of the DMC washing step in the sample preparation before XPS.

Fourth, the O 1s overlay plots in Figure 4.9b indicate that neither electrolyte gives the common SEI component Li_2O which would be positioned at ∼528.4 eV [72].

Fifth, the peak associated with FSI and TFSI anions in F 1s plots (Figures 4.7a and 4.10a) have two possible origins. They may stem from undecomposed salt or partially decomposed salt components being incorporated into the SEI layer or from electrolyte residues left on the surface even after washing with DMC.

Sixth, the doublets at 166.7 eV in the S 2p core peak (Figure 4.11a) are assigned to S=O

bonds, an Si 2p plasmon effect, and an X-ray-induced degradation product. The cycled anode only contains ∼1 at% Si at the surface and the contribution of the plasmon effect to the peak at 166.7 eV is therefore probably quite small. In addition, the sample with LiFSI:Emi contains less Si compounds than LiTFSI:Emi (Table 4.2), but has a more pronounced shoulder at 166.7 eV, further indicating that the plasmon effect is not a major contributor.

Lastly, it should be noted that the peak at ∼688 eV in F 1s plots may also be attributed to CF_3 compounds [123], however the lack of the characteristic CF_3 peak at ∼294 eV in C 1s [108] rules out this possibility. The lack of CF_3 components in LiTFSI:Emi and LiTFSI:Ph is surprising as LiTFSI is known to yield CF_3 with both EmiFSI and carbonate electrolytes and with graphite and Li metal anodes due to easier cleavage of the C-S bond than the C-F bond in LiTFSI [123, 124]. It may be the case that CF_3 reacts further with nearby Li ions to yield LiF [125] as both LiTFSI:Ph and LiTFSI:Emi show more LiF than the corresponding electrolytes with LiFSI. Furthermore, the absence of CF_3 is an indication that there is very little salt residue from the electrolyte on the sample surface.

Comparison of survey spectra and atomic composition of the surface

Survey spectra in Figure 4.5 and the corresponding atomic percentages of the surface in Table 4.2 show that some Si signal is still seen for the cycled anodes. Although atomic percentages based on survey spectra are not accurate measurements, the remaining Si signal can give an indication of the thickness of the SEI layer, or more generally of the covering effect of the SEI because its thickness might not be uniform. Both $P_{111i4}FSI$ electrolytes give more Si signal than EmiFSI, in agreement with electrochemical results showing a thicker SEI with EmiFSI.

In terms of the N 1s peak, the clear presence of nitrogen compounds in LiFSI:Ph and LiTFSI:Ph seen from Table 4.2 and the lack of any nitrogen in the uncycled anode is indicative of a decomposition of the FSI or TFSI anions in the phosphonium electrolytes. Both electrolytes with EmiFSI give more nitrogen-containing compounds than with $P_{111i4}FSI$, in addition to more sulphur compounds. However, the difference between EmiFSI and $P_{111i4}FSI$ is larger for N 1s than for S 2p. This is most likely related to decomposition of the Emi cation which was also concluded from voltage profiles in Figure 4.4b. Both EmiFSI electrolytes contain more sulphur than LiFSI:Ph and LiTFSI:Ph which would indicate more anion decomposition, however F 1s does not confirm this trend, particularly for LiFSI:Emi which contains a smaller amount of fluorine than the other electrolytes.

All cycled anodes contain a large amount of oxygen. Oxygen is present in a 2:1 ratio with sulphur in both FSI and TFSI anions, but O 1s accounts for much more than twice the atomic percentage of the surface compared to S 2p. This means that there must be another source of oxygen in the samples, with the surface oxide layer on Si being a likely source as Li_xSiO_y is known to be a part of the SEI on Si anodes [72].

Further, LiFSI typically contains chlorine impurities as it is a byproduct of the production process of the salt [83]. The lack of chlorine signal in LiFSI:Emi and LiFSI:Ph is a sign of the LiFSI salt being of high quality.

The Li 1s core peak is often not included in articles showing XPS results. The Kratos Element Library in CasaXPS lists Li 1s with a very low relative sensitivity factor of 0.025 (relative to F 1s), meaning that it has a small peak in the XPS spectrum that can easily give distorted values of atomic percentages. Roughly 1/4 of the surface is attributed to Li.

5.2.3 The effect of LiFSI and LiTFSI on the SEI layer

Although regarded to provide good fits of the XPS spectra, the deconvolution of core peaks in Figures 4.6 to 4.8 cannot be regarded to be exact. The hard task of performing a perfect deconvolution was the main motivation to instead present XPS data of the cycled anodes as overlay plots, as done in Figures 4.9 to 4.12. These overlay plots, in combination with survey spectra, the corresponding atomic composition at the surface, and electrochemical data, are now used to evaluate the effects of LiFSI and LiTFSI on the SEI layer on Si anodes.

Results from XPS analysis seem to generally support the double-layer model for LiFSI:Emi and LiTFSI:Emi presented by Yamagata et al. [88]. First, the C 1s spectrum in Figure 4.9a shows a shift towards C-OH, C-O-C, and C-N bonds for LiTFSI:Emi compared to LiFSI:Emi. As LiFSI:Emi in the O 1s spectrum in Figure 4.9b generally shows a higher peak at energies corresponding to carbon single and double bonded to oxygen than LiTFSI:Emi does, C-N bonds is assumed to contribute to the shift in the C 1s spectrum for LiTFSI:Emi. More C-N bonds indicate more cation decomposition, in line with the double-layer model. The same conclusion cannot be drawn from C-N bonds in N 1s (Figure 4.10b), however the effect of the unknown X-ray degradation product in N 1s could be an explanation as to why the relative amounts of C-N bonds in LiFSI:Emi and LiTFSI:Emi do not match between C 1s and N 1s. An identical double-layer model cannot be transferred to the phosphonium electrolytes as the P 2p core peak in Figure 4.12a shows drastically more phosphonium cations being incorporated into the SEI for LiFSI:Ph than for LiTFSI:Ph.

A possible consequence of Emi cations contributing more to the SEI layer with LiTFSI:Emi is that LiFSI:Emi should contain more decomposition products from the salt/FSI anions. More of the unknown salt degradation product in N 1s and more S=O bonds in S 2p with LiFSI:Emi than LiTFSI:Emi support this hypothesis, but less NSO_2^- in N 1s, slightly less salt-related compounds in S 2p and less fluorine compounds in F 1s, both LiF and salt-related compounds, disagree and indicate more salt decomposition for LiTFSI:Emi. For F 1s, though, this might be affected by LiTFSI having three times as many F atoms as LiFSI.

There is a larger contribution of the phosphonium cation to the SEI for LiFSI:Ph than for LiTFSI:Ph, and this can also be seen in C 1s (Figure 4.9a) with more C-C and C-H bonds being present for LiFSI:Ph, in addition to more signal from binding energies that can in part be attributed to C-P bonds. Why P_{111i4}^+ contributes more to the SEI without LiTFSI present is unknown. One possibility could be that the incorporation of the phosphonium cation in the SEI occurs after the cell voltage has passed 2.15 V. At this point, significant decomposition of (salt) anions in LiTFSI:Ph has already occurred which might prevent the incorporation process of the cation. Another possibility is that the SEI formed with LiFSI:Ph is more porous as it contains less LiF, thereby allowing more phosphonium cations to be trapped within the porous structure.

The composition of the various peaks that so far have been referred to as "(unknown) salt degradation products" is now given some attention. Several decomposition mechanisms of FSI and TFSI anions have previously been shown in the literature, usually involving radical-containing intermediate products [81, 112, 115, 126, 125]. A possible reduction mechanism of FSI^- involves breaking of the S-F bonds [115, 126]:

$$N(SO_2F)_2^- + e^- \longrightarrow N(SO_2F)_2^{2-\bullet} \longrightarrow SO_2NSO_2F^{-\bullet} + F^- \xrightarrow{+e^- + 2Li^+} O_2NSO_2^- + 2\,LiF$$

The S-N bond may also be broken [126] to yield:

$$N(SO_2F)_2^- + e^- \longrightarrow NSO_2F^{-\bullet} + SO_2F^{-\bullet} \xrightarrow{+2e^- + 2Li^+} NSO_2^- + SO_2^{-\bullet} + 2\,LiF$$

Decomposition of the TFSI anion usually proceeds via a cleavage of the S-N bond [81]:

$$N(SO_2CF_3)_2^- + e^- \longrightarrow N(SO_2CF_3)_2^{2-\bullet} \longrightarrow NSO_2CF_3^{-\bullet} + SO_2CF_3^-$$

These CF_3-containing (intermediate) products may then decompose further to yield LiF [125].

The exact decomposition mechanisms of LiFSI and LiTFSI in this work are not known, however it is clear that many of the reactions release F^- that form LiF, explaining the high LiF content seen in XPS data. The "(unknown) salt degradation products" showing up in XPS results are attributed to the myriad of compounds containing S, N, O, and F that form in addition to LiF.

LiF is believed to yield a SEI layer that promotes structural stability of the SEI [70] and supports rapid transport of Li^+ through grain boundary diffusion, especially when Li_2CO_3 is present [32, 127]. LiTFSI appears to give more LiF than LiFSI. Both anodes cycled in phosphonium electrolytes contain more LiF (Figure 4.10a) and show better Coulombic efficiencies than EmiFSI, a sign of a more stable SEI. However, LiTFSI:Ph has a SEI with more LiF than LiFSI:Ph does, but shows a lower Coulombic efficiency. The possible benefits on cell performance of more LiF in the SEI is generally believed to be outweighed by increased viscosity and reduced ionic conductivity in the bulk electrolyte with LiTFSI compared to LiFSI and with P_{111i4}FSI compared to EmiFSI.

Lastly, differences in the Si 2p spectra in Figure 4.11b will be discussed. The overall Si 2p signal has previously in this discussion been related to the thickness of the SEI layer. The Li_xSi alloy is mostly not believed to be a part of the actual SEI layer, but instead represents Li trapped within outer regions of the Si particles, as seen from Figure 2.9. The lack of a SiO_2 peak for the cycled anodes indicates that all the oxygen in the original surface oxide layer has reacted and is now found in Li_xSiO_y compounds or in other oxygen-containing SEI components. Further, LiTFSI yields similar amounts of Li_xSi and Li_xSiO_y whereas LiFSI yields more Li_xSi. The differences in SEI coverage should not affect this observation as the two components are compared within the spectrum from a single electrolyte and not across different electrolytes. As the amount of SiO_2 originally at the surface is equal, this difference in Li_xSiO_y to Li_xSi ratio seems to indicate that LiFSI promotes more of the oxygen in SiO_2 to form other SEI components apart from Li_xSiO_y, however clear evidence of this hypothesis is not seen in the other XPS spectra.

5.3 The effect of TEP on cell performance

The results in Section 4.3 clearly show that TEP decomposes when added to a LiTFSI:Emi electrolyte and that more decomposition occurs with more TEP added. The decomposition of TEP has a negative effect on initial capacity and rate performance of the cells, particularly for TEP40.

With an assumption that all deviation from a 100 % Coulombic efficiency is attributed to SEI formation, the thickness of the SEI layers after the first cycle will be largest for TEP40, followed by TEP20 and LiTFSI:Emi. This can further be seen to have a direct impact on

overpotentials in voltage profiles and potentiostatic hold step fractions, in agreement with a thicker SEI layer, or more generally a SEI with reduced Li^+ transport properties, forming with more TEP added. Although TEP20 exhibits a reduced viscosity and improved ionic conductivity compared to LiTFSI:Emi, as shown in Section 4.1, the negative effects of TEP reduction have a greater influence on capacities, rate performance, and overpotentials, yielding an overall reduced cell performance.

Decomposition of TEP seems to occur mainly in the very first cycle as the voltage profiles in Figures 4.16c and 4.16d show no signs of another reduction plateau at ∼2.7 V. This is also supported by Coulombic efficiencies of TEP20 and TEP40 being comparable to LiTFSI:Emi for later cycles, although TEP40 shows a lower Coulombic efficiency than LiTFSI:Emi and TEP20 in the last C/20 cycles.

The decomposition products of TEP in this work are unknown as XPS or other characterization techniques were not employed for cells containing a TEP electrolyte, but previous reports on decomposition products of TEP include for instance $LiPO_3$ [116]. Others have reported the evolution of ethylene gas upon TEP reduction [93]. Combining these two observations might suggest a decomposition mechanism where one or more of the alkyl side groups on TEP are split off and create ethylene gas, while the remaining molecule reacts with Li ions to form $LiPO_3$ or similar compounds. This would suggest that the SEI layers for electrolytes with TEP are maybe not that much thicker than with LiTFSI:Emi as a comparison of voltage profiles in Figure 4.16b might indicate, considering that gaseous decomposition products of TEP would not contribute to a thicker SEI layer.

Table 4.3 shows the amount of capacity ascribed to initial electrolyte decomposition. The TEP content in the electrolytes is 43.2 mmol for TEP20 and 86.4 mmol for TEP40. Comparing these values shows that significantly more electrons are involved in the initial TEP decomposition than there are moles of TEP present in the electrolytes, which indicates a multi-step reduction mechanism of TEP that may fit well with a hypothesis of alkyl side groups being split off from the main molecule.

Three possible tactics to prevent TEP reduction are now presented. First, highly concentrated electrolytes are considered. Li ions have a coordination number of $n = 4$ with TEP and a high salt concentration can be used to deplete the electrolyte of free TEP molecules and create a more stable Li-ion solvate that reduces the reactivity of TEP [116]. This has been shown to yield stable performance of LiTFSI-TEP and LiFSI-TEP electrolytes [30, 116] and of the closely related LiFSI-TMP electrolyte [128].

Second, TEP can be used as a cosolvent together with solvents that themselves have good SEI-forming abilities. If a desired component in the bulk electrolyte decomposes before TEP, it can form a good SEI layer and prevent TEP decomposition. This has been shown to work with a combination of known carbonates and TEP or TMP [6, 95].

Lastly, an additive can be added to the electrolyte to be preferentially decomposed instead of TEP at higher potentials vs Li/Li^+ to form a stable SEI layer. This method has been reported in the literature and has been shown to hinder reduction of both TMP [94] and TEP [30, 93, 116]. This method has been attempted with the FEC additive in this work and is discussed in the following section.

5.4 The effect of FEC on cell performance

The addition of FEC appears to suppress the reduction of the LiTFSI salt at 2.2 V, the Emi cation at 2.8 V, and TEP at 2.7 V, as evident from voltage profiles in Figure 4.16b. Both electrolytes with FEC added show a more gradual voltage profile until lithiation begins at ∼3.2 V. This is similar to the expected behavior of an electrolyte containing FEC known from carbonate electrolytes, with FEC initially decomposing to create a good SEI that prevents decomposition of the other electrolyte components [32]. However, Coulombic efficiencies of the first cycle are lower for electrolytes with FEC. With the assumption that a Coulombic efficiency below 100 % is attributed to SEI formation, this should mean that a significant amount of decomposition of the electrolytes occurs at higher potentials alongside lithiation. A closer look at the voltage profiles of Emi:FEC and TEP20:FEC at ∼3.35 V shows that they are somewhat "unstable", indicative of something more than just an orderly lithiation process taking place. Both FEC electrolytes seem to exhibit similar or even slightly larger overpotentials in the second cycle than their corresponding electrolytes without FEC, as seen from voltage profiles and potentiostatic hold step fractions. As the bulk of the electrolytes can be regarded to not be significantly influenced by the addition of 5 wt% FEC, this should indicate that SEI layers formed after the first cycle with FEC have somewhat worse Li^+ transport properties than those without FEC which may be explained by an increased thickness of the SEI. For the last C/20 rate, the Coulombic efficiency of cells with FEC added is superior to those without FEC. Emi:FEC does indeed seem to have a slightly more stable capacity in the least four cycles. Regarding TEP20:FEC, the capacity of TEP20 in the last cycles is so much greater than for TEP20:FEC that a comparison of their stability would probably be too affected by the difference in expansion of the Si particles to give any definitive results.

There are very few articles in the literature discussing the addition of FEC to ILs. FEC has been shown to be preferentially reduced instead of the salt or the IL in a 1 M $LiPF_6$ in EC:EMC:EmiTFSI (21:49:30 vol%) + 5 wt% FEC electrolyte and subsequently create a stable SEI layer on a graphite electrode in a half cell with Li metal [33]. With the IL 1-butyl-4-methylpyridinium TFSI ($PP_{14}TFSI$), a $PP_{14}TFSI$:PC:FEC (60:30:10 wt%) electrolyte with 0.5 mol/kg lithium difluoro(oxalate)borate was tested with a LiNiMnO cathode and a Li metal anode and showed stable performance due to a beneficial SEI layer forming with FEC [129]. These two experiments may arguably illustrate that there is no apparent reason to expect that FEC would act very differently together with an IL compared to a carbonate electrolyte, although the two ILs reported are somewhat different to EmiFSI and a mixture of IL and carbonates were used in both instances.

In this work, it may therefore not be the combination of an IL and FEC that is the problem, but rather the Si anode itself. A possible hypothesis to explain the dissatisfying behavior of cells with a FEC-containing electrolyte would be that although FEC initially appears to form a protective SEI layer, it cannot withstand the expansion of Si particles upon lithiation and it cracks, allowing the electrolyte to be decomposed. Previously cited sources in Section 5.3 showing reduced TEP decomposition with FEC used a graphite half cell [116], LFP, $LiNiMnCoO_2$ and $Li_4Ti_5O_{12}$ half cells [30], and a full cell with a carbon-coated SiO anode and a $LiNi_{0.8}Co_{0.15}Al_{0.05}O_2$ cathode. Neither would have experienced electrode expansion similar to the Si anodes in this work. The hypothesis of Si expansion being responsible for cells with FEC performing poorly can be supported by previous experiments with Si anodes and carbonate electrolytes where the FEC additive generated a not so flexible SEI that could not

handle the massive expansion of the Si particles, at least when compared to a more flexible SEI forming with VC as an additive [31]. The addition of VC to the electrolytes in this work might therefore have improved their performance more than what FEC could do. However, it seems that FEC in general is considered to give a relatively stable performance of Si anodes, at least in various carbonate-based electrolytes [16, 130].

In summary, FEC appears to have a negative effect on cell capacity, rate performance, and electrolyte decomposition when added to LiTFSI:Emi and TEP20 electrolytes. The cracking of an inflexible SEI generated with FEC upon the massive expansion of Si particles may be *one* contributing factor to explain the poor performance of cells with FEC, but the formulation of any definitive conclusion will not be attempted here.

Chapter 6

Conclusion

The aim of this work was to improve the performance and understanding of Si anodes in combination with ILs for LIBs. A threefold approach was used and included (1) evaluating the effects that two different Li salts, LiFSI and LiTFSI, had on cycling stability, SEI formation, rate performance, and ionic conductivity of battery cells with two different ILs, $P_{111i4}FSI$ and EmiFSI, (2) assessing the use of TEP and TMMP as cosolvents for EmiFSI, and (3) evaluating FEC as a potential additive in EmiFSI-based electrolytes with and without a cosolvent. Eight different electrolytes were mixed, only two of which had previously been tested with Si anodes, and EIS measurements and electrochemical cycling of pouch cells were used to evaluate the performance of Si anodes in a pseudo-full cell setup with a capacitively oversized LFP cathode. A selection of anodes were characterized by means of XPS to investigate the effect of LiFSI and LiTFSI on the composition of the SEI layer.

The results obtained in this work showed that electrolytes containing LiFSI have a reduced viscosity and improved ionic conductivity compared to those with LiTFSI, in line with previous reports in the literature [20, 27]. These properties appear to have a direct impact on the rate performance of cells, with LiFSI-based electrolytes outperforming LiTFSI at increased (dis)charging rates in both EmiFSI and $P_{111i4}FSI$. An investigation of voltage profiles and Coulombic efficiency plots revealed that LiFSI is more reactive at low and high cell potentials, particularly in EmiFSI, but that more decomposition occurs at intermediate potentials with LiTFSI.

Regarding Coulombic efficiency and cycling stability, electrochemical data cannot determine clear differences related to LiFSI and LiTFSI as the differences between the two salts are generally small and the effects are opposite in EmiFSI compared to in $P_{111i4}FSI$. However, the improved cycling stability and Coulombic efficiency of $P_{111i4}FSI$ compared to EmiFSI are substantially more noticeable.

Electrochemical data and XPS measurements showed that the initial SEI layer formed with $P_{111i4}FSI$ electrolytes are thicker compared to those cycled in EmiFSI and a lower Coulombic efficiency for EmiFSI-based electrolytes indicates that the SEI layer grows more upon repeated (dis)charge cycles for EmiFSI than for $P_{111i4}FSI$.

XPS measurements showed that SEI layers with LiFSI and LiTFSI as Li salt are generally very similar, consisting for the most part of known decomposition products of the IL cation and FSI and TFSI anions. In addition, the surface oxide layer on Si particles in the electrode was seen to contribute to the SEI by being lithiated to form Li_xSiO_y compounds or by acting

as a source of oxygen in the formation of other SEI components. Characterization with XPS revealed that electrolytes with LiTFSI give a SEI containing more LiF, without it having a visible improvement on cell performance as frequently reported in the literature [32, 70]. More LiF is also generated with phosphonium-based electrolytes than with EmiFSI.

For EmiFSI, a combination of electrochemical results and XPS measurements indicate that FSI anions minimize the decomposition of the Emi cation, in line with a model previously developed for graphite anodes by Yamagata et al. [88] and until now only hypothesized to also be valid for Si anodes [27]. The phosphonium cation is believed to not decompose, but nevertheless contributed to the SEI by being incorporated into the layer in an undecomposed state. Significantly more phosphonium cations were seen in the SEI layer when LiFSI was used compared to LiTFSI, without the reason for this being known.

In conclusion, LiFSI seems to be the salt of choice in P_{111i4}FSI electrolytes based on an improved ionic conductivity, cycling stability, and overall cell performance compared to LiTFSI. However, both electrolytes with P_{111i4}FSI appear to be far too viscous to be used in commercial batteries in their current state. EmiFSI electrolytes were less viscous and had better ionic conductivities, but still exhibited a relatively poor rate performance. In EmiFSI, there seems to be a trade-off between improved capacity and slightly better Coulombic efficiency with LiTFSI and a better rate performance with LiFSI.

Regarding the use of cosolvents, TMMP was quickly ruled out as a potential cosolvent for EmiFSI, at least for the concentrations used in this work (15 and 25 wt% TMMP), due to their immiscibility. TEP was miscible with EmiFSI and seemed to reduce the viscosity of the electrolyte, but showed worse ionic conductivities at higher concentrations of TEP, maybe related to TEP having a low permittivity. Further, TEP underwent a major decomposition process during the first charge cycle and a thick SEI layer forming is believed to explain the reduced capacity, increased overpotential, and poor rate performance of electrolytes containing TEP.

FEC was evaluated as a possible electrolyte additive by being added in an amount of 5 wt% to an EmiFSI electrolyte and to an electrolyte of EmiFSI containing 20 wt% TEP. FEC was successful in initially limiting the decomposition of other electrolyte components, however it appears that the SEI layer formed with FEC did not manage to prevent electrolyte decomposition at higher cell potentials, perhaps related to the massive expansion of the Si particles, ultimately yielding lower Coulombic efficiencies in the first cycle. The addition of FEC to the electrolyte resulted in a cell with worse rate performance and greater overpotentials, both with and without TEP present. The combination of TEP and FEC appears to be particularly unsuited, with significantly lowered capacities observed.

The findings in this thesis and recommendations for further work will hopefully be a small, but positive contribution to the development and implementation of safe and high energy density LIBs, an important challenge to tackle for batteries to realize their full potential in the important fight against climate change.

Chapter 7

Further work

In order to investigate the three different approaches employed in this work to improve the performance of ILs in combination with Si anodes, a varied, but limited amount of electrochemical cycling and characterization methods have been used. This thesis leaves several important questions unanswered.

Unless a major breakthrough in synthetization of ILs is accomplished, ILs will persist to have higher viscosities than current carbonate-based electrolytes. This fact, in combination with their superior thermal stability, make IL electrolytes particularly suited for high-temperature operation. It can therefore be more appropriate to evaluate the cells at an elevated temperature, for instance 80 °C. The improved capacity of LiTFSI compared to LiFSI in EmiFSI, in addition to its superior thermal and chemical stability, might then be more important than its negative effect on ionic conductivity and rate performance, as the rate performance of all cells would likely be improved at elevated temperatures either way.

EIS measurements provided insight into resistances and ionic conductivities of the cells, but did not paint a complete picture of all relevant electrolyte properties. The lack of quantification of the Li^+ transport number is one major shortcoming of the simple EIS measurements performed in this work. Further, performing EIS measurements both before and after electrochemical cycling in combination with increasingly more complex equivalent circuit models of the cells can help quantify some of the overpotential phenomena present.

The use of XPS in this work provided important information on the contents of the SEI layer and assisted in confirming and understanding results from electrochemical measurements. Additional and complementary characterization techniques can give deeper insight into electrolyte decomposition and SEI formation. Some notable methods include electrochemical techniques like cyclic voltammetry, microscopy techniques such as scanning electron microscopy (SEM), surface-sensitive characterization techniques such as FTIR and Raman spectroscopy, and cross-sectional investigations using for instance a combination of focused ion beam (FIB) and energy-dispersive X-ray spectroscopy (EDX) methods. Performing post-mortem characterization of cells with TEP added to the electrolytes can confirm that it is a thick SEI layer forming that is responsible for the poor cycling performance of electrolytes containing TEP. Post-mortem characterization can also help in understanding why the addition of FEC did not improve cell performance, as would be expected, and assist in explaining its poor interplay with the TEP cosolvent.

Based on the results from this work, FEC is believed to initially stop decomposition of

other electrolyte components, but that extensive electrolyte decomposition occurs at higher cell potentials. It can therefore be relevant to charge a cell, stop it just before lithiation occurs, and characterize the SEI to confirm that it consist mainly of known decomposition products of FEC. Further, characterizing the SEI after the first charge and discharge cycle can verify the hypothesis of extensive decomposition occurring at higher cell potentials.

It is apparent that FEC is not a suitable additive to be used alone with EmiFSI or in a combination of EmiFSI and TEP. There are multiple known SEI-forming additives in the literature that can be tested. If the hypothesis of FEC yielding a too rigid SEI layer that cannot withstand Si expansion is true, the addition of VC to the electrolyte, which is known to yield a more flexible SEI [31], would perhaps be the most relevant additive to test first. A combination of FEC and VC might allow TEP to successfully be utilized as a cosolvent for EmiFSI. Another strategy to stop the decomposition of TEP in the cell can be to use a very high concentration of Li salt, as this has been shown to prevent decomposition of a pure TEP electrolyte [30, 116].

This work showed that TMMP cannot be used as a cosolvent for EmiFSI at concentrations of 15 and 25 wt%. A determination of the solubility of TMMP in EmiFSI can provide information on if there are any relevant concentrations for which TMMP is suitable to be used as a cosolvent for EmiFSI.

Lastly, this work has only tested two different cosolvents to be used with LIBs and there are countless alternatives remaining untested. A suggested approach forward is to select a variety of low-priced solvents with low viscosity and good Li^+ solvation properties that are known to resist decomposition and maintain a good performance in a tough electrochemical environment and further assess their relevance as cosolvents by testing them in LIB cells.

Chapter 8

Bibliography

[1] V. Masson-Delmotte et al. *Summary for Policymakers. In: Global Warming of 1.5° C. An IPCC Special Report on the impacts of global warming of 1.5° C above pre-industrial levels and related global greenhouse gas emission pathways, in the context of strengthening the global response.* Tech. rep. World Meteorological Organization, 2018, p. 32. URL: http://www.ipcc.ch/report/sr15/.

[2] V. Etacheri et al. "Challenges in the development of advanced Li-ion batteries: A review". In: *Energy and Environmental Science* 4.9 (Sept. 2011), pp. 3243–3262. ISSN: 17545692. DOI: 10.1039/c1ee01598b.

[3] S. Comello and S. Reichelstein. "The emergence of cost effective battery storage". In: *Nature Communications* 10.1 (Dec. 2019). ISSN: 20411723. DOI: 10.1038/s41467-019-09988-z.

[4] The Royal Swedish Academy of Sciences Press release. *The Nobel Prize in Chemistry 2019 (accessed 2019.11.14)*. 2019. URL: https://www.nobelprize.org/uploads/2019/10/press-chemistry-2019-2.pdf.

[5] J. B. Goodenough and Y. Kim. "Challenges for Rechargeable Li Batteries". In: *Chemistry of Materials* 22.3 (Feb. 2010), pp. 587–603. ISSN: 0897-4756. DOI: 10.1021/cm901452z.

[6] C. Wang, A. J. Appleby, and F. E. Little. "Charge-discharge stability of graphite anodes for lithium-ion batteries". In: *Journal of Electroanalytical Chemistry* 497.1-2 (2001), pp. 33–46. ISSN: 00220728. DOI: 10.1016/S0022-0728(00)00447-2.

[7] S. Chae et al. "Integration of Graphite and Silicon Anodes for the Commercialization of High-Energy Lithium-Ion Batteries". In: *Angewandte Chemie International Edition* 59 (Oct. 2019), pp. 110–135. ISSN: 14337851. DOI: 10.1002/anie.201902085.

[8] S. Kalnaus, K. Rhodes, and C. Daniel. "A study of lithium ion intercalation induced fracture of silicon particles used as anode material in Li-ion battery". In: *Journal of Power Sources* 196.19 (Oct. 2011), pp. 8116–8124. ISSN: 03787753. DOI: 10.1016/j.jpowsour.2011.05.049.

[9] T. Yoon et al. "Capacity fading mechanisms of silicon nanoparticle negative electrodes for lithium ion batteries". In: *Journal of the Electrochemical Society* 162.12 (2015), A2325–A2330. ISSN: 19457111. DOI: 10.1149/2.0731512jes.

[10] M. Nie et al. "Silicon solid electrolyte interphase (SEI) of lithium ion battery characterized by microscopy and spectroscopy". In: *Journal of Physical Chemistry C* 117.26 (July 2013), pp. 13403–13412. ISSN: 19327447. DOI: 10.1021/jp404155y.

[11] H. Shobukawa et al. "Electrochemical reaction and surface chemistry for performance enhancement of a Si composite anode using a bis(fluorosulfonyl)imide-based ionic liquid". In: *Journal of Materials Chemistry A* 4.39 (2016), pp. 15117–15125. DOI: 10.1039/c6ta06447g.

[12] S. Hess, M. Wohlfahrt-Mehrens, and M. Wachtler. "Flammability of Li-Ion battery electrolytes: Flash point and self-extinguishing time measurements". In: *Journal of the Electrochemical Society* 162.2 (2015), A3084–A3097. ISSN: 19457111. DOI: 10.1149/2.0121502jes.

[13] V. R. Koch et al. "The intrinsic anodic stability of several anions comprising solvent-free ionic liquids". In: *Journal of the Electrochemical Society* 143.3 (1996), pp. 798–803. ISSN: 00134651. DOI: 10.1149/1.1836540.

[14] B. Garcia et al. "Room temperature molten salts as lithium battery electrolyte". In: *Electrochimica Acta* 49.26 (Oct. 2004), pp. 4583–4588. ISSN: 00134686. DOI: 10.1016/j.electacta.2004.04.041.

[15] A. Balducci et al. "Development of safe, green and high performance ionic liquids-based batteries (ILLIBATT project)". In: *Journal of Power Sources* 196.22 (Nov. 2011), pp. 9719–9730. ISSN: 03787753. DOI: 10.1016/j.jpowsour.2011.07.058.

[16] K. Xu. "Electrolytes and Interphases in Li-Ion Batteries and Beyond". In: *Chemical Reviews* 114.23 (2014), pp. 11503–11618. DOI: 10.1021/cr500003w.

[17] H. Matsumoto et al. "Fast cycling of Li/LiCoO2 cell with low-viscosity ionic liquids based on bis(fluorosulfonyl)imide [FSI]-". In: *Journal of Power Sources* 160.2 (Oct. 2006), pp. 1308–1313. ISSN: 03787753. DOI: 10.1016/j.jpowsour.2006.02.018.

[18] D. Molina Piper et al. "Stable silicon-ionic liquid interface for next-generation lithium-ion batteries". In: *Nature Communications* 6 (2015), pp. 1–10. DOI: 10.1038/ncomms7230.

[19] K. Tsunashima and M. Sugiya. "Physical and electrochemical properties of low-viscosity phosphonium ionic liquids as potential electrolytes". In: *Electrochemistry Communications* 9.9 (Sept. 2007), pp. 2353–2358. ISSN: 13882481. DOI: 10.1016/j.elecom.2007.07.003.

[20] H. B. Han et al. "Lithium bis(fluorosulfonyl)imide (LiFSI) as conducting salt for nonaqueous liquid electrolytes for lithium-ion batteries: Physicochemical and electrochemical properties". In: *Journal of Power Sources* 196.7 (Apr. 2011), pp. 3623–3632. ISSN: 03787753. DOI: 10.1016/j.jpowsour.2010.12.040.

[21] R. Kerr et al. "High-Capacity Retention of Si Anodes Using a Mixed Lithium/Phosphonium Bis(fluorosulfonyl)imide Ionic Liquid Electrolyte". In: *ACS Energy Letters* 2.8 (Aug. 2017), pp. 1804–1809. ISSN: 23808195. DOI: 10.1021/acsenergylett.7b00403.

[22] S. Tsuzuki, K. Hayamizu, and S. Seki. "Origin of the low-viscosity of [Emim][(FSO2)2N] ionic liquid and its lithium salt mixture: Experimental and theoretical study of self-diffusion coefficients, conductivities, and intermolecular interactions". In: *Journal of Physical Chemistry B* 114.49 (Dec. 2010), pp. 16329–16336. ISSN: 15205207. DOI: 10.1021/jp106870v.

[23] V. Sharova et al. “Comparative study of imide-based Li salts as electrolyte additives for Li-ion batteries”. In: *Journal of Power Sources* 375 (Jan. 2018), pp. 43–52. ISSN: 03787753. DOI: 10.1016/j.jpowsour.2017.11.045.

[24] K. Xu. “Nonaqueous liquid electrolytes for lithium-based rechargeable batteries”. In: *Chemical Reviews* 104.10 (Oct. 2004), pp. 4303–4417. ISSN: 00092665. DOI: 10.1021/cr030203g.

[25] Z. Xu et al. “Electrolytes for advanced lithium ion batteries using silicon-based anodes”. In: *Journal of Materials Chemistry A* 7.16 (2019), pp. 9432–9446. ISSN: 20507496. DOI: 10.1039/c9ta01876j.

[26] T. Sugimoto et al. “Application of bis(fluorosulfonyl)imide-based ionic liquid electrolyte to silicon-nickel-carbon composite anode for lithium-ion batteries”. In: *Journal of Power Sources* 195.18 (Sept. 2010), pp. 6153–6156. ISSN: 03787753. DOI: 10.1016/j.jpowsour.2010.01.011.

[27] Y. Matsui et al. “Design of an electrolyte composition for stable and rapid charging-discharging of a graphite negative electrode in a bis(fluorosulfonyl)imide-based ionic liquid”. In: *Journal of Power Sources* 279 (Apr. 2015), pp. 766–773. ISSN: 03787753. DOI: 10.1016/j.jpowsour.2015.01.070.

[28] A. Guerfi et al. “Improved electrolytes for Li-ion batteries: Mixtures of ionic liquid and organic electrolyte with enhanced safety and electrochemical performance”. In: *Journal of Power Sources* 195.3 (Feb. 2010), pp. 845–852. ISSN: 03787753. DOI: 10.1016/j.jpowsour.2009.08.056.

[29] A. Eftekhari, Y. Liu, and P. Chen. “Different roles of ionic liquids in lithium batteries”. In: *Journal of Power Sources* 334 (Dec. 2016), pp. 221–239. ISSN: 03787753. DOI: 10.1016/j.jpowsour.2016.10.025.

[30] L. Jiang et al. “Safer Triethyl-Phosphate-Based Electrolyte Enables Nonflammable and High-Temperature Endurance for a Lithium Ion Battery”. In: *ACS Applied Energy Materials* 3.2 (Feb. 2020), pp. 1719–1729. ISSN: 25740962. DOI: 10.1021/acsaem.9b02188.

[31] T. Jaumann et al. “Lifetime vs. rate capability: Understanding the role of FEC and VC in high-energy Li-ion batteries with nano-silicon anodes”. In: *Energy Storage Materials* 6 (Jan. 2017), pp. 26–35. ISSN: 24058297. DOI: 10.1016/j.ensm.2016.08.002.

[32] E. Peled and S. Menkin. “Review - SEI: Past, present and future”. In: *Journal of the Electrochemical Society* 164.7 (2017), A1703–A1719. ISSN: 19457111. DOI: 10.1149/2.1441707jes.

[33] I. A. Profatilova et al. “Electrochemical and thermal properties of graphite electrodes with imidazolium- and piperidinium-based ionic liquids”. In: *Journal of Power Sources* 192.2 (July 2009), pp. 636–643. ISSN: 03787753. DOI: 10.1016/j.jpowsour.2009.03.041.

[34] C. Julien et al. *Lithium Batteries*. Switzerland: Springer, Cham, 2016. ISBN: 978-3-319-19107-2. DOI: 10.1007/978-3-319-19108-9{_}2.

[35] J. B. Goodenough and K. S. Park. “The Li-ion rechargeable battery: A perspective”. In: *Journal of the American Chemical Society* 135.4 (Jan. 2013), pp. 1167–1176. ISSN: 00027863. DOI: 10.1021/ja3091438.

[36] Y. Qi, A. Van Der Ven, and P. Balbuena. *Batteries-Theory, Modeling, and Simulation.* Pennington, New Jersey: Electrochemical Society Inc., 2015. ISBN: 9781623323080.

[37] M. Osiak et al. "Structuring materials for lithium-ion batteries: Advancements in nanomaterial structure, composition, and defined assembly on cell performance". In: *Journal of Materials Chemistry A* 2.25 (July 2014), pp. 9433–9460. ISSN: 20507496. DOI: 10.1039/c4ta00534a.

[38] L. Fransson et al. "Influence of carbon black and binder on Li-ion batteries". In: *Journal of Power Sources* 101.1 (Oct. 2001), pp. 1–9. ISSN: 03787753. DOI: 10.1016/S0378-7753(01)00481-5.

[39] S. T. Myung, Y. Hitoshi, and Y. K. Sun. "Electrochemical behavior and passivation of current collectors in lithium-ion batteries". In: *Journal of Materials Chemistry* 21.27 (July 2011), pp. 9891–9911. ISSN: 09599428. DOI: 10.1039/c0jm04353b.

[40] S. Goriparti et al. "Review on recent progress of nanostructured anode materials for Li-ion batteries". In: *Journal of Power Sources* 257 (2014), pp. 421–443. ISSN: 03787753. DOI: 10.1016/j.jpowsour.2013.11.103.

[41] S. S. Zhang and T. R. Jow. "Aluminum corrosion in electrolyte of Li-ion battery". In: *Journal of Power Sources* 109.2 (July 2002), pp. 458–464. ISSN: 03787753. DOI: 10.1016/S0378-7753(02)00110-6.

[42] D. Andre et al. "Future generations of cathode materials: an automotive industry perspective". In: *Journal of Materials Chemistry A* 3 (2015), pp. 6709–6732. DOI: 10.1039/c5ta00361j.

[43] C. Julien et al. "Comparative Issues of Cathode Materials for Li-Ion Batteries". In: *Inorganics* 2.1 (Mar. 2014), pp. 132–154. ISSN: 2304-6740. DOI: 10.3390/inorganics2010132.

[44] M. Yoshio, T. Tsumura, and N. Dimov. "Electrochemical behaviors of silicon based anode material". In: *Journal of Power Sources* 146 (2005), pp. 10–14. ISSN: 03787753. DOI: 10.1016/j.jpowsour.2005.03.143.

[45] F. Wu and G. Yushin. "Conversion cathodes for rechargeable lithium and lithium-ion batteries". In: *Energy and Environmental Science* 10.2 (Feb. 2017), pp. 435–459. ISSN: 17545706. DOI: 10.1039/c6ee02326f.

[46] P. Poizot et al. "Nano-sized transition-metal oxides as negative-electrode materials for lithium-ion batteries". In: *Nature* 407.6803 (Sept. 2000), pp. 496–499. ISSN: 00280836. DOI: 10.1038/35035045.

[47] E. A. Olivetti et al. "Lithium-Ion Battery Supply Chain Considerations: Analysis of Potential Bottlenecks in Critical Metals". In: *Joule* 1.2 (Oct. 2017), pp. 229–243. ISSN: 25424351. DOI: 10.1016/j.joule.2017.08.019.

[48] G. André, M. Godin, and P. Sud. "Child labour, agency and family dynamics: The case of mining in Katanga (DRC)". In: *Childhood* 21.2 (2014), pp. 161–174. DOI: 10.1177/0907568213488966.

[49] P. P. Prosini. "Modeling the voltage profile for LiFePO 4". In: *Journal of the Electrochemical Society* 152.10 (2005). ISSN: 00134651. DOI: 10.1149/1.2006607.

[50] J. Gao et al. "Brief overview of electrochemical potential in lithium ion batteries". In: *Phys. B* 25.1 (2016), p. 18210. DOI: 10.1088/1674-1056/25/1/018210.

[51] J. Chen, S. Wang, and M. S. Whittingham. "Hydrothermal synthesis of cathode materials". In: *Journal of Power Sources* 174.2 (Dec. 2007), pp. 442–448. ISSN: 03787753. DOI: 10.1016/j.jpowsour.2007.06.189.

[52] J. Chen. "Recent progress in advanced materials for lithium ion batteries". In: *Materials* 6.1 (2013), pp. 156–183. ISSN: 19961944. DOI: 10.3390/ma6010156.

[53] W. Xu et al. "Lithium metal anodes for rechargeable batteries". In: *Energy and Environmental Science* 7.2 (Jan. 2014), pp. 513–537. ISSN: 17545706. DOI: 10.1039/c3ee40795k.

[54] M. T. McDowell et al. "25th Anniversary Article: Understanding the Lithiation of Silicon and Other Alloying Anodes for Lithium-Ion Batteries". In: *Advanced Materials* 25.36 (Sept. 2013), pp. 4966–4985. ISSN: 09359648. DOI: 10.1002/adma.201301795.

[55] K. Ogata et al. "Revealing lithium-silicide phase transformations in nano-structured silicon-based lithium ion batteries via in situ NMR spectroscopy". In: *Nature Communications* 5 (Feb. 2014). ISSN: 20411723. DOI: 10.1038/ncomms4217.

[56] M. Ashuri, Q. He, and L. L. Shaw. "Silicon as a potential anode material for Li-ion batteries: Where size, geometry and structure matter". In: *Nanoscale* 8.1 (Jan. 2016), pp. 74–103. ISSN: 20403372. DOI: 10.1039/c5nr05116a.

[57] H. Wu et al. "Stable cycling of double-walled silicon nanotube battery anodes through solid-electrolyte interphase control". In: *Nature Nanotechnology* 7.5 (2012), pp. 310–315. ISSN: 17483395. DOI: 10.1038/nnano.2012.35.

[58] R. Yi et al. "Micro-sized Si-C Composite with Interconnected Nanoscale Building Blocks as High-Performance Anodes for Practical Application in Lithium-Ion Batteries". In: *Advanced Energy Materials* 3.3 (Mar. 2013), pp. 295–300. ISSN: 16146832. DOI: 10.1002/aenm.201200857.

[59] N. Liu et al. "Rice husks as a sustainable source of nanostructured silicon for high performance Li-ion battery anodes". In: *Scientific Reports* 3.1 (May 2013), pp. 1–7. ISSN: 20452322. DOI: 10.1038/srep01919.

[60] A. Magasinski et al. "Toward efficient binders for Li-ion battery Si-based anodes: Polyacrylic acid". In: *ACS Applied Materials and Interfaces* 2.11 (Nov. 2010), pp. 3004–3010. ISSN: 19448244. DOI: 10.1021/am100871y.

[61] I. Kovalenko et al. "A major constituent of brown algae for use in high-capacity Li-ion batteries". In: *Science* 334.6052 (Oct. 2011), pp. 75–79. ISSN: 10959203. DOI: 10.1126/science.1209150.

[62] F. Wang et al. "Engineering of carbon and other protective coating layers for stabilizing silicon anode materials". In: *Carbon Energy* 1.2 (2019), pp. 219–245. ISSN: 2637-9368. DOI: 10.1002/cey2.24.

[63] P. Limthongkul et al. "Electrochemically-driven solid-state amorphization in lithium-silicon alloys and implications for lithium storage". In: *Acta Materialia* 51.4 (Feb. 2003), pp. 1103–1113. ISSN: 13596454. DOI: 10.1016/S1359-6454(02)00514-1.

[64] B. Key et al. "Real-Time NMR Investigations of Structural Changes in Silicon Electrodes for Lithium-Ion Batteries". In: *Journal of the American Chemical Society* 131.26 (July 2009), pp. 9239–9249. ISSN: 0002-7863. DOI: 10.1021/ja8086278.

[65] B. Key et al. "Pair distribution function analysis and solid state NMR studies of silicon electrodes for lithium ion batteries: Understanding the (de)lithiation mechanisms". In: *Journal of the American Chemical Society* 133.3 (Jan. 2011), pp. 503–512. ISSN: 00027863. DOI: 10.1021/ja108085d.

[66] A. Wang et al. "Review on modeling of the anode solid electrolyte interphase (SEI) for lithium-ion batteries". In: *Computational Materials* 4.1 (Dec. 2018). ISSN: 20573960. DOI: 10.1038/s41524-018-0064-0.

[67] E. Peled. "The Electrochemical Behavior of Alkali and Alkaline Earth Metals in Nonaqueous Battery Systems—The Solid Electrolyte Interphase Model". In: *Journal of The Electrochemical Society* 126.12 (1979), p. 2047. ISSN: 00134651. DOI: 10.1149/1.2128859.

[68] P. Verma, P. Maire, and P. Novák. "A review of the features and analyses of the solid electrolyte interphase in Li-ion batteries". In: *Electrochimica Acta* 55.22 (Sept. 2010), pp. 6332–6341. ISSN: 00134686. DOI: 10.1016/j.electacta.2010.05.072.

[69] A. Würsig et al. "Film formation at positive electrodes in lithium-ion batteries". In: *Electrochemical and Solid-State Letters* 8.1 (2005). ISSN: 10990062. DOI: 10.1149/1.1836114.

[70] K. Schroder et al. "The Effect of Fluoroethylene Carbonate as an Additive on the Solid Electrolyte Interphase on Silicon Lithium-Ion Electrodes". In: *Chemistry of Materials* 27.16 (Aug. 2015), pp. 5531–5542. ISSN: 15205002. DOI: 10.1021/acs.chemmater.5b01627.

[71] N. S. Choi et al. "Effect of fluoroethylene carbonate additive on interfacial properties of silicon thin-film electrode". In: *Journal of Power Sources* 161.2 (Oct. 2006), pp. 1254–1259. ISSN: 03787753. DOI: 10.1016/j.jpowsour.2006.05.049.

[72] B. Philippe et al. "Nanosilicon Electrodes for Lithium-Ion Batteries: Interfacial Mechanisms Studied by Hard and Soft X-ray Photoelectron Spectroscopy". In: *Chemistry of Materials* 24 (2012), pp. 1107–1115. DOI: 10.1021/cm2034195.

[73] J. Feng. "Electrolytes for Advanced LIBs". In: *Recent Advances in Energy Storage Materials and Devices*. Ed. by L. Lu and N. Hu. Vol. 12. Millersville, PA 17551, USA: Materials Research Forum LLC, May 2017. Chap. 6, pp. 125–163. ISBN: 978-1-945291-27-2. DOI: 10.21741/9781945291272-6.

[74] R. Fong. "Studies of Lithium Intercalation into Carbons Using Nonaqueous Electrochemical Cells". In: *Journal of The Electrochemical Society* 137.7 (1990), p. 2009. ISSN: 00134651. DOI: 10.1149/1.2086855.

[75] R. Hayes, G. G. Warr, and R. Atkin. "Structure and Nanostructure in Ionic Liquids". In: *Chemical Reviews* 115.13 (2015), pp. 6357–6426. ISSN: 15206890. DOI: 10.1021/cr500411q.

[76] T. Welton. "Room-Temperature Ionic Liquids . Solvents for Synthesis and Catalysis". In: *Chemical Reviews* 99 (1999), pp. 2071–2084. ISSN: 0009-2665. DOI: 10.1021/cr980032t.

[77] X. Liu, T. J. Vlugt, and A. Bardow. "Maxwell-stefan diffusivities in binary mixtures of ionic liquids with dimethyl sulfoxide (DMSO) and H2O". In: *Journal of Physical Chemistry B* 115.26 (July 2011), pp. 8506–8517. ISSN: 15205207. DOI: 10.1021/jp203026c.

[78] A. S. Best, A. I. Bhatt, and A. F. Hollenkamp. "Ionic Liquids with the Bis(fluorosulfonyl) imide Anion: Electrochemical Properties and Applications in Battery Technology". In: *Journal of The Electrochemical Society* 157.8 (June 2010), A903. ISSN: 00134651. DOI: 10.1149/1.3429886.

[79] S. Seki et al. "Lithium secondary batteries using modified-imidazolium room-temperature ionic liquid". In: *Journal of Physical Chemistry B* 110.21 (June 2006), pp. 10228–10230. ISSN: 15206106. DOI: 10.1021/jp0620872.

[80] D. R. MacFarlane et al. "Pyrrolidinium imides: A new family of molten salts and conductive plastic crystal phases". In: *Journal of Physical Chemistry B* 103.20 (1999), pp. 4164–4170. ISSN: 10895647. DOI: 10.1021/jp984145s.

[81] P. C. Howlett et al. "Characterization of the Lithium Surface in N-Methyl-N-alkylpyrrolidinium Bis(trifluoromethanesulfonyl)amide Room-Temperature Ionic Liquid Electrolytes". In: *Journal of The Electrochemical Society* 153.3 (Feb. 2006), A595. ISSN: 00134651. DOI: 10.1149/1.2164726.

[82] Y. Wang et al. "Accelerating rate calorimetry studies of the reactions between ionic liquids and charged lithium ion battery electrode materials". In: *Electrochimica Acta* 52.22 (June 2007), pp. 6346–6352. ISSN: 00134686. DOI: 10.1016/j.electacta.2007.04.067.

[83] M. Kerner et al. "Thermal stability and decomposition of lithium bis(fluorosulfonyl)imide (LiFSI) salts". In: *RSC Advances* 6 (2016), pp. 23327–23334. DOI: 10.1039/c5ra25048j.

[84] G. M. Girard et al. "Role of Li concentration and the SEI layer in enabling high performance Li metal electrodes using a phosphonium bis(fluorosulfonyl)imide ionic liquid". In: *Journal of Physical Chemistry C* 121.39 (2017), pp. 21087–21095. ISSN: 19327455. DOI: 10.1021/acs.jpcc.7b01929.

[85] G. M. Girard et al. "Electrochemical and physicochemical properties of small phosphonium cation ionic liquid electrolytes with high lithium salt content". In: *Physical Chemistry Chemical Physics* 17.14 (Apr. 2015), pp. 8706–8713. ISSN: 14639076. DOI: 10.1039/c5cp00205b.

[86] M. Kerner et al. "Ionic liquid based lithium battery electrolytes: fundamental benefits of utilising both TFSI and FSI anions?" In: *Physical Chemistry Chemical Physics* 17.29 (Aug. 2015), pp. 19569–19581. ISSN: 14639076. DOI: 10.1039/c5cp01891a.

[87] K. Fujii et al. "Structural aspect on Li ion solvation in room-temperature ionic liquids". In: *Electrochemistry in Ionic Liquids: Volume 1: Fundamentals*. Ed. by A. A. J. Torriero. Switzerland: Springer, Cham, Jan. 2015. Chap. 10, pp. 317–332. ISBN: 9783319134857. DOI: 10.1007/978-3-319-13485-7{_}10.

[88] M. Yamagata et al. "Charge-discharge behavior of graphite negative electrodes in bis(fluorosulfonyl)imide-based ionic liquid and structural aspects of their electrode/electrolyte interfaces". In: *Electrochimica Acta* 110 (2013), pp. 181–190. ISSN: 00134686. DOI: 10.1016/j.electacta.2013.03.018.

[89] S. Sayah et al. "A bis(fluorosulfonyl)imide based ionic liquid as safe and efficient electrolyte for Si/Sn-Ni/C/Al composite anode". In: *Electrochimica Acta* 243 (July 2017), pp. 197–206. ISSN: 00134686. DOI: 10.1016/j.electacta.2017.05.056.

[90] H. Srour, H. Rouault, and C. Santini. "Imidazolium Based Ionic Liquid Electrolytes for Li-Ion Secondary Batteries Based on Graphite and LiFePO 4". In: *Journal of The Electrochemical Society* 160.1 (Nov. 2013), A66–A69. ISSN: 0013-4651. DOI: 10.1149/2.025301jes.

[91] A. Deshpande et al. "Enhancement of lithium ion mobility in ionic liquid electrolytes in presence of additives". In: *Journal of Physical Chemistry C* 117.48 (Dec. 2013), pp. 25343–25351. ISSN: 19327447. DOI: 10.1021/jp409498w.

[92] J. Feng et al. "Understanding the interactions of phosphonate-based flame-retarding additives with graphitic anode for lithium ion batteries". In: *Electrochimica Acta* 114 (Dec. 2013), pp. 688–692. ISSN: 00134686. DOI: 10.1016/j.electacta.2013.10.104.

[93] K. Matsumoto, K. Inoue, and K. Utsugi. "A highly safe battery with a non-flammable triethyl-phosphate-based electrolyte". In: *Journal of Power Sources* 273 (Jan. 2015), pp. 954–958. ISSN: 03787753. DOI: 10.1016/j.jpowsour.2014.09.086.

[94] X. Wang et al. "High-Concentration Trimethyl Phosphate-Based Nonflammable Electrolytes with Improved Charge–Discharge Performance of a Graphite Anode for Lithium-Ion Cells". In: *Journal of The Electrochemical Society* 153.1 (Dec. 2006), A135. ISSN: 00134651. DOI: 10.1149/1.2136078.

[95] B. S. Lalia et al. "A mixture of triethylphosphate and ethylene carbonate as a safe additive for ionic liquid-based electrolytes of lithium ion batteries". In: *Journal of Power Sources* 195.21 (Nov. 2010), pp. 7426–7431. ISSN: 03787753. DOI: 10.1016/j.jpowsour.2010.05.040.

[96] E. P. Roth and C. J. Orendorff. "How electrolytes influence battery safety". In: *Electrochemical Society Interface* 21.2 (2012), pp. 45–49. ISSN: 19448783. DOI: 10.1149/2.F04122if.

[97] K. Naoi et al. "Nonflammable Hydrofluoroether for Lithium-Ion Batteries: Enhanced Rate Capability, Cyclability, and Low-Temperature Performance". In: *Journal of The Electrochemical Society* 156.4 (2009), A272. ISSN: 00134651. DOI: 10.1149/1.3073552.

[98] G. Nagasubramanian and C. J. Orendorff. "Hydrofluoroether electrolytes for lithium-ion batteries: Reduced gas decomposition and nonflammable". In: *Journal of Power Sources* 196.20 (Oct. 2011), pp. 8604–8609. ISSN: 03787753. DOI: 10.1016/j.jpowsour.2011.05.078.

[99] Ø. Lindgård. *Evaluation of LiTFSI as Electrolyte Salt in EmiFSI-based Ionic Liquid Electrolytes to be used with Silicon Anodes for Lithium-Ion Batteries*. Tech. rep. Specialization project (TMT4510), Department of Materials Science and Engineering, NTNU, 2019.

[100] V. Renman. *The Battery Bible, an internal document at the Department of Materials Science and Engineering, NTNU*. 2019.

[101] J. F. Moulder et al. *Handbook of X-ray Photoelectron Spectroscopy*. Ed. by J. Chastain. Minnesota: Perkin-Elmer Corporation, 1992. ISBN: 978-0964812413.

[102] J. Alvarado et al. "A carbonate-free, sulfone-based electrolyte for high-voltage Li-ion batteries". In: *Materials Today* 21.4 (2018), pp. 341–353. DOI: 10.1016/j.mattod.2018.02.005.

[103] G. T. Cheek et al. "Electrochemical Studies of Imidazolium Carboxylate Adducts in a Room-Temperature Ionic Liquid". In: *ECS Transactions* 64.4 (Aug. 2014), pp. 161–169. ISSN: 1938-6737. DOI: 10.1149/06404.0161ecst.

[104] K. W. Schroder et al. "Examining Solid Electrolyte Interphase Formation on Crystalline Silicon Electrodes: Influence of Electrochemical Preparation and Ambient Exposure Conditions". In: *J. Phys. Chem. C* 116 (2012), p. 14. DOI: 10.1021/jp307372m.

[105] G. Greczynski and L. Hultman. "C 1s Peak of Adventitious Carbon Aligns to the Vacuum Level: Dire Consequences for Material's Bonding Assignment by Photoelectron Spectroscopy". In: *ChemPhysChem* 18.12 (June 2017), pp. 1507–1512. ISSN: 14397641. DOI: 10.1002/cphc.201700126.

[106] C. Moreno-Castilla, M. V. López-Ramón, and F. Carrasco-Marín. "Changes in surface chemistry of activated carbons by wet oxidation". In: *Carbon* 38.14 (Jan. 2000), pp. 1995–2001. ISSN: 00086223. DOI: 10.1016/S0008-6223(00)00048-8.

[107] S. Malmgren et al. "Consequences of air exposure on the lithiated graphite SEI". In: *Electrochimica Acta* 105 (2013), pp. 83–91. ISSN: 00134686. DOI: 10.1016/j.electacta.2013.04.118.

[108] *Thermo Scientific XPS: Knowledge Base - XPS Simplified (ThermoFischer Scientific)*. 2020. URL: https://xpssimplified.com/periodictable.php.

[109] H. Takezawa et al. "Electrochemical behaviors of nonstoichiometric silicon suboxides (SiO x) film prepared by reactive evaporation for lithium rechargeable batteries". In: *Journal of Power Sources* 244 (Dec. 2013), pp. 149–157. ISSN: 03787753. DOI: 10.1016/j.jpowsour.2013.02.077.

[110] Z. Liu et al. "Investigation of the Electrode/Ionic Liquid Interphase: Chemical Reactions of an Ionic Liquid and a Lithium Salt with Lithiated Graphite Probed by X-ray Photoelectron Spectroscopy". In: *Journal of Physical Chemistry C* 123.16 (Apr. 2019), pp. 10325–10332. ISSN: 19327455. DOI: 10.1021/acs.jpcc.8b11549.

[111] B. Philippe. "Insights in Li-ion Battery Interphases through Photoelectron Sepctroscopy Depth Profiling". PhD thesis. Acta Universitatis Upsaliensis, 2013.

[112] B. Philippe et al. "Improved Performances of Nanosilicon Electrodes Using the Salt LiFSI: A Photoelectron Spectroscopy Study". In: *Journal of the American Chemical Society* 135 (2013), pp. 9829–9842. DOI: 10.1021/ja403082s.

[113] P. Parikh et al. "Role of Polyacrylic Acid (PAA) Binder on the Solid Electrolyte Interphase in Silicon Anodes". In: *Chemistry of Materials* 31.7 (Apr. 2019), pp. 2535–2544. ISSN: 15205002. DOI: 10.1021/acs.chemmater.8b05020.

[114] F. Buchner et al. "Intercalation and Deintercalation of Lithium at the Ionic Liquid-Graphite(0001) Interface". In: *Journal of Physical Chemistry Letters* 8.23 (Dec. 2017), pp. 5804–5809. ISSN: 19487185. DOI: 10.1021/acs.jpclett.7b02530.

[115] G. M. Girard et al. "Spectroscopic Characterization of the SEI Layer Formed on Lithium Metal Electrodes in Phosphonium Bis(fluorosulfonyl)imide Ionic Liquid Electrolytes". In: *ACS Applied Materials and Interfaces* 10.7 (Feb. 2018), pp. 6719–6729. ISSN: 19448252. DOI: 10.1021/acsami.7b18183.

[116] Z. Zeng et al. "Non-flammable electrolytes with high salt-to-solvent ratios for Li-ion and Li-metal batteries". In: *Nature Energy* 3.8 (Aug. 2018), pp. 674–681. ISSN: 20587546. DOI: 10.1038/s41560-018-0196-y.

[117] G. H. Wrodnigg, J. O. Besenhard, and M. Winter. "Cyclic and acyclic sulfites: New solvents and electrolyte additives for lithium ion batteries with graphitic anodes?" In: *Journal of Power Sources* 97-98 (July 2001), pp. 592–594. ISSN: 03787753. DOI: 10.1016/S0378-7753(01)00536-5.

[118] M. N. Kobrak. "Electrostatic interactions of a neutral dipolar solute with a fused salt: A new model for solvation in ionic liquids". In: *Journal of Physical Chemistry B* 111.18 (May 2007), pp. 4755–4762. ISSN: 15206106. DOI: 10.1021/jp066112f.

[119] H. Weingärtner. "Understanding ionic liquids at the molecular level: Facts, problems, and controversies". In: *Angewandte Chemie - International Edition* 47.4 (Jan. 2008), pp. 654–670. ISSN: 14337851. DOI: 10.1002/anie.200604951.

[120] C. Chiappe, M. Malvaldi, and C. S. Pomelli. "Ionic liquids: Solvation ability and polarity". In: *Pure and Applied Chemistry* 81.4 (Jan. 2009), pp. 767–776. ISSN: 1365-3075. DOI: 10.1351/PAC-CON-08-09-08.

[121] J. Li et al. "Asymmetric Rate Behavior of Si Anodes for Lithium-Ion Batteries: Ultrafast De-Lithiation versus Sluggish Lithiation at High Current Densities". In: *Advanced Energy Materials* 5.6 (Mar. 2015), p. 1401627. ISSN: 16146832. DOI: 10.1002/aenm.201401627.

[122] B. J. Tielsch and J. E. Fulghum. "Differential Charging in XPS. Part I: Demonstration of Lateral Charging in a Bulk Insulator Using Imaging XPS". In: *Surface and Interface Analysis* 24.1 (Jan. 1996), pp. 28–33. ISSN: 1096-9918. DOI: 10.1002/(SICI)1096-9918(199601)24:1<28::AID-SIA66>3.0.CO;2-G.

[123] M. Wang et al. "Effect of LiFSI Concentrations to Form Thickness- and Modulus-Controlled SEI Layers on Lithium Metal Anodes". In: *Journal of Physical Chemistry C* 122.18 (May 2018), pp. 9825–9834. ISSN: 19327455. DOI: 10.1021/acs.jpcc.8b02314.

[124] T. Sugimoto et al. "Ionic liquid electrolyte systems based on bis(fluorosulfonyl)imide for lithium-ion batteries". In: *Journal of Power Sources* 189.1 (Apr. 2009), pp. 802–805. ISSN: 03787753. DOI: 10.1016/j.jpowsour.2008.07.053.

[125] B. S. Parimalam and B. L. Lucht. "Reduction Reactions of Electrolyte Salts for Lithium Ion Batteries: LiPF6, LiBF4, LiDFOB, LiBOB, and LiTFSI". In: *Journal of The Electrochemical Society* 165.2 (2018), A251–A255. DOI: 10.1149/2.0901802jes.

[126] A. Basile. "Identifying the Solid-Electrolyte Interphase formed on Lithium Metal Electrodes using Room temerature Ionic liquid based Electrolytes". PhD thesis. RMIT University, 2014.

[127] Q. Zhang et al. "Synergetic Effects of Inorganic Components in Solid Electrolyte Interphase on High Cycle Efficiency of Lithium Ion Batteries". In: *Nano Letters* 16 (2016), pp. 2011–2016. DOI: 10.1021/acs.nanolett.5b05283.

[128] J. Wang et al. "Fire-extinguishing organic electrolytes for safe batteries". In: *Nature Energy* 3.1 (Jan. 2018), pp. 22–29. ISSN: 20587546. DOI: 10.1038/s41560-017-0033-8.

[129] L. Dong et al. “Safe Hybrid Electrolytes Based on Ionic Liquid and Carbonate Solvents for High-Temperature Li-rich Lithium-Ion Battery”. In: *Int. J. Electrochem. Sci.* 15 (2020), pp. 2948–2960. DOI: 10.20964/2020.04.30.

[130] V. Etacheri et al. “Effect of fluoroethylene carbonate (FEC) on the performance and surface chemistry of Si-nanowire li-ion battery anodes”. In: *Langmuir* 28.1 (Jan. 2012), pp. 965–976. ISSN: 07437463. DOI: 10.1021/la203712s.

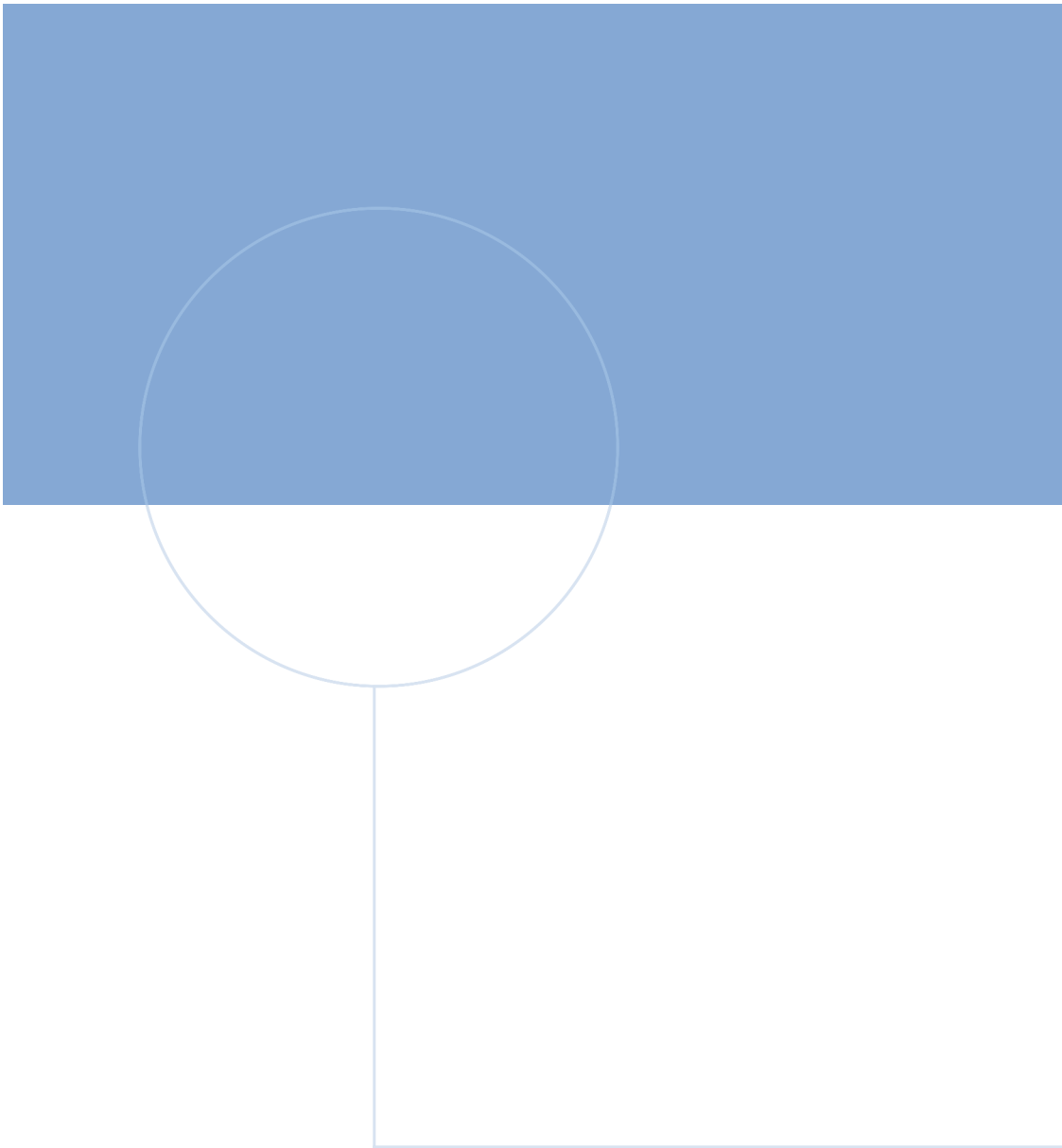

NTNU

Norwegian University of
Science and Technology